THE MOISTURE AND THERMAL REGIMES OF A BARE SOIL IN THE LOWER FRASER VALLEY DURING SPRING

by

MICHAEL DAVID NOVAK

B.Eng., McGill University, 1970

M.Sc., University of Western Ontario, 1971

A THESIS SUBMITTED IN PARTIAL FULFILLMENT OF THE REQUIREMENTS FOR THE DEGREE OF DOCTOR OF PHILOSOPHY

in

THE FACULTY OF GRADUATE STUDIES

Department of Soil Science

We accept this thesis as conforming

to the required standard

THE UNIVERSITY OF BRITISH COLUMBIA

August 1981

In presenting this thesis in partial fulfilment of the requirements for an advanced degree at the University of British Columbia, I agree that the Library shall make it freely available for reference and study. I further agree that permission for extensive copying of this thesis for scholarly purposes may be granted by the head of my department or by his or her representatives. It is understood that copying or publication of this thesis for financial gain shall not be allowed without my written permission.

Department of Soil Science

The University of British Columbia
2075 Wesbrook Place
Vancouver, Canada
V6T 1W5

Date 18/10/81

ABSTRACT

Half-hourly measurements of the surface energy balance components and soil temperatures were made at Agassiz, B.C., in the spring and early summer of 1978 at two adjacent bare-soil sites, one of which was culti-packed, while the other was disc-harrowed. The latent and sensible heat flux densities were measured using the energy balance/Bowen ratio technique with reversing psychrometer units. Soil surface heat flux density, G_o, was calculated using the null-alignment procedure from half-hourly measurements of soil temperature at 30 depths down to 1 m and volumetric soil heat capacity calculated from measurements of bulk density, organic matter fraction, and moisture content measured gravimetrically at least every 2 days.

The bulk density of the upper 10 cm of soil was reduced 10 - 20% by the disc-harrowing. Net radiation was reduced by 7% and evaporation by 40% at the disc-harrowed site during a 16-day almost-rainless period. Surface drying was greater at the disc-harrowed site, which in conjunction with the lower bulk density led to a greater reduction in near-surface volumetric soil heat capacity and thermal conductivity. The daily average of G_o was not affected by either the tillage or surface drying, although its diurnal amplitude was reduced by the disc-harrowing. Both daily and daytime averages of near-surface soil temperature were higher and nighttime averages slightly lower at the disc-harrowed site. Surface drying increased the diurnal amplitudes of near surface soil temperatures, particularly for the disc-harrowed site. The effects of the disc-harrowing and surface drying on the soil thermal regime were mostly attributed to the resulting reductions in near-surface thermal properties. The relative increase in atmospheric admittance that occurred with surface drying exceeded the corresponding decrease in soil admittance at both sites.

It was concluded that the increase in atmospheric admittance, which was attributed to the greater atmospheric instability under the resulting stronger lapse rates, must be included when partitioning available energy at the earth's surface. Daily and daytime averages of G_o at each site could be expressed as simple functions of either the solar irradiance alone or net radiation and some measure of near-surface soil moisture status. Nighttime average G_o at both sites could be expressed as a function of a cloudiness ratio based upon the daytime average of solar irradiance.

To calculate soil temperature, the exact solution to the equations of heat transfer for a homogeneous finite layer overlying a homogeneous semi-infinite layer with G_o as a boundary condition was derived. The theory was found to be useful in assessing the effects of tillage and drying on daily average temperature. However, for relatively wet sites such as at Agassiz, the derivation of a solution in which the variation of k and C with depth and time is better represented than by the simple two-layered model is desirable. The results showed that all methods that calculate soil temperature using G_o as a boundary condition are sensitive to small systematic errors in G_o over periods greater than 10 days. Calculation of diurnal variations of soil temperature using the harmonic solution to the two-layered model was tested. This procedure underestimated the diurnal variation of the surface temperature on cloudy days and overestimated on clear days when the soil surface was dry, particularly at the culti-packed site.

An empirical equation developed by Idso's group at Phoenix, Arizona to calculate daily average evaporation rates during all 3 drying stages of a bare soil was tested and discussed on the basis of available

evaporation theory. The results show that the Idso expression for potential evaporation rate did not apply at Agassiz due to differences in the advection regimes at the two locations. The Agassiz potential evaporation rate data was well represented by the Priestley-Taylor equation with a_{PT} ("alpha") = 1.27 ± 0.1. It was concluded that Idso's equation for potential evaporation rate has no greater generality than the Priestley-Taylor or other such semi-empirical approach. The concept of expressing the stage III rates as proportional to the expression for potential evaporation rate worked marginally well at the culti-packed site and quite well at the disc-harrowed site. It was concluded that for soils with stage III rates much greater than 50% of potential evaporation rate more complete procedures are necessary for calculating evaporation rates during extended drying periods.

TABLE OF CONTENTS

LIST OF TABLES

LIST OF FIGURES

Page

LIST OF SYMBOLS

Roman Symbols

a	Constant in the Laplace transforms of T_1, T_2 ($J^{-1} m^2 °C s^{\frac{1}{2}}$).
a_{PT}	Priestley-Taylor coefficient, "alpha".
A_1, A_2	Constants in the Laplace transform of T_1 (°C s).
b	Constant in the Laplace transforms of T_1, T_2 ($s^{\frac{1}{2}}$).
B	Bowen ratio, H/LE.
B_1, B_2	Constants in the Laplace transform of T_2 (°C s).
c	Constant in the Laplace transforms of T_1, T_2 ($s^{\frac{1}{2}}$).
c_s^{org}	Specific heat of organic matter (1.93 kJ kg^{-1} $°C^{-1}$).
c_s^{min}	Specific heat of mineral matter (0.71 kJ kg^{-1} $°C^{-1}$).
c_s^{w}	Specific heat of water (4.185 kJ kg^{-1} $°C^{-1}$).
c_p	Specific heat of air (1.0 kJ kg^{-1} $°C^{-1}$).
$C = C(z,t)$	Soil volumetric heat capacity at depth z and time t (MJ m^{-3} $°C^{-1}$).
C_a	Atmospheric volumetric heat capacity (1.2 kJ m^{-3} $°C^{-1}$).
C_f	Fluid volumetric heat capacity (MJ m^{-3} $°C^{-1}$).
C_1	Soil volumetric heat capacity of upper finite layer (MJ m^{-3} $°C^{-1}$).
C_2	Soil volumetric heat capacity of lower semi-infinite layer (MJ m^{-3} $°C^{-1}$).
$(C_1)_{max}$	Maximum value of C_1, "wet value" (MJ m^{-3} $°C^{-1}$).
$(C_1)_{min}$	Minimum value of C_1, "dry value" (MJ m^{-3} $°C^{-1}$).
d	Depth of upper finite layer (cm).
D_{1d}	Daily damping depth of the upper finite layer, $(2 k_1 C_1^{-1} \omega_d^{-1})^{\frac{1}{2}}$ (cm).
D_{2d}	Daily damping depth of the lower semi-infinite layer, $(2 k_2 C_2^{-1} \omega_d^{-1})^{\frac{1}{2}}$ (cm).

D_{2a} Annual damping depth of the lower semi-infinite layer, $(2\ k_2\ C_2^{-1}\ \omega_a)^{\frac{1}{2}}$ (cm).

e Vapour pressure (kPa).

e_a Vapour pressure in the atmosphere (kPa).

e_z Vapour pressure in the atmosphere at height z (kPa).

$e^*=e^*(T)$ Saturated vapour pressure function (kPa).

e_z^* Saturated vapour pressure in the atmosphere at height z (kPa).

e_o^* Saturated vapour pressure at the soil surface temperature, T_o (kPa).

$f(z)$ Initial soil temperature distribution function (°C).

f_{org}^m Dry-mass fraction of soil organic matter.

f_{min}^m Dry-mass fraction of mineral content.

f_w^m Dry-mass fraction of moisture content.

F Constant in square-root of time expression for bare soil evaporation with PLE = ∞ (W m^{-2} $d^{\frac{1}{2}}$).

$g_o=g_o(s)$ Laplace transform of $G_o(t)$ (W m^{-2} s).

$G=G(z,t)=G_z$ Soil heat flux density at depth z and time t (W m^{-2}).

$G_o=G_o(t)$ Soil surface heat flux density (W m^{-2}).

$G_o(j)$ Soil surface heat flux density of the j^{th} pulse interval (W m^{-2}).

G_o^{24} 24-hour average of G_o (W m^{-2}).

G_o^d Daytime average of G_o (W m^{-2}).

G_{vL} Soil heat flux density due to the transport of latent heat by vapour movement, $\rho_w L_w v$ (W m^{-2}).

G_{vL}^{θ} Soil heat flux density due to the transport of latent heat by vapour movement along moisture gradients, $-\rho_w L_w \kappa_{\theta v} \frac{d\theta v}{dz}$ (W m^{-2}).

h_z Bulk vapour and heat transfer coefficient, similarly assumed (m s^{-1}).

$h_{LE}=h_{LE}(z,t)$ Volumetric rate at which energy is being used for evaporation in the soil (W m^{-3}).

H Sensible surface heat flux density into the atmosphere ($W\ m^{-2}$).

H_1, H_2 Values of H at sites 1 and 2 respectively ($W\ m^{-2}$).

i Unit imaginary number, $\sqrt{-1}$.

j Dummy integer.

$k=k(z,t)$ Soil thermal conductivity at depth z and time t ($W\ m^{-1}\ °C^{-1}$).

k_{20} Average daily soil thermal conductivity at 20 cm depth determined from the times for which null-points did exist in the profile ($W\ m^{-1}\ °C^{-1}$).

k_1 Soil thermal conductivity of the upper finite layer ($W\ m^{-1}\ °C^{-1}$).

k_2 Soil thermal conductivity of the lower semi-infinite layer ($W\ m^{-1}\ °C^{-1}$).

$(k_1)_{max}$ Maximum value of k , "wet value" ($W\ m^{-1}\ °C^{-1}$).

$(k_1)_{min}$ Minimum value of k , "dry value" ($W\ m^{-1}\ °C^{-1}$).

LE Latent surface heat flux density into the atmosphere ($W\ m^{-2}$).

LE_I, LE_{II}, LE_{III} Latent heat flux density during the respective evaporation stages I, II, and III from a bare soil ($W\ m^{-2}$).

L_N Net longwave radiation flux density at the soil surface ($W\ m^{-2}$).

$(L_N)_1$, $(L_N)_2$ Values of L_N at sites 1 and 2, respectively ($W\ m^{-2}$).

$(L\downarrow)_1$, $(L\downarrow)_2$ Down-coming longwave radiation flux densities received at the soil surfaces at sites 1 and 2, respectively ($W\ m^{-2}$).

$L_t^{-1}\{y\}$ Inverse Laplace transform of y (°C).

L_w Latent heat of vapourization of water ($2.5\ MJ\ kg^{-1}$).

MSSR Maximum steady-state latent heat flux density from a bare soil with a water table located at some depth below the surface ($W\ m^{-2}$).

n Dummy integer.

p Parameter given by $C_f \, v \, (2k)^{-1}$ (cm^{-1}).

P Porosity of the soil

P_1 Parameter given by $\kappa_1 \, t \, d^{-2}$.

PLE Potential surface latent heat flux density ($W \, m^{-2}$).

PLE_{Ag} Values of PLE at Agassiz ($W \, m^{-2}$).

q Fraction S/S_{max}, with S_{max} = 340 $W \, m^{-2}$ on a daily average basis.

$q_v = q_v(z,t)$ Vapour flux density in the soil (positive upward) at depth z and time t ($kg \, m^{-2} \, s^{-1}$).

r_a Parameter given by $\dfrac{\sqrt{k_1 \, C_1} - \sqrt{k_2 \, C_2}}{\sqrt{k_1 \, C_1} + \sqrt{k_2 \, C_2}}$.

r_b Parameter given by $\dfrac{\sqrt{k_1 \, C_1}}{\sqrt{k_1 \, C_1} + \sqrt{k_2 \, C_2}}$.

R Absolute value of complex numbers on sections 1 and 5 of the contour used to evaluate the inverse Laplace transform of $x(s)$ (s^{-1}).

R^2 Squared correlation coefficient in a linear least-squared statistical regression of data.

R_N Net radiation flux density at the soil surface ($W \, m^{-2}$).

R_v Gas constant for water vapour (460 $J \, kg^{-1} \, °C^{-1}$).

s Laplace transform variable (s^{-1}).

s_v Slope of the saturation vapour pressure versus temperature function (kPa $°C^{-1}$).

S Solar radiation flux density (solar irradiance) at the soil surface, assumed horizontal ($W \, m^{-2}$).

S_N Net solar radiation flux density at the soil surface ($W \, m^{-2}$).

S_{max} Maximum value of S measured (340 W m^{-2} on a daily basis).

t Time (d, h, or s).

t(j) Time at the midpoint of the j^{th} pulse interval.

t_1 Average time of sunrise (4.5 h).

t_2 Average time of sunset (20.5 h).

t_{III} Time required to reach the transition to stage III (d).

$T=T(z,t)=T_z$ Soil temperature at depth z and time t (°C).

$T_o=T_o(t)$ Soil surface temperature (°C).

T_a Atmospheric (air) temperature (°C).

$T_1=T_1(z,t)$ Soil temperature at depth z and time t in the upper finite layer (°C).

$T_2=T_2(z,t)$ Soil temperature at depth z and time t in the lower semi-infinite layer (°C).

$(T_o)_1,(T_o)_2$ Soil surface temperatures at sites 1 and 2, respectively (°C).

$(T_a)_1,(T_a)_2$ Air temperatures (70 cm height) at sites 1 and 2 respectively (°C).

T_{aa} Annual average soil temperature (°C).

T_{max} Daily maximum soil temperature at some depth (°C).

T_{min} Daily minimum soil temperature at some depth (°C).

v Steady-state velocity (positive downward) with which a fluid is moving in the soil (m d^{-1}).

$x = x(s)$ Laplace transform, $y(s)/g_o(s)$ (°C W^{-1} m^2).

$y=y(s)$ General form of terms in the Laplace transforms of T_1, T_2 (°C s).

$y_1=y_1(s)$ Laplace transform of T_1 (°C s).

$y_2=y_2(s)$ Laplace transform of T_2 (°C s).

z Depth in soil or height in atmosphere (cm or m).

z_k Depth at which G is known at some time t (cm).

z_n Depth of a null-point in the soil temperature profile (cm).

Greek Symbols

α	Soil albedo.
α_d	Dry soil albedo.
α_w	Wet soil albedo.
β	Soil surface wetness partitioning factor, $(\alpha_d - \alpha)/(\alpha_d - \alpha_w)$.
γ	A real value of s that lies to the right of all singularities of x(s) (s^{-1}).
γ_v	Psychrometric constant ($\cong$ 0.066 kPa $°C^{-1}$).
δ	Parameter used in empirical bare soil evaporation formulas; defined on p. 122.
ε	Absolute-value of complex numbers on section 3 of the contour used to evaluate the inverse Laplace transform of x(s) (s^{-1}).
ε_s	Emissivity of the soil surface.
ε_a	Emissivity of the atmosphere.
$(\varepsilon_s)_1, (\varepsilon_s)_2$	Emissivities of the soil surfaces at sites 1 and 2, respectively.
η_a, η_o	Phase parameters.
θ	Argument of a complex number.
$\theta_v = \theta_v(z,t)$	Soil volumetric moisture content at depth z and time t (cm^3 water/cm^3 soil).
κ_a	Atmospheric eddy diffusivity, similarity assumed ($m^2\ s^{-1}$).
κ_H, κ_{LE}	Atmospheric eddy diffusivities for sensible and latent heat respectively ($m^2\ s^{-1}$).
κ_1	Soil thermal diffusivity of the upper finite layer, $k_1\ C_1^{-1}$ ($cm^2\ d^{-1}$).
κ_2	Soil thermal diffusivity of the lower semi-infinite layer, $k_2\ C_2^{-1}$ ($cm^2\ d^{-1}$).

$\kappa_{\theta v}$ Hydraulic vapour diffusivity ($m^2\ s^{-1}$).

λ Dummy integration variable(s).

μ Thermal admittance parameter of a homogeneous medium, $\sqrt{k\ C}$ ($J\ m^{-2}\ °C^{-1}\ s^{-\frac{1}{2}}$).

μ_s Effective soil thermal admittance, $\frac{\|G_o\|}{\|T_o\|\sqrt{\omega}}$ ($J\ m^{-2}\ °C^{-1}\ s^{-\frac{1}{2}}$).

μ_a Effective atmospheric thermal admittance, $\frac{\|H\|}{\|T_o\|\sqrt{\omega}}$ ($J\ m^{-2}\ °C^{-1}\ s^{-\frac{1}{2}}$).

$(\mu_s)_{max}$ Maximum possible value of μ_s ($J\ m^{-2}\ °C^{-1}\ s^{-\frac{1}{2}}$).

ν Dummy integration variable ($s^{-\frac{1}{2}}$).

ξ Dummy integration variable, ν^2 (s^{-1}).

ρ_b Soil bulk density, i.e. mass of dry soil per volume of soil ($kg\ m^{-3}$).

ρ_w Density of water (1000 $kg\ m^{-3}$).

ρ_a Density of the atmosphere (1.2 $kg\ m^{-3}$).

ρ_v Density of water vapour in the pore space of the soil ($kg\ m^{-3}$).

σ Stefan-Boltzmann constant ($5.67 \times 10^{-8}\ W\ m^{-2}\ °C^{-4}$).

τ Width of the square pulses used to represent $G_o(t)$ (d).

ϕ_a Potential temperature of the atmosphere (°C).

ω Angular frequency of a sinusoidal oscillation (d^{-1} or h^{-1}).

ω_a Angular frequency of an annual cycle ($2\pi/365\ d^{-1}$).

ω_d Angular frequency of a daily cycle ($2\pi/24\ h^{-1}$).

ACKNOWLEDGEMENTS

The study was supported by grants from Agriculture Canada and the British Columbia Ministry of Agriculture. I was personally supported by the National Science and Engineering Research Council of Canada as well as by a U.B.C. teaching assistantship and a summer scholarship. The research site and facilities were provided by the Agriculture Canada Research Station at Agassiz, B.C.

I am grateful to the faculty, staff, and students of the Department of Soil Science for their help and friendship during my years of study at U.B.C. Particular acknowledgement goes to my supervisor, Dr. Andy Black, whose advice and encouragement greatly contributed to the success of the research. As well the understanding and support of my friends and family is appreciated.

Pat Wong contributed his electronics ability during the critical field study phase of the research. Rafael Moreno drafted the figures and Jeeva Jonahs typed the manuscript.

INTRODUCTION

Soil temperature is one of the major limiting factors in agriculture and forestry in Canada, often determining the length of the growing season and ultimate yields. It is dependent upon the soil volumetric heat capacity, thermal conductivity, and surface heat flux density (the quantity of heat that enters or leaves a unit area of soil surface per unit time). For a given soil both the volumetric heat capacity and thermal conductivity are mainly functions of moisture content and bulk density. These functions have been well established for different soil textures. Relatively few studies have dealt with the soil surface heat flux density; especially how it is affected by changes in the other surface energy balance components (the net radiation, sensible heat, and latent heat flux density). In many areas the latent heat flux density accounts for a large part of the net radiation flux density, at least during certain times of the year. This prompted the author to study, as part of this thesis, whether the reduction of evaporation by the creation of a mulched surface layer would lead to an increase in the soil surface heat flux density. Such a layer forms naturally when a bare soil dries by evaporation. Artificially loosening the surface soil enhances this process. Soil hydraulic conductivity generally decreases more rapidly than thermal conductivity as soil moisture content decreases. A steady-state argument then suggests, all other factors being equal, that the natural formation of a soil mulch should result in an increase in soil surface heat flux density.

The relationships between the soil surface heat flux density and the surface energy balance components were investigated in a study that

took place on a bare soil in the spring and early summer of 1978 at the Agriculture Canada Research Station at Agassiz, B.C. Two contrasting tillage treatments were studied, culti-packed versus disc-harrowed. The results of this study form the basis of the three chapters comprising this thesis, which has been written in paper format.

In Chapter 1 the effects of tillage and soil drying on the surface energy balance components (particularly the soil heat flux density), and temperatures, thermal properties, and moisture contents at Agassiz are reported. Relationships between soil surface heat flux density and easily measured meteorological and soil variables are developed.

In Chapter 2 the exact solution to the equations governing heat transfer in a two-layered model of a drying or tilled soil with the soil surface heat flux density as the upper boundary condition is derived. This solution is tested against the daily average soil temperatures measured at Agassiz using the measured daily average soil surface heat flux density as the boundary condition. Furthermore, the possibility of using the harmonic solution to the equations of heat transfer for the two-layered soil to predict daily maximum and minimum temperatures is assessed.

In Chapter 3 an empirical equation developed in Phoenix, Arizona to calculate the daily average evaporation rate of a bare soil during all 3 stages of drying is tested with the Agassiz measurements and discussed on the basis of available evaporation theory. The Priestley-Taylor method of describing potential evaporation rate is also evaluated for the bare soil at Agassiz.

CHAPTER 1

THE EFFECTS OF DRYING AND TILLAGE ON THE SURFACE HEAT FLUX DENSITY OF A BARE SOIL

THE EFFECTS OF DRYING AND TILLAGE ON THE SURFACE HEAT FLUX DENSITY OF A BARE SOIL

1.1 Introduction

The modification of the thermal regimes of bare soils by tillage and by surface drying is important in the practical management of agronomic systems. The temperature (T) distribution in a one-dimensional soil profile, in which internal heat sources or sinks are absent and internal convective heat exchange can be neglected, is governed by the partial differential equation

$$C\frac{\partial T}{\partial t} = \frac{\partial}{\partial z}\left(k\frac{\partial T}{\partial z}\right) \qquad (1)$$

where t is the time, z is the depth in the soil, k is the soil thermal conductivity, and C is the volumetric soil heat capacity. In general, k and C are functions of z, t, and T (Carslaw and Jaeger, 1959). Solutions of (1) when the thermal properties are not constant, as is usually the case in a drying or tilled soil, can be carried out numerically on a computer (Wierenga and de Wit, 1970; Hanks et al., 1971). Van Duin (1954) and van Wijk and Derksen (1966) modelled the effects of surface drying and tillage by representing the thermal properties as step functions with respect to depth, with the step occurring at the same depth for both k and C. The solution of (1) requires the specification of both initial and boundary conditions. For the surface boundary condition often the temperature (T_o) is assumed to be given as a function of time. However in assessing the effects of drying and tillage on the thermal regime of a soil, one of the major objectives is to predict their effect on surface temperature, which precludes specifying this function a priori.

An alternate and completely equivalent procedure is to specify the surface soil heat flux density as a given function of time. This flux density is coupled to the dynamics of heat, moisture, and radiation transfer in both the soil and atmosphere, as can be seen from the surface energy balance equation,

$$R_N = S_N + L_N = LE + H + G_o \qquad (2)$$

where R_N, S_N, and L_N are the net, net solar, and net longwave radiation flux densities respectively and LE, H, and G_o are the latent, sensible, and soil surface heat flux densities respectively. Analysis of these dynamics for a large range of atmospheric and soil conditions is difficult and has not been fully carried out. Lettau (1951) presented an analysis of the diurnal and annual heat budgets of the earth's surface assuming that evaporation was constant, the flux densities R_N, G_o, and H in (2) were harmonic functions of time, soil thermal properties were constant, and the atmospheric eddy diffusivity, K_a, increased linearly with height. The effects of buoyancy were neglected and the linear relationship between diffusivity and height, which accounted for turbulence due to wind and surface roughness, was shown to be strictly applicable up to heights ~ 30 cm.

Poppendiek (1952), Staley (1956), and Stearns (1966) all presented experimental results showing that K_a increased strongly with height to heights of ~ 3 - 40 m and exhibited large diurnal variations (being ~ 3 - 100 times greater during the daytime than at night). Furthermore both Staley (1956) and Priestley (1959) reported that K_a was at least bounded, if not decreasing, for heights above 20 to 100 m. Since surface fluctuations are felt to heights of at least 100 - 400 m (de Vries, 1957), Lettau's

(1951) assumption regarding κ_a is subject to error.

Van Wijk and de Vries (1966) modified Lettau's theory somewhat by also representing LE, L_N, and S_N as harmonic functions of time. LE was assumed to be in phase with H and L_N with T_o, while S_N reached a maximum at solar noon. In their investigations both van Duin (1954) and van Wijk and Derksen (1966) used Lettau's theory to determine the amplitudes of the diurnal and annual time courses of G_o for their layered soils. According to these authors the ratio of the amplitude of G_o to that of H decreased with both tillage and drying (particularly for diurnal variations) due to the decrease in both C and k near the soil surface. κ_a was unaffected since windspeed and surface roughness were assumed constant. These authors also used the simple assumption that the amplitude of G_o remained unchanged with tillage and drying, as speculated by de Vries (1975).

Relatively few field studies of the effect of drying or tillage on soil heat flux density have been published. Idso et al. (1975a) reported that the daytime total soil surface heat flux densities in May and September at Phoenix, Arizona doubled when a bare Avondale loam dried out completely at the surface, although in December there was no increase. A similar increase was shown for a bare Williams loam at Sidney, Montana in September. The increase in soil heat flux density with drying for May and September at Phoenix occurred despite an indicated decrease in R_N of about 40%. In an earlier experiment in Israel, Fuchs and Hadas (1972) reported only a slight increase in the fraction of R_N dissipated as soil heat when a bare Negev loessial soil dried out following an irrigation in June. According to their Figure 5, the diurnal variations of soil surface heat flux density were similar for both wet and dry days,

despite a reduction in daytime average evaporation of about 210 W m^{-2} on the dry day. In the study of Wierenga and de Wit (1970) at Davis, California, their Figure 4 showed an increase in the diurnal amplitude of soil surface heat flux density of about 40% following irrigation in the summer of a bare Yolo silt-loam. The figure also indicated that the daily averages of the soil heat flux densities were similar for both days. Allmaras et al. (1977) reported the results of experiments with four kinds of tillage on bare Nicollet clay-loam and Doland loam/silt-loam soils in western Minnesota. Their results are difficult to summarize and explain. They showed that daytime average soil surface heat flux densities were somewhat lower (in one year) for the plowed treatment compared with the plow-packed treatment, despite greater values of R_N for the former (attributed to greater surface roughness). However soil heat flux densities for the roto-tilled treatment were similar to or slightly higher than those for the plow-packed treatment. The results suggested that heat transfer by turbulent convection within the near-surface soil was significant at higher porosities.

The purpose of this chapter is to report on the effects of tillage and soil drying on the surface energy balance components (particularly the soil heat flux density), and temperatures, thermal properties, and moisture contents of a bare soil in the Lower Fraser Valley, B.C., during the spring and early summer of 1978. A major objective of this work was to find useful relationships between soil surface heat flux density and easily measured meteorological and soil variables.

1.2 Experimental Procedure

The study was carried out on the Agriculture Canada Research

Station at Agassiz, British Columbia (49° 15'N, 121° 46' W). The experiments were conducted in a 145 x 175 m level field normally used for horticultural trials but kept bare for this study (Appendix I, Figure 1). The surrounding fields were quite level and supported crops throughout the study. The soil was a Monroe series loam/silt-loam (Degraded Eutric Brunisol) which developed from Fraser River deposits. Profiles showed little textural variability to depths ranging from 50 to 100 cm, below which coarser textured layers were often encountered. The water table was located between 1 and 2 m below the soil surface.

Two major experiments were conducted. The first consisted of a long-term study (May 10 to July 21) of a firmly packed area referred to as site 1. Preparation of this site took place in the first week of May and consisted of disc-harrowing followed by firm packing with a culti-packer. The second experiment was a shorter study (July 6 to July 21) of an area, referred to as site 2, in which the topmost 10 cm of soil had been loosened by two passes of the disc-harrow. This disc-harrowing took place on June 28 on about one third of the field, which consequently reduced the size of site 1 by this amount. The instrumentation, which was identical for both experiments, was centrally located in each site. The sites were maintained free of weeds by periodic applications of glyphosate, a broad spectrum herbicide.

Half-hourly average values of the surface energy balance components were obtained throughout each day. Net radiation flux density at each site was measured with a Swissteco S-1 net radiometer mounted 65 cm above the soil surface. The signal from the site 1 net radiometer was integrated using a dual-ramping voltage integrator (Tang et al., 1976). The half-hourly value of net radiation at site 2 was approximated by taking a two-hour

running average of the ratio of site 2 to site 1 half-hourly instantaneous measurements of net radiation, and multiplying by the site 1 integrated half-hourly value. This procedure was reasonable since the ratio seldom varied by more than 5 to 10% over a two-hour period. Solar irradiance was measured with a Kipp and Zonen CM5 pyranometer and a voltage integrator. The albedo was measured half-hourly at each site using an inverted Kipp and Zonen pyranometer located at 60 cm above the soil surface. Field calibrations of all the radiation instruments by a beam-radiation shading technique (Tanner, 1963) were consistent with the manufacturers' calibrations. Windspeed was measured with a sensitive Cassella anemometer located at a height of 95 cm at site 1. Wind direction at this same height and location was measured with a Climet 012-6C vane. Precipitation and other standard meteorological variables were measured routinely by the research station staff at a climate station adjacent to the study area.

Latent and sensible heat flux densities were measured using the energy balance/Bowen ratio technique which uses the equation: $LE = (R_N - G_o)/(1 + B)$, where B is the Bowen ratio (H/LE). The Bowen ratios were measured with reversing psychrometer units designed and built at U.B.C. and fully described in Black and McNaughton (1971) and Tang (1976). Each unit consisted of two shielded, aspirated ($\sim 3.5 m\ s^{-1}$) psychrometers each containing germanium diodes which measured the vertical wet-bulb and dry-bulb temperature differences over a distance of 50 cm. The sensitivities of each pair of wet-bulb and dry-bulb diodes were matched to within 0.5%. The positions of the psychrometers were automatically reversed every 15 minutes to remove any systematic errors. There was one psychrometer unit per site. The Bowen ratio was calculated from the relation

$$B = \frac{K_H}{K_{LE}} \gamma_v \frac{\overline{\Delta\phi_a}}{\overline{\Delta e_a}} \qquad (3)$$

where $\Delta\phi_a$, Δe_a are the vertical differences in potential temperature and vapour pressure respectively, and γ_v is the psychrometric constant. The usual assumption was made that the atmospheric eddy diffusivities for both latent and sensible heat were similar ($K_H = K_{LE}$) and Δe_a was corrected for the natural decrease of pressure with height. The bars refer to averages over 20 minutes of every 30 minute measurement period, the other 10 minutes being reserved for equilibration after the reversals.

The similarity assumption has been verified by many researchers for both lapse and nocturnal inversion conditions (Dyer, 1967; Oke, 1970), although recently Verma et al. (1978) and Motha et al. (1979) showed that this assumption did not hold for strongly advective conditions. However such conditions generally did not occur during this study since midday Bowen ratios were almost always greater than zero. The absolute wet-bulb and dry-bulb temperatures of one of the psychrometers in each unit was measured once every half-hour. The psychrometers were mounted within 1 m of the soil surfaces which resulted in a minimum fetch-height ratio of 80:1. The prevailing wind direction was such that this ratio was unaffected by division of the field into the two sites. Windspeeds during the daytime were generally quite low, usually falling in the range 1 to 2 m s^{-1}. Periodic manual checks with Lambrecht psychrometers as well as visual inspections of the wicks indicated that the psychrometric units operated properly throughout the experiments. Evaporation calculated from gravimetric measurements of changes in soil moisture storage on May 30 and June 5 at site 1 agreed well with the evaporation measured by the energy balance/Bowen ratio instrumentation. Furthermore, half-hourly

evaporation rates measured by both Bowen ratio units operating together at site 1 on July 22 were in agreement to within 5%. Further details about these checks of the Bowen ratio units are in Chapter 3. A photograph of the two units on July 22 is in Appendix I, Figure 2.

Soil heat flux densities at the surface and at other depths of interest were calculated half-hourly from measured soil temperatures and volumetric heat capacities using a slightly modified version of the null-alignment method described by Kimball and Jackson (1975). Soil temperatures were measured at half-hour intervals by a bank of 30 matched copper-constantan thermocouples installed at 0.2, 0.5, 1.0, 1.5, 2.0, 2.5, 3.0, 3.5, 4.0, 4.5, 5.0, 6.0, 7.0, 8.0, 9.0, 10.0, 12.0, 14.0, 16.0, 18.0, 21.0, 24.0, 27.0, 32.0, 37.0, 42.0, 52.0, 62.0, 82.0, and 105.0 cm depths. The thermocouples were positioned at the desired depths using a framework consisting of acrylic and stainless steel tubing, as described in Appendix I, Figure 3. The required absolute temperature was measured to ±0.1°C using an FD-300 silicon diode placed at the 105 cm depth (Tang et al., 1974). The temperatures at the remaining depths were determined by measuring the temperature differences between any given depth and that immediately below to ±0.03°C using the thermocouples. Soil volumetric heat capacity was calculated from bulk density (ρ_b), dry-mass fractions of organic matter (f^m_{org}), mineral content (f^m_{min}), and moisture content (f^m_w) and specific heats according to

$$C = \rho_b (c_s^{org} f^m_{org} + c_s^{min} f^m_{min} + c_s^w f^m_w) \qquad (4)$$

where the values used for the specific heats of organic matter (c_s^{org}), mineral matter (c_s^{min}), and water (c_s^w) were 1.93, 0.71, and 4.185 kJ kg^{-1} $°C^{-1}$ respectively. Bulk density was measured at 5 cm

intervals to a depth of 50 cm and at 10 cm intervals below 50 cm. Organic matter fraction was estimated from measurements made by combustion of some of the bulk density samples at ~ 400°C, and $f^m_{min} = 1 - f^m_{org}$. Moisture content was measured gravimetrically to a depth of 21 cm at least every two days, and to a depth of 80 - 100 cm every 6 to 10 days. Each sample was a composite of 3 profiles usually taken near midday and oven-dried to ~ 105°C. Sampling depths were 0 - 0.5, 0-2, 2-4, 4-6, 6-9, 9-12, 12-15, 15-18, 18-21, 21-25, 25-30, 30-35, 35-40, 40-45, 45-50, 50-60, 60-70, 70-80 cm .... Sampling of the upper 21 cm of soil was done with the standard Oakfield core sampler (2 cm inner diameter), except for the 0-9 cm layer at site 2 which could not be sampled in this manner due to its loosened condition. Instead it was sampled by carefully and quickly scraping off soil from the desired intervals with a spatula.

To carry out the soil heat flux calculations both the temperatures and volumetric heat capacities were smoothed with cubic spline polynomials, first in time using the routine of Reinsch (1967) and then with depth using Kimball's (1976) routine (7 knots, located at 1, 2, 4, ..., 64 cm, were used for the temperatures and 3 knots, located at 2, 8, 32 cm, for the heat capacities). Both these routines were available as standard packages at the U.B.C. Computing Centre (Lee, 1978). The heat flux densities at various depths were calculated using an integrated form of (1), as follows:

$$G(z,t) = G(z_k,t) - \int_{z_k}^{z} C\frac{\partial T}{\partial t}\, dz \qquad (5)$$

where $G(z_k,t)$ is a heat flux density, known at some depth z_k for each time t. For those times for which a null-point, defined by $\frac{\partial T}{\partial z} = 0$, existed in the temperature profile (only depths in the interval 2 - 25 cm

were considered), it was assumed that

$$G(z_k,t) = G(z_n,t) = 0 \qquad (6)$$

where z_n is the depth of the null-point, i.e. isothermal heat flow along moisture gradients was neglected. The depth z_n was determined by finding the zero of the $\frac{\partial T}{\partial z}$ function. Both this calculation and the evaluation of the integral in (5) were performed with packaged routines (ZERO2 and CADRE respectively) available through the U.B.C. Computing Centre (Lee, 1979; Madderom, 1978). For the times for which a null-point did not exist in the profile, the heat flux density at the 20 cm depth was calculated according to Fourier's law:

$$G(z_k,t) = -k(z_k,t)\,\frac{\partial T}{\partial z}(z_k,t) = G(20\text{ cm},t) = -k_{20}\frac{\partial T}{\partial z}\,(20\text{ cm},t) \qquad (7)$$

where k_{20} was the average thermal conductivity at 20 cm determined from the times, on the day in question, for which null-points did exist in the profile. The accuracy of (7) was acceptable because k_{20} did not vary significantly throughout each day and the absolute values of heat flux density at 20 cm were generally small compared with those near the surface. The half-hourly soil heat flux densities calculated from (5), (6), and (7) were in good agreement with those measured with heat flux plates constructed by the author at U.B.C. in a manner similar to that of Fuchs and Tanner (1968), after application of Philip's (1961) correction to account for the difference between soil and plate thermal conductivities. Furthermore half-hourly site 1 soil heat flux densities, calculated using the null-alignment procedure described above with soil temperatures from a back-up profile of 6 FD-300 silicon diodes, located at the 1, 2.5, 5, 10, 20, 50 cm depths, agreed to within 40 W m^{-2} with those calculated from

the thermocouple systems. The heat flux densities presented in this chapter have not been corrected for the overestimate of the daytime 0 - 2.5 cm depth soil temperatures by the thermocouple systems for dry soil conditions (full details in Chapter 2). Calculations show that the error in G_o for these conditions was < 10 W m^{-2} for half-hourly averages and < 2 W m^{-2} for daily averages. Soil thermal conductivities at various depths of interest were calculated half-hourly from the soil heat flux densities and the smoothed temperature gradients (corrected for the above-mentioned overestimate) using Fourier's law.

Data acquisition for the experiments was with a Hewlett-Packard 2070A data logger and 3489A paper tape punch system, a Wescor DL-520 data logger, and integrator/mechanical counter-printer systems designed and built at U.B.C. The accuracy of the Hewlett-Packard system was about 0.5%. The Wescor data logger, with a resolution of 3 μV was used exclusively for the soil thermocouple difference signals. The accuracy of the integrators was about 0.2%.

The resolution in the measurement of temperature differences by the psychrometer units was less than 0.01°C. The minimum midday temperature difference between top and bottom psychrometers (either wet-bulb or dry-bulb) on clear days was ~ 0.35°C and the accuracy of the absolute air temperatures was ~ 0.5°C. The errors in the R_N and G_o measurements for these conditions were ~ 5% and ~ 10 - 15% respectively. This led to the typical errors in B, LE, and H shown in Table 1.1. It must be emphasized that the resolution in time of the measurements of all four surface energy balance components should be much better than the absolute errors indicated. This is of importance when considering the effects of drying.

B	0.5	1.0	3.0
ERROR IN B(%)	9	12	24
ERROR IN LE(%)	16	20	32
ERROR IN H(%)	19	20	20

TABLE 1.1: Typical midday uncertainties in clear-day measurements of B, LE, and H, using the analysis of Fuchs and Tanner (1970), for the Bowen ratio psychrometer units. The maximum midday Bowen ratio observed at site 1 was ~ 1.3 while values as high as 3.8 were observed at site 2.

1.3 Results and Discussion

A. Cumulative Surface Energy Densities

Total daily precipitation and 24-hour average solar irradiance (S), which are presented in Figure 1.1, indicate the variability of the weather conditions during the study. The weather, which was typical of the region, as described by Hay and Oke (1976), was dominated mostly by cyclonically generated Pacific frontal rainstorms of moderate intensity, especially during May. This is indicated by both the size and frequency of rainfall events. The decrease in the frequency of rainfall in late June and July was due to the establishment of the usual summer high pressure system over the region. About 2/3 of the days were cloudy and the average drying period was about 2-4 days, with a maximum of 10 days.

The cumulative 24-hour average energy densities for both sites are shown in Figure 1.2. The energy density units used (W m^{-2} d) are such that division by the number of days in a given period of interest yields the average energy flux density for that period in W m^{-2}. During the site 1 study period the net radiation flux density was approximately 60% of the solar irradiance (Figure 1.2a). Since the daytime average albedo of the soil at both sites varied from 0.065 ± 0.01 when the surface was wet to 0.165 ± 0.01 when it was dry, the net longwave radiation exchange from soil to sky at site 1 was about 30% of the solar irradiance. Latent, sensible, and soil heat flux densities at site 1 represented about 40, 15, and 5% of the solar irradiance and 68, 24, and 8% of the net radiation flux density respectively during the site 1 study period. The overall linearity of the cumulative latent heat curve from May 17 to June 28 indicates that near potential evaporation rates were maintained on average at site 1 for the first 2/3 of the experiment. This can be attributed to

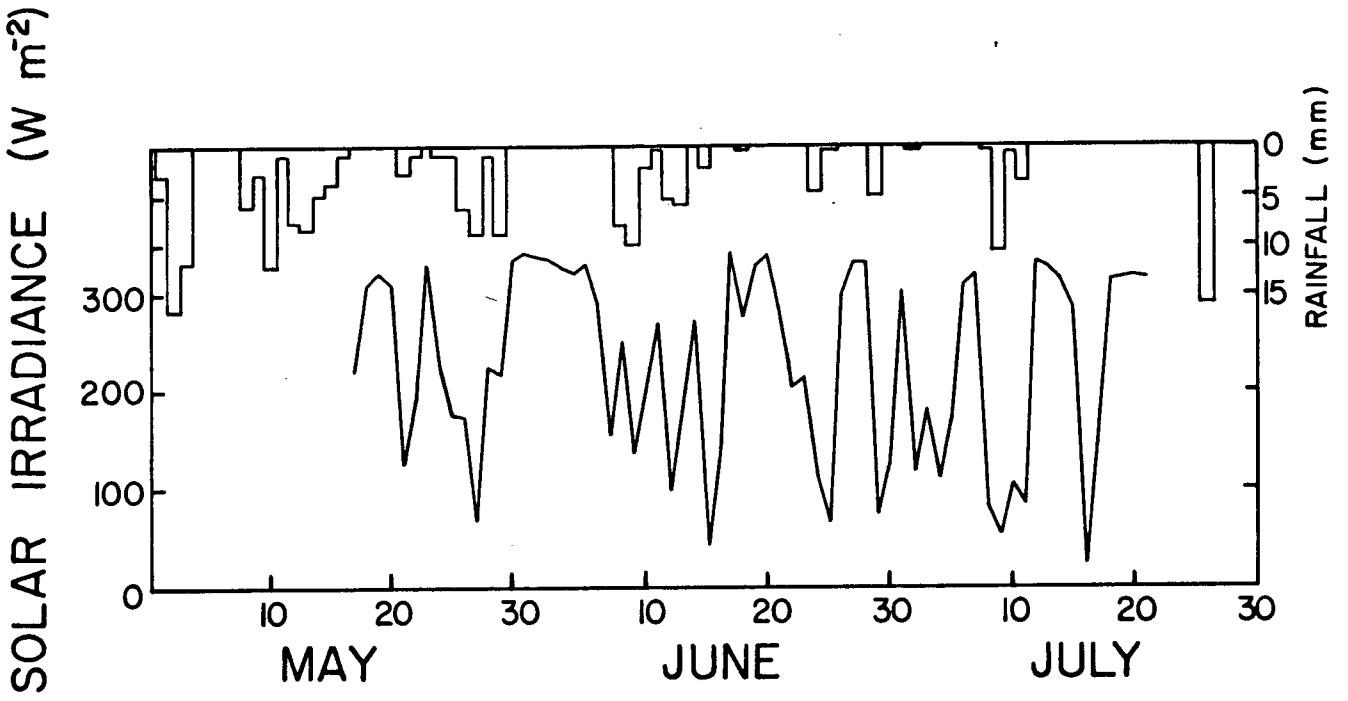

FIGURE 1.1: Total daily precipitation measured at Agassiz in May, June, and July, 1978 and 24-hour average solar irradiance measured during the study.

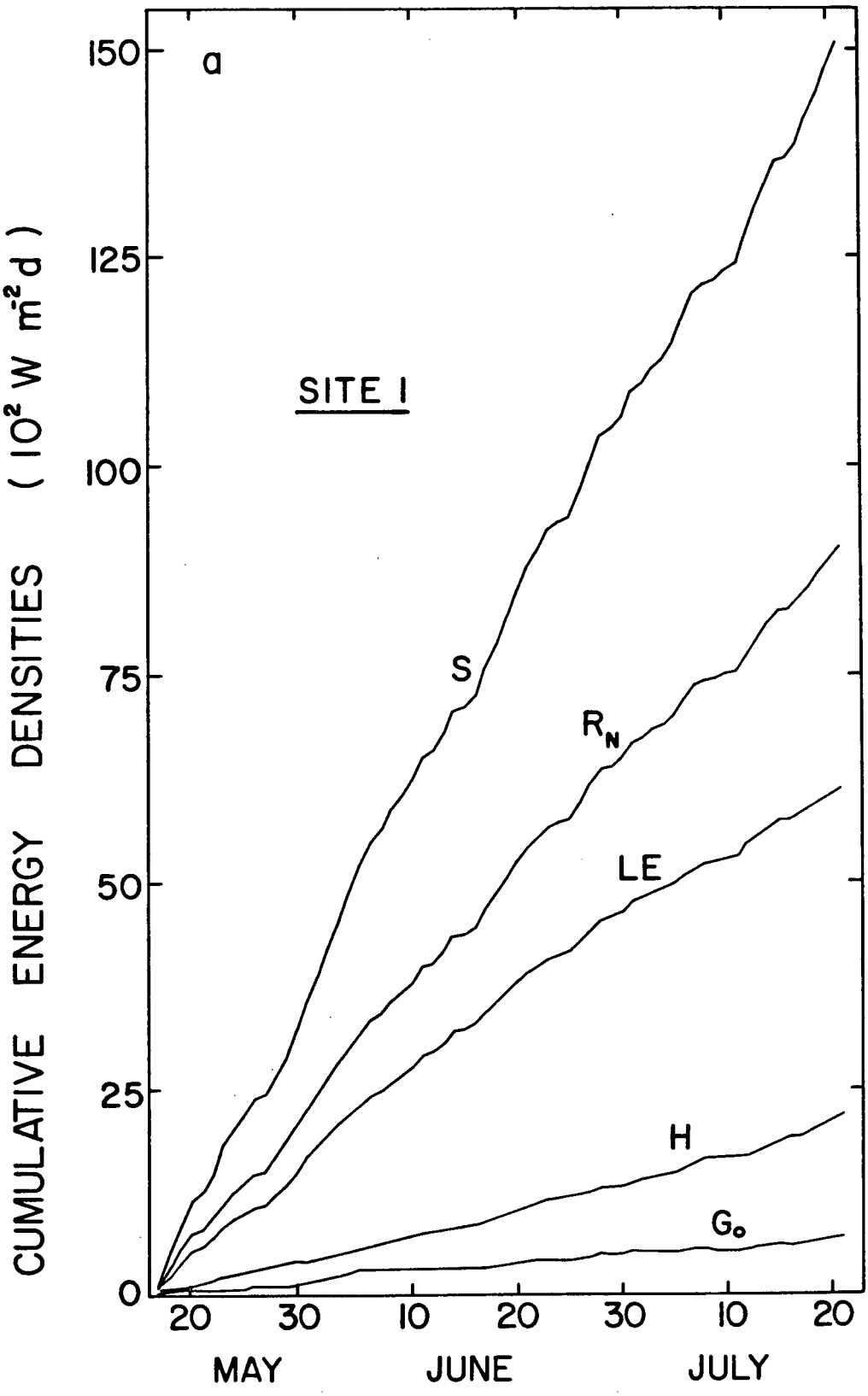

FIGURE 1.2a: Cumulative 24-hour average energy densities at site 1 for the period May 17 to July 21. May 17 was the first day that all 5 densities shown were measured.

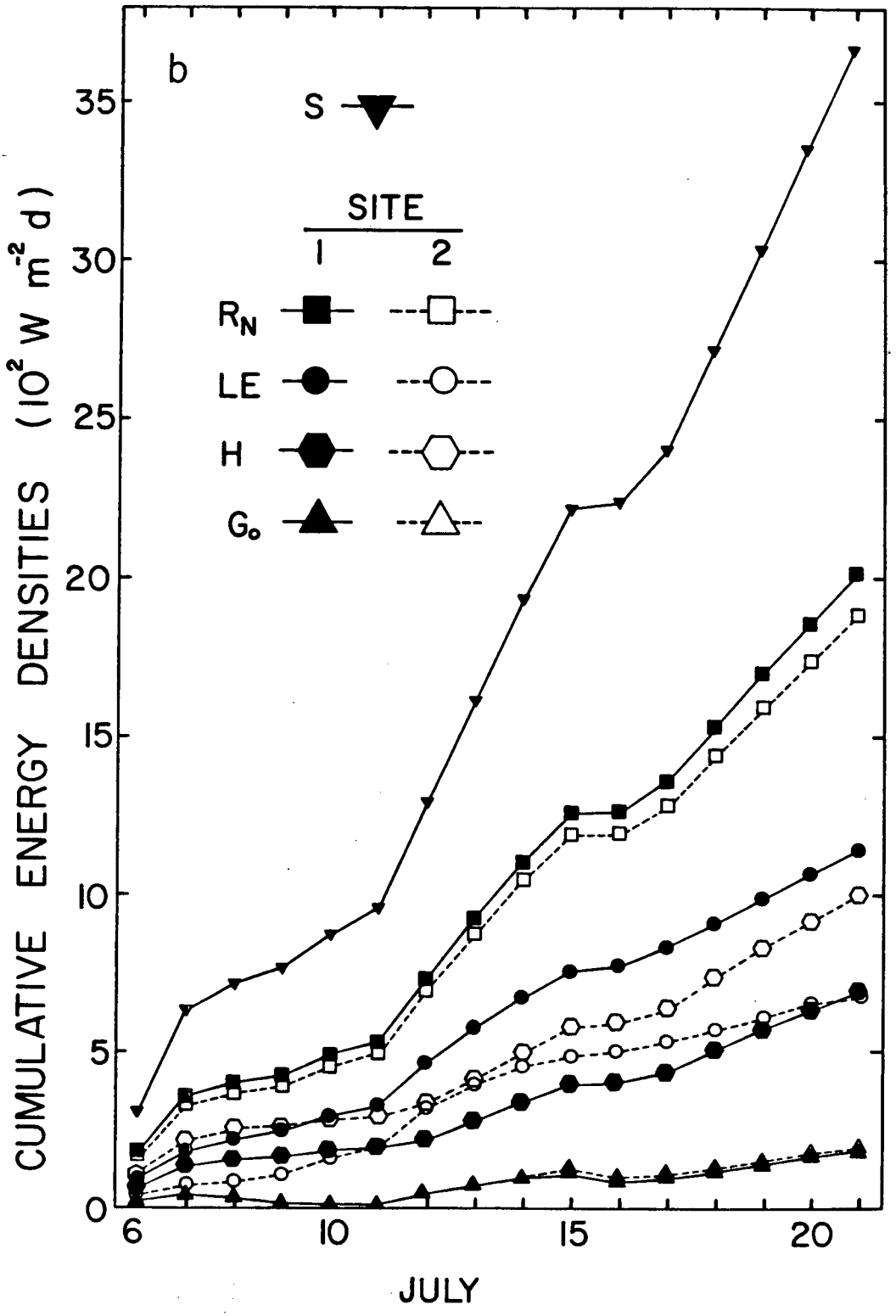

FIGURE 1.2b: As in Figure 1.2a except for both sites 1 and 2 for the period July 6 to 21.

the frequent rainfall events and cloudy days, the hydraulic conductivity characteristics of the packed soil, and the presence of the water table at the 1-2 m depth. However during the last few weeks of the experiment the near surface soil moisture fell to levels such that the overall evaporation at site 1 was considerably less than the potential rate. Consequently the effect of drying on soil heat flux density at site 1 was examined over a range of 24-hour average latent heat flux densities varying from 75 to 180 W m^{-2} on clear days.

Examination of Figure 1.2b shows that disc-harrowing had a marked effect on the energy balance of the soil surface during the site 2 study period. The average latent heat flux density at site 2 was about 60% of that at site 1. This was attributed to changes in moisture retention and hydraulic conductivity in the loosened upper 10 cm of soil. The average net radiation flux density at site 2 was about 7% lower than at site 1, mainly due to higher site 2 daily average surface temperatures, although somewhat higher albedos at this site were also a factor. The average sensible heat flux density at site 2 exceeded that at site 1 by about 44%. Examination of the cumulative soil heat density curves show that the 24-hour average soil heat flux densities at both sites were similar. Hence the higher daily average soil surface temperatures at site 2 noted above were mainly attributed to differences in soil thermal properties. Clear-day 24-hour average latent heat flux densities at site 2 varied from 35 to 130 W m^{-2}. Latent, sensible, and soil heat flux densities represented about 19, 27, and 5% of the solar irradiance and 37, 53, and 10% of the net radiation flux density respectively during the site 2 study period. The corresponding figures for site 1 during this period were 31, 19, 5% and 57, 34, 9% respectively.

B. Soil Physical and Thermal Properties

Measured bulk densities, organic matter fractions, and moisture contents are presented in Table 1.2. The disc-harrowing at site 2 reduced the 0 - 10 cm bulk densities by about 10 - 20 percent. For the densities below 10 cm no systematic differences between the sites were noted. The organic matter fractions, being somewhat higher than those reported for non-cultivated soils of the same series, were consistent with the past history of the field as a well-fertilized site used for horticultural trials. At site 2 the minimum moisture contents measured in the 0 - 9 cm layer were significantly lower than at site 1, although below 9 cm they were similar. This is in agreement with the expected result that the increase in porosity of the near surface soil at site 2 would result in a moisture retention curve that at the wet end has a volumetric moisture content that decreases more rapidly with decreasing (more negative) soil matric potential. Table 1.2 indicates that the maximum moisture contents at site 1 were higher than those at site 2. This reflects the longer study period at site 1. Maximum moisture contents of the layers in the upper 21 cm at site 1 during the site 2 study period were only 0.02 - 0.04 higher than at site 2. The low moisture contents in the 70 - 80 cm layer were due to the coarser textures often found below 50 cm.

The effects of moisture content and porosity on the soil thermal properties are evident in Table 1.3, in which the ranges of volumetric heat capacities and thermal conductivities at both sites are presented. In general, the conductivities are in good agreement with those reported recently in other studies for silt-loam (Riha et al., 1980; Parikh et al., 1979) and loam (Sepaskhah and Boersma, 1979) soils of similar porosities and moisture contents. However the minimum surface values at both sites, and

DEPTHS (cm)		0 - 5	5 - 10	10 - 15	15 - 20	20 - 25	40 - 45	70 - 80
BULK DENSITY ($kg\ m^{-3}$)	SITE 1	990	1072	1128	1128	1210	1070	1237
	SITE 2	880	856	1155	1185	1208	1082	1268
DRY-MASS FRACTION OF ORGANIC MATTER		0.072	0.067	0.063	0.058	0.053	0.033	0.027

DEPTHS (cm)			0-0.5	0-2	2-4	4-6	6-9	9-12	12-15	15-18	18-21	40-45	70-80
DRY-MASS FRACTION OF MOISTURE CONTENT	SITE 1	MAX.	0.39	0.40	0.41	0.41	0.42	0.42	0.42	0.42	0.42	0.45	0.34
	10/05-21/07	MIN.	0.04	0.11	0.24	0.26	0.28	0.29	0.30	0.31	0.32	0.32	0.10
	SITE 2	MAX.	0.31	0.31	0.32	0.32	0.32	0.33	0.33	0.34	0.34	0.36	0.21
	6/07-21/07	MIN.	0.03	0.04	0.17	0.23	0.26	0.28	0.30	0.31	0.32	0.33	0.17

TABLE 1.2: Measured bulk densities and dry-mass fractions of organic matter and moisture content. The maximum and minimum moisture contents represent the range of values observed in the indicated period at each site.

DEPTHS (cm)			0.0	1.0	2.5	5.0	10.0	20.0
SITE 1 10/05-21/07	C ($MJ\ m^{-3}\ °C^{-1}$)	MAX.	2.4	2.4	2.5	2.6	2.8	2.9
		MIN.	1.0	1.2	1.8	1.9	2.2	2.4
	k ($W\ m^{-1}\ °C^{-1}$)	MAX.	0.8	0.8	0.8	0.9	1.0	1.1
		MIN.	0.2	0.5	0.6	0.7	0.8	0.9
SITE 2 6/07-21/07	C ($MJ\ m^{-3}\ °C^{-1}$)	MAX.	1.8	1.8	1.9	1.9	2.5	2.6
		MIN.	0.8	0.8	1.3	1.5	2.3	2.5
	k ($W\ m^{-1}\ °C^{-1}$)	MAX.	0.6	0.6	0.6	0.7	0.9	1.1
		MIN.	0.1	0.2	0.4	0.6	0.8	1.0

TABLE 1.3: The ranges of soil volumetric heat capacities and thermal conductivities at sites 1 and 2 during the indicated periods. The conductivities were calculated from measured nighttime and daytime average soil heat flux densities and temperature gradients using (7). The volumetric heat capacities were calculated from measured bulk densities, organic matter fractions, and moisture contents using (4). Both C and k values are reported to ±0.1 in their respective units.

the 1 cm value at site 2, are somewhat lower than the values reported ($\simeq$ 0.2 - 0.3 W m^{-1} $°C^{-1}$) by the above authors for moisture contents < 0.05. This may have been due to the assumption that no evaporation occurred below the surface at each site, as discussed in Appendix III.

Both early morning and late evening visual observations, as well as albedo data on overcast days, demonstrated that greater rewetting of the soil surface by upward moisture flow occurred at site 1 than at site 2 during periods of low solar irradiance. In calculating the soil heat flux densities, the diurnal variations in C due to this recharge of near-surface moisture were neglected since the required detailed moisture content data was unavailable. Since gravimetric sampling was generally carried out near midday, the magnitudes of the nighttime near-surface soil heat flux densities were probably somewhat underestimated on days with dry soil surface conditions (particularly at site 1). Nevertheless on such days calculated surface thermal conductivities increased from day-time values ~ 0.2 to nighttime values ~ 0.5 W m^{-1} $°C^{-1}$ at site 1 and from ~ 0.1 to ~ 0.2 W m^{-1} °C at site 2. These values were consistent with the greater rewetting that occurred at site 1. Diurnal variations in thermal conductivity for depths below about 2.5 cm for dry soil conditions and at all depths for wet soil conditions were less than about 20%.

Examining the site 1 k and C data in Table 1.3 shows that below about the 5 cm depth, the percentage change in these properties during the site 1 study period was not very great (< 30%) despite the fact that this experiment lasted more than two months. Comparing cumulative evaporation with cumulative precipitation at site 1 for the period May 10 - July 21 shows that the former exceeded the latter by 110 mm, whereas the net change in moisture storage in the topmost 21 cm for this period was about 20-30 mm.

This indicates that considerable upward moisture flow from deep in the profile took place. The above figures suggest a flow rate of as much as 1 - 1.5 mm d^{-1} from the water table.

C. Effects of Tillage

The nighttime, daytime and 24-hour average soil surface heat flux densities and surface temperatures measured at both sites during the site 2 study period are presented in Figures 1.3a and 1.3b respectively. The average daylength during this period was about 16 hours and the only rainfall was ~ 15 mm received on July 8 - 11. During the period July 12-21, the upper layers of soil at both sites dried steadily, except during the overcast interval centered on July 16 during which some rewetting of the surfaces by upward moisture movement occurred.

Figure 1.3a shows that daytime averages of G_o were generally lower and nighttime averages generally higher (less negative) at site 2 than at site 1. The differences were more marked at night, on clear days, and for dry soil conditions. On clear days the differences in both daily maximum and minimum half-hourly values of G_o were ≈ 30-60 W m^{-2}. Furthermore differences in half-hourly values of G_o extended down to depths ~ 10-20 cm. However, 24-hour average values of G_o were similar at both sites, as mentioned in section 1.3-A.

Despite the generally smaller diurnal variations of G_o at site 2 compared with site 1, Figure 1.3b shows that daytime averages of T_o were generally higher and nighttime averages slightly lower at site 2 compared with site 1. In addition, 24-hour averages of T_o at site 2 were generally higher than at site 1. The greatest difference between maximum and minimum values of T_o, which occurred on clear days with the lowest moisture

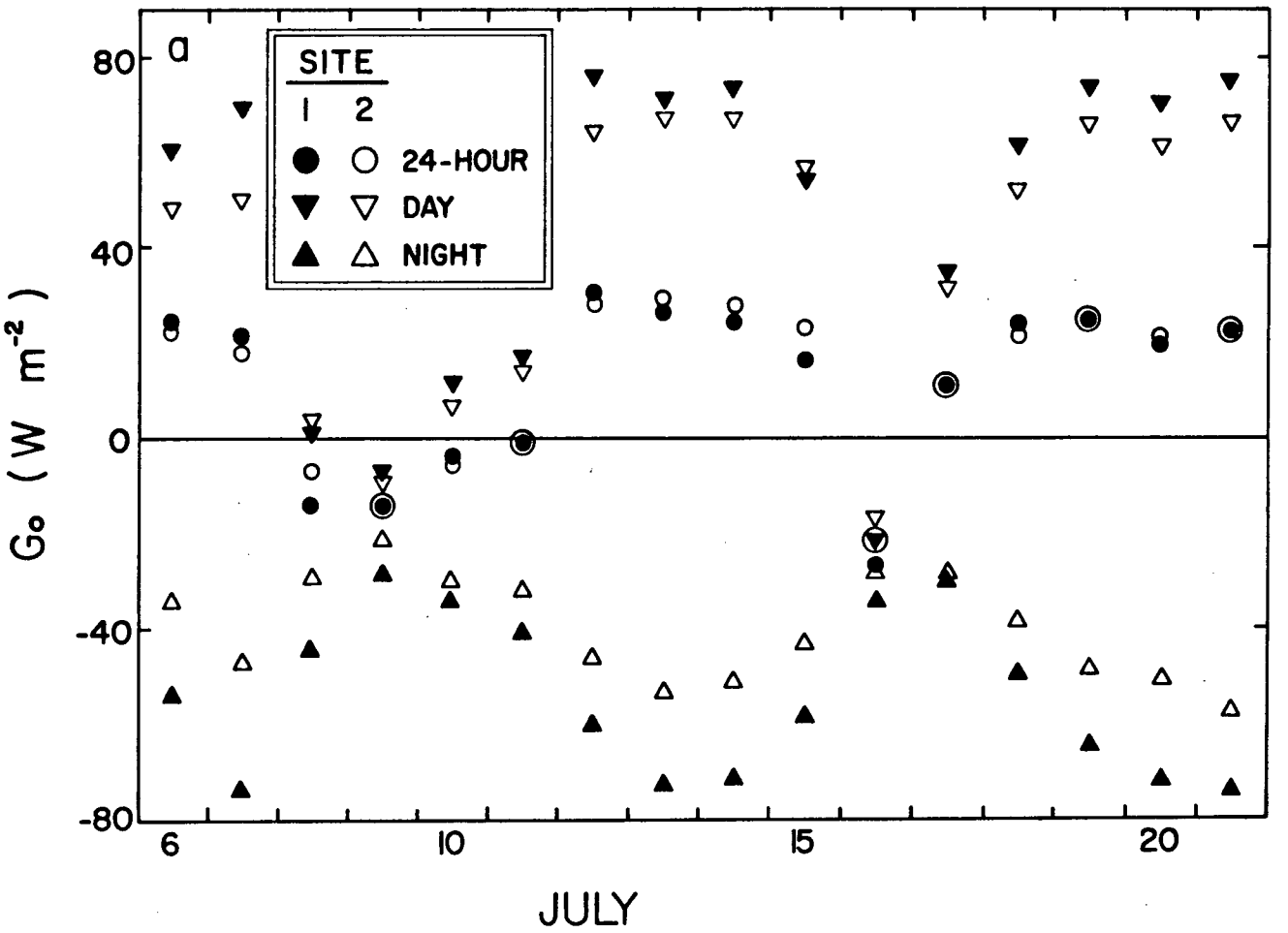

FIGURE 1.3a: Daily (24-hour), daytime, and nighttime average soil surface heat flux densities at sites 1 and 2 during the period July 6 to 21.

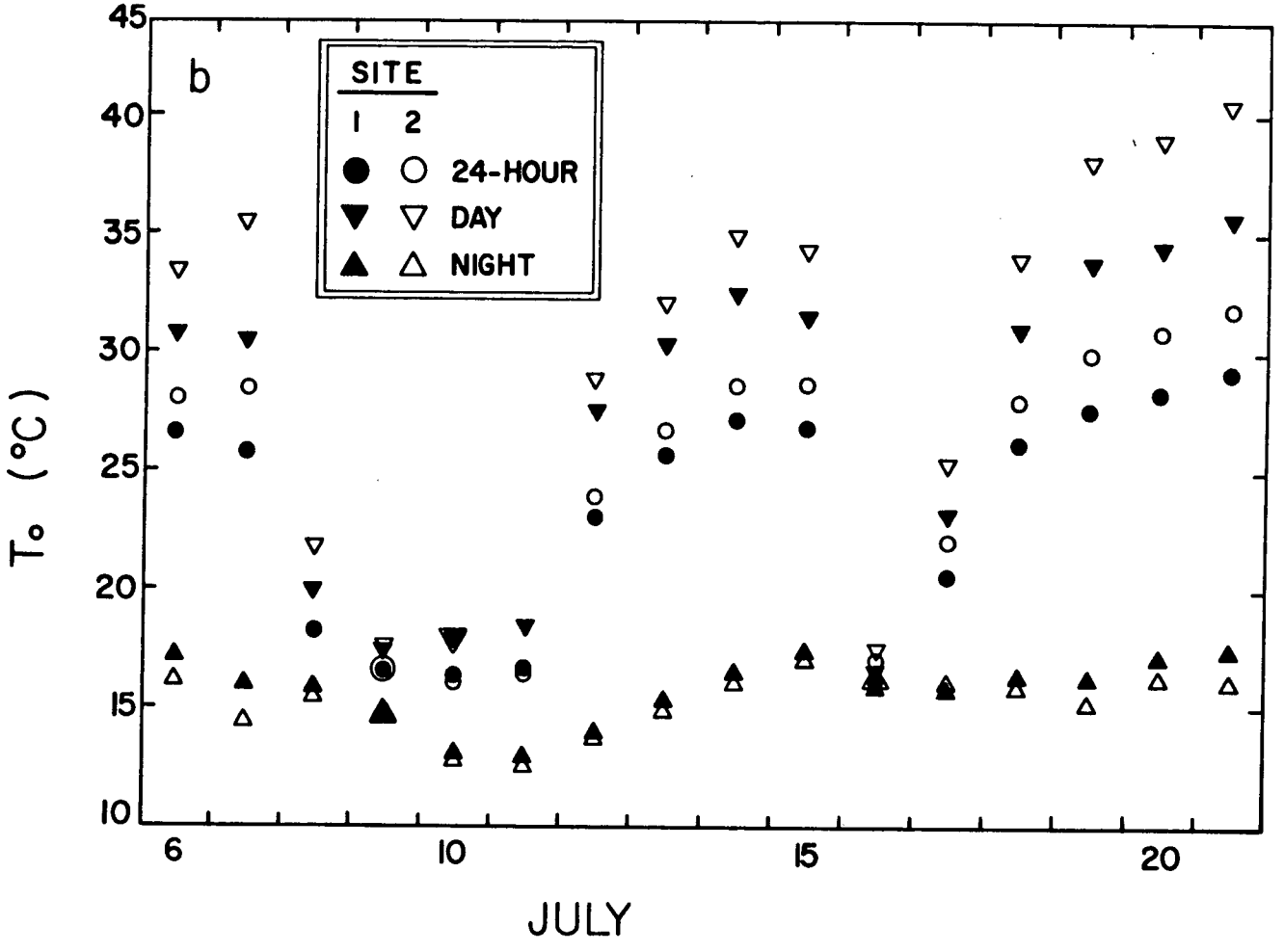

FIGURE 1.3b: As in Figure 1.3a except for soil surface temperatures. The temperatures have been corrected for the overestimate by the thermocouple systems for dry soil conditions (see Chapter 2).

contents (July 19-21), were 29 - 32°C at site 1 and 39 - 42°C at site 2. On July 12, the clear day with the highest soil moisture contents, these differences in T_o were 25.5°C and 29.0°C at sites 1 and 2 respectively. Differences between the soil temperatures of the two sites for depths below 2.5 cm were < 2 - 3°C. For very cloudy and rainy days, especially when the soil surface was wet, as during July 9-11, the differences in surface temperatures and temperatures at depth were small. This indicates that there was little heat accumulation effect from previous days.

It is of interest to note that the effects of disc-harrowing and drying on soil surface heat flux density at Agassiz were similar to those observed in an experiment carried out by the author on a cultivated Lumbum peat soil in the Lower Fraser Valley in spring 1977 (Novak and Black, 1978). In that experiment surface heat flux densities and temperatures were measured (at 2-hour intervals) at both well-drained and poorly-drained sites until plowing, disc-harrowing and planting operations occurred, after which they were measured at the well-drained site only. The tillage operations reduced the bulk density of the 0 - 10 cm layer from 310 to 240 kg m^{-3} at the well-drained site. The 0 - 10 cm bulk density at the poorly-drained site was 265 kg m^{-3} (the higher value at the well-drained site was attributed to shrinkage with drying). Diurnal courses of soil surface heat flux density on two clear days with similar solar irradiance are shown in Figure 1.4. Moisture contents of the 0 - 5 cm surface layer on these days were 2.5, 2.1, and 1.6 kg water/kg dry soil at the poorly-drained, well-drained, and tilled sites respectively. The surface soil heat flux density was not greatly affected by the drying due to drainage. However the diurnal variations of G_o were reduced following the tillage by 30 - 60 W m^{-2}. Estimates of the 24-hour average G_o yielded values in the range

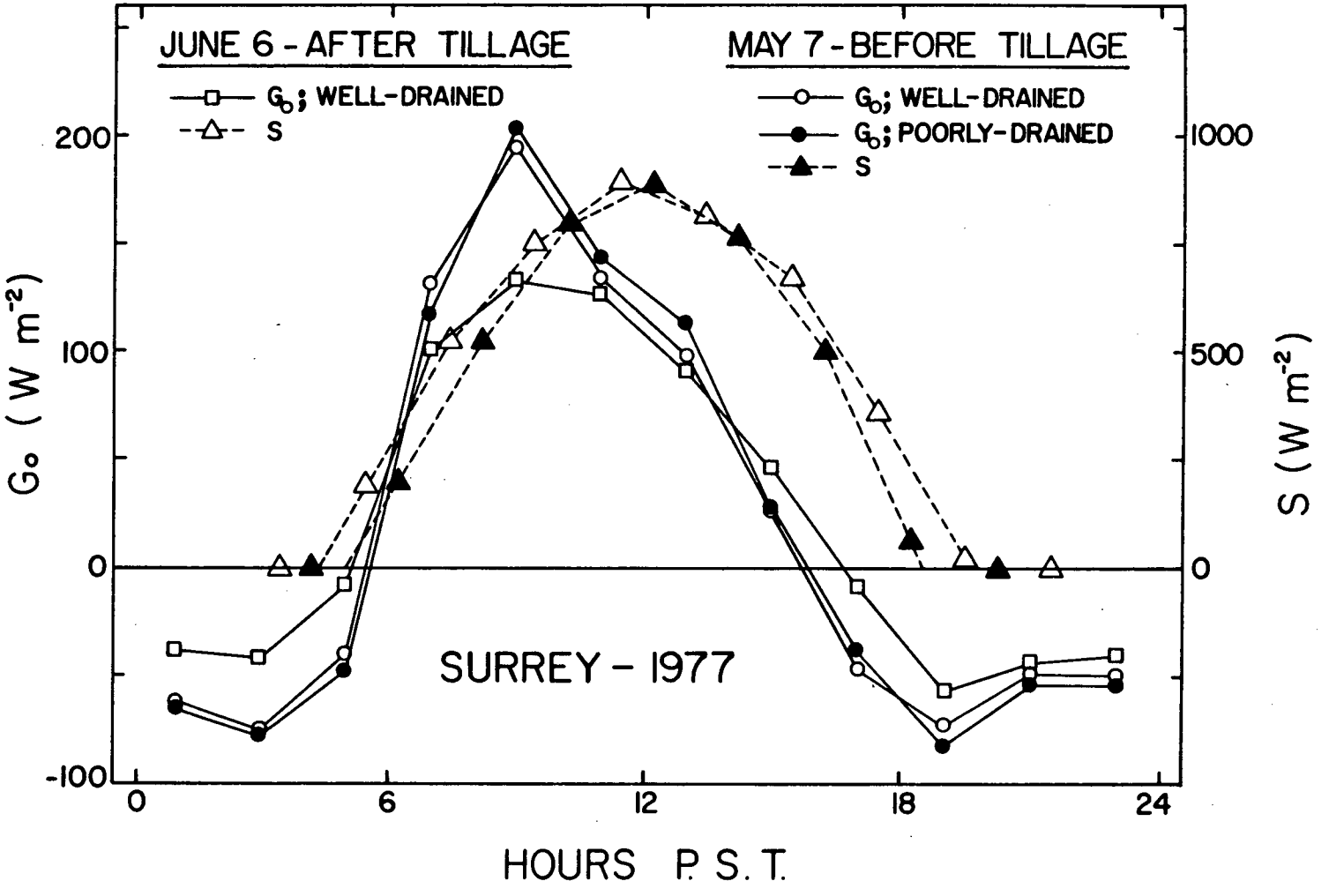

FIGURE 1.4: Diurnal courses of soil surface heat flux density and solar irradiance on a bare lumbum peat soil at Surrey on May 7 and June 6, 1977.

15 - 20 W m^{-2} for all 3 curves. The diurnal variations in surface temperature before the tillage (≈ 23 - 24°C) were similar for both the well-drained and poorly-drained sites. For the well-drained site following the tillage, the variation increased to 27 - 28°C. The reduction in the diurnal variation of G_o and the corresponding increase in that of T_o following the tillage operations were analogous to the results at Agassiz.

D. Diurnal Variations

Half-hourly measurements of the surface energy balance components on selected days are presented in Figure 1.5. The R_N, H, and LE data were all smoothed by taking running averages over 1½ hour intervals (weighted according to 1, 2, 1) since it was felt that the calculated values of G_o had been inherently smoothed to this extent in the null-alignment procedure. On May 31, a clear day, advection of warm, dry air was the maximum observed during the study and soil moisture contents were high. On June 9, typical of a rainy day with highly variable cloud cover, about 40% of the clear-sky solar irradiance was received. July 12 and July 21 were clear days representative of wet (at site 1 not as wet as on May 31) and dry near-surface soil moisture conditions at both sites, as can be seen from the magnitudes of LE. Advection was minimal on these two days.

In both the analyses of Lettau (1951) and van Wijk and de Vries (1966), it was assumed that the diurnal variation about the daily average of each of the surface energy balance components and soil and air temperatures could be represented by a sinusoidal function with a 24-hour period. Figure 1.5 demonstrates that for the energy balance components on the clear days this assumption was a reasonable first-order approximation. One major reason for the departures from sinusoidal behaviour is the shape

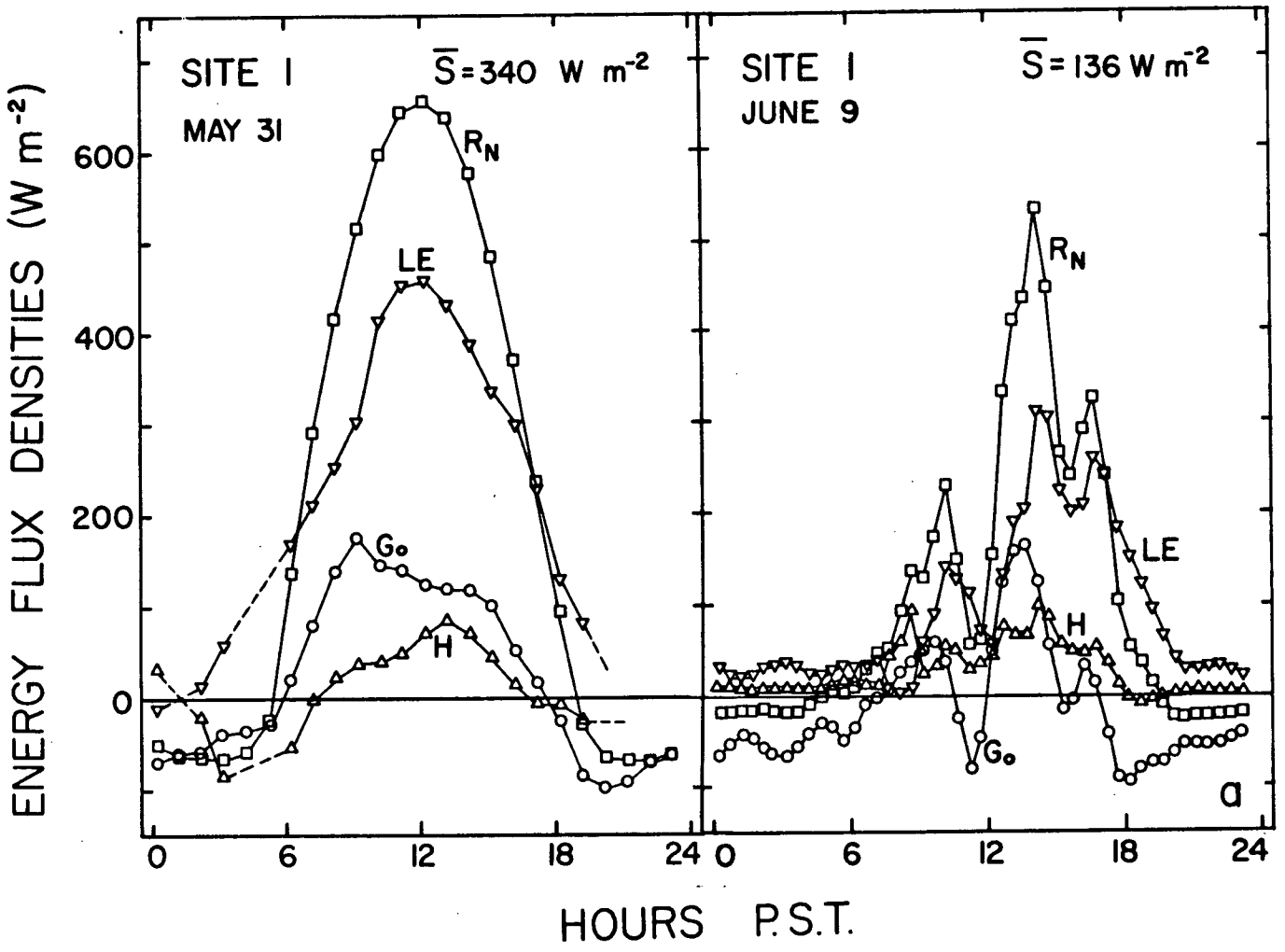

FIGURE 1.5a: Diurnal courses of the surface energy balance components at site 1 on June 9 and May 31. Every half-hour value was plotted for June 9 while for May 31 only the value from the first half-hour of every hour was used. Also indicated is the 24-hour average solar irradiance. The dashed lines indicate $-1.5 < B < -0.5$.

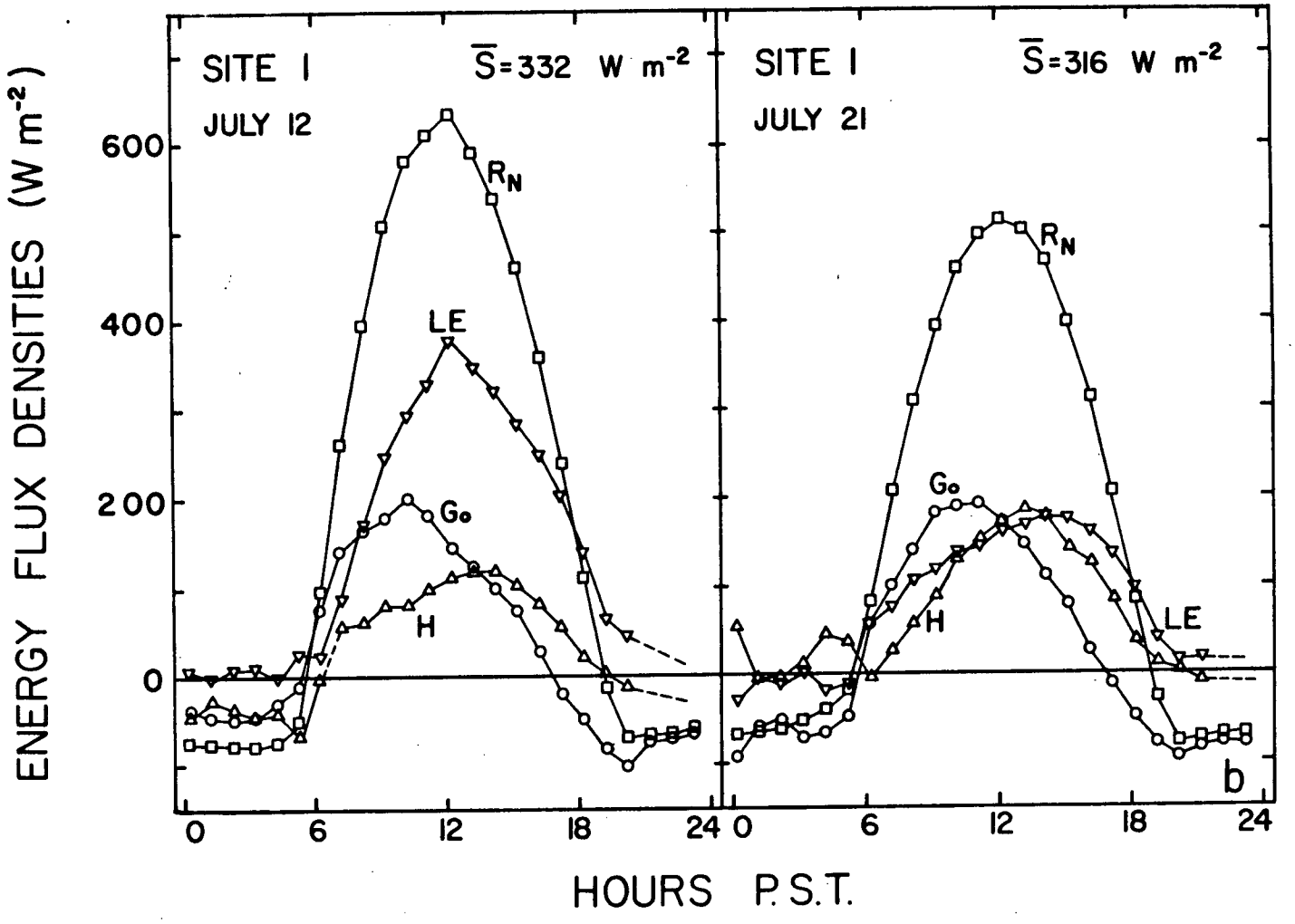

FIGURE 1.5b: As in Figure 1.5a except for July 12 and July 21.

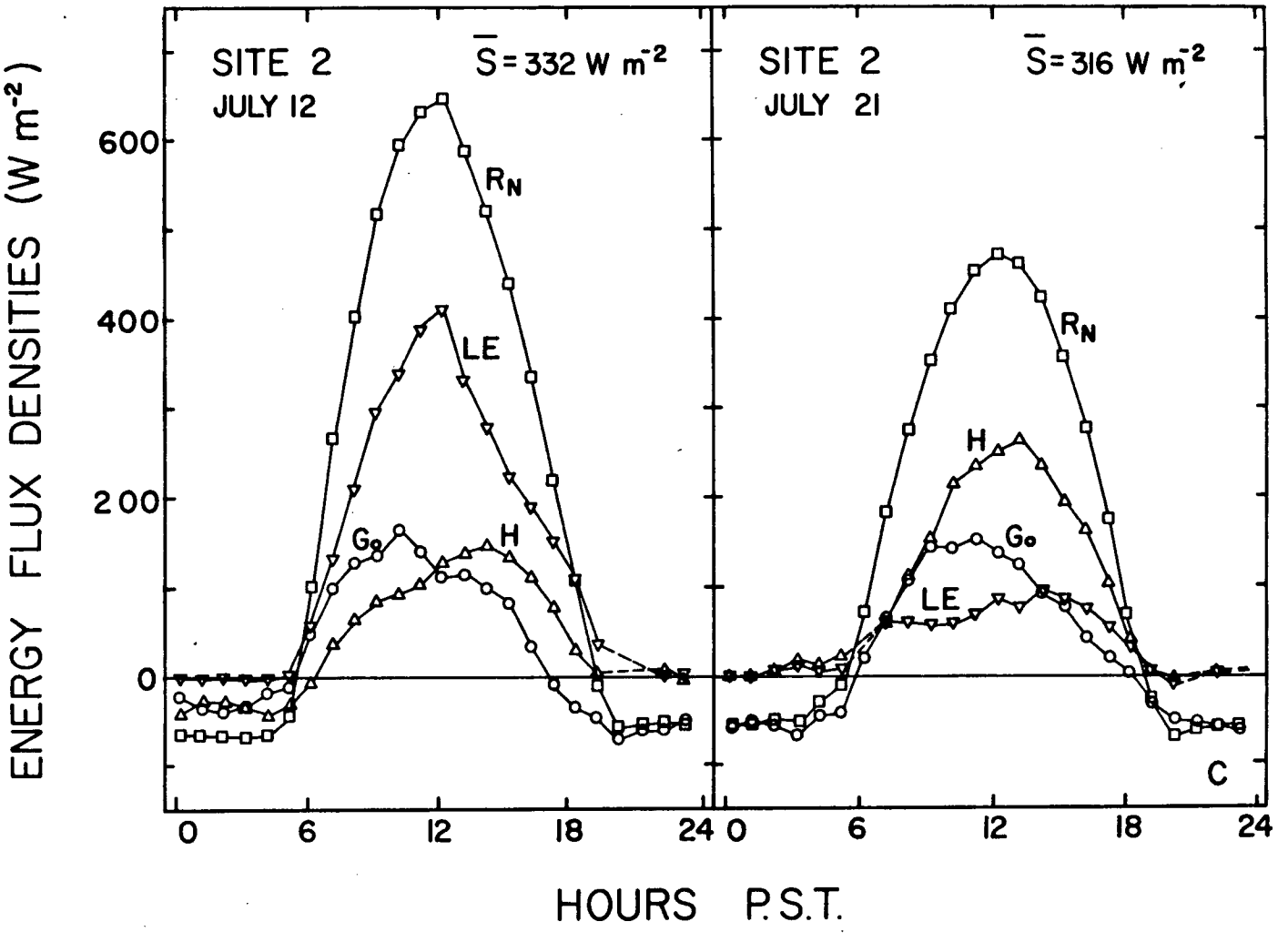

FIGURE 1.5c: As in Figure 1.5a except for site 2 on July 12 and July 21.

of the solar irradiance curve which sharply levels off to zero during the night. It would be expected that at other times of the year and in other latitudes, for which the daylengths are less than those experienced in this study (15.5 - 16.5 hours), the deviations from sinusoidal behaviour would be greater. Examination of the clear-day solar irradiance measurements showed that on any day the differences in the times at which the half-hourly values were equal to the 24-hour average value was 10.5 ± 0.5 hours, compared with 12 hours for exact sinusoidal behaviour. This fact is reflected in all of the surface energy balance components.

The diurnal phase lags of the energy balance components are indicated by the times at which they attain maximum values on clear days. At both sites G_o usually reached a maximum 1 - 3 hours before local solar noon and H and LE usually 0 - 2 hours after local solar noon, while R_N was in phase with the solar irradiance. T_o at both sites lagged G_o by 2-4 hours and H by 0-1 hour. Examination of all of the clear-day data did not reveal any consistent shifts in the phases of any of the components as a result of soil drying. Much of the observed day to day scatter implicit in the indicated ranges appeared to be related to advective effects, as well as errors in identifying the peak due to short-term random meteorological fluctuations.

Priestley (1959), pg. 105 pointed out that if two semi-infinite homogeneous media, initially isothermal, are supplied with energy at their common boundary only, then irrespective of the form of the time variation of this energy flux density, the ratio of their surface heat flux densities would be equal to the ratio of their respective thermal admittances ($\mu = \sqrt{kC}$). Application of this result to the assessment of the partitioning of (R_N - LE) between G_o and H at the soil-atmosphere interface meets with

the following main difficulties: (i) either the soil or the atmosphere is an energy source, such as occurs when either cold or warm air respectively is advected into an area, (ii) the thermal properties of either the soil or the atmosphere vary with depth or height respectively, and (iii) the thermal properties of these media vary with time.

The first difficulty may be avoided, at least on clear days, by using the amplitudes of the variations of the surface energy balance components, as suggested by Lettau (1951). In addition both Lettau's (1951) analysis for the case in which the atmospheric diffusivity increases with height and van Wijk and Derksen's (1966) analysis for layered soils indicate that it is always possible to define an effective thermal admittance for a medium in which both C and k vary with z, by analogy with the homogeneous case. This effective admittance will be a function of the depth or height to which the heat flux density penetrates, the form of the time variation of the heat flux density, and the manner in which the thermal properties vary with z. For harmonic fluctuations, the effective thermal admittances of the soil (μ_s) and the atmosphere (μ_a) are defined as

$$\mu_s = \frac{||G_o||}{||T_o|| \sqrt{\omega}}; \quad \mu_a = \frac{||H||}{||T_o|| \sqrt{\omega}} \tag{8}$$

where ω is the angular frequency of the oscillations and $||\ ||$ indicates the amplitude of the enclosed entity. As to whether it is always possible to define on effective admittance when the thermal properties vary with time is not clear. This should be a less serious problem in the soil for which the relative diurnal variations of k and C are usually much less than the relative diurnal variation of K_a in the atmosphere, which as noted in the introduction can be as much as 1 - 2 orders of magnitude in the

lower 40 m. The theoretical analyses of Poppendick (1952) and Lettau (1954) show that when thermal properties vary sinusoidally then higher harmonics will be produced for sinusoidal surface boundary conditions. Furthermore, if one of G_o, H, or T_o contains such harmonics then evidently (8) could not be used to define an effective admittance.

Atmospheric diffusivities at 70 cm above the surfaces generally varied from < 0.04 $m^2\ s^{-1}$ during the nighttime to about 0.13 - 0.18 $m^2\ s^{-1}$ during the daytime on clear days. This was due to an increase in both free and forced convection, since both windspeeds and lapse rates at this height were usually greater during the daytime. This change in atmospheric diffusivity between daytime and nighttime usually occurred fairly abruptly, as in the results of Staley (1956). The diurnal variations in soil thermal properties have already been discussed in section 1.3-B. Higher harmonics were not noted in any of the clear-day heat flux density or temperature traces, including those at depth in the soil and at the psychrometer levels in the atmosphere. As indicated earlier, the phases of these were relatively unaffected by the tillage and drying. Consequently it was felt that effective admittances calculated using (8) would be meaningful and would reflect both daytime and nighttime values of the thermal properties.

The clear-day values of $||R_N||$, $||G_o||$, $||H||$, and $||T_o||$ from both sites are plotted versus $||LE||$ in Figure 1.6. The amplitudes were calculated by halving the difference between the measured daily maximum and minimum values. Also shown are some of the trajectories defined by the data points in two drying periods, May 30 to June 5 and July 12 to 21. Each point is separated from the previous one (indicated by the solid directed line) by one day. The dashed lines in the latter period indicate that cloudy days intervened on July 15-17. Values of $||S||$ on the clear days varied

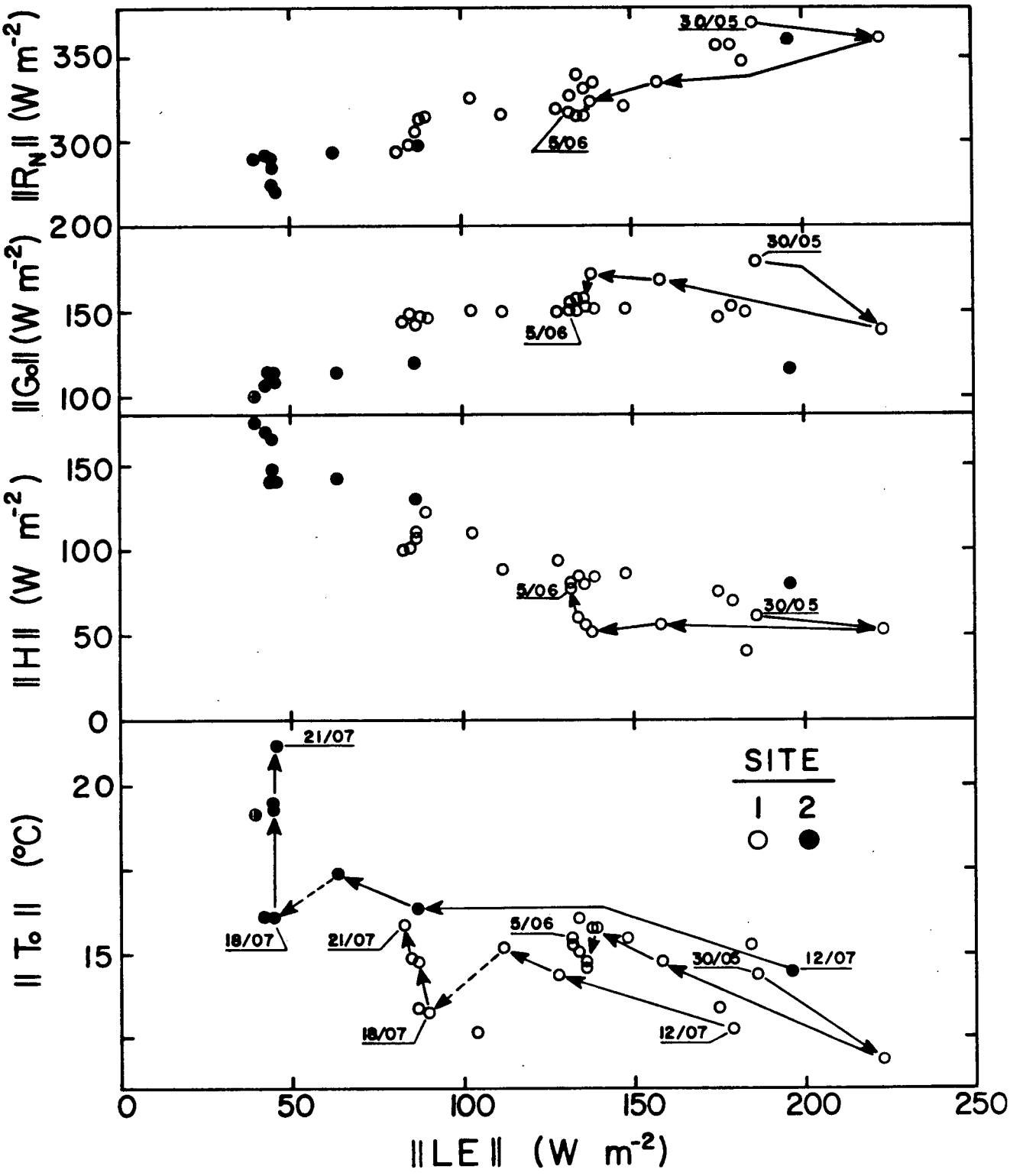

FIGURE 1.6: Plot of the diurnal amplitudes of R_N, G_o, H, and T_o on clear days at both sites versus the diurnal amplitude of LE. Some of the trajectories defined by the data points in the drying periods May 30 to June 5 and July 12 to 21 are indicated.

by < 7%, i.e. from 430 to 460 W m^{-2}. Clear days were defined as those with 24-hour average S > 0.9 S_{max}, where $S_{max} = 340\ W\ m^{-2}$. Note that $||R_N|| \neq ||G_o|| + ||H|| + ||LE||$ because of the phase lags between these components.

Figure 1.6 shows that $||R_N||$ decreased as $||LE||$ decreased as a result of soil drying. The decrease in $||R_N||$ was due to the increase in surface albedo as well as the increase in $||T_o||$ shown. $||G_o||$ at each site remained approximately constant, or perhaps decreased slightly as $||LE||$ decreased. The lower values of $||G_o||$ at site 2 compared with site 1 have already been discussed in section 1.3-C.

Somewhat higher values of $||G_o||$ at site 1 were measured during the May 30 to June 5 period, as shown. The complexity of the relationship between windspeed, warm-air advection, $||LE||$, and $||G_o||$ is indicated by the decrease in $||G_o||$ and increase in $||LE||$ on May 31 compared with May 30, followed by the increase in $||G_o||$ and decrease in $||LE||$ on June 1. The daytime average windspeed on May 31 was 4.1 m s^{-1} (95 cm height) while the daytime average lapse rate (70 cm height) was 0.047 °C m^{-1}. These were the highest and lowest values, respectively, measured during the study.

Figure 1.6 shows that $||H||$ at both sites increased as $||LE||$ decreased. Values of $||T_o||$ also increased as $||LE||$ decreased, particularly at site 2. The trajectories of the two drying periods show that the increase in $||T_o||$ with drying at site 1 was more marked within a given drying period than when all of the points are considered together. This is of importance for remote sensing applications in which either daily evaporation or soil moisture status are calculated from the measured diurnal variations of T_o (Idso et al., 1975b; Idso et al., 1975c).

Effective daily thermal admittances of the soil and atmosphere at both sites, calculated from the clear-day data using (8) with $\omega = \omega_d = 7.27 \times 10^{-5}$ s^{-1} are presented in Table 1.4. The "wet" values shown are averages over the days with $\|LE\| > 175$ W m^{-2} while the "dry" values are averages over the days with $\|LE\| < 100$ W m^{-2}. The indicated ranges of uncertainty were estimated from the variability of the effective admittances calculated on these days. Also shown are effective daily atmospheric diffusivities calculated using $\kappa_a = \mu_a^2 C_a^{-2}$, with the atmospheric heat capacity $C_a = 1.2$ kJ m^{-3} $°C^{-1}$.

The table shows that effective soil admittances at both sites decreased in response to drying, particularly at site 2. This was mainly due to the increase of $\|T_o\|$ with drying already mentioned. At site 1, during the period May 30 to June 5, μ_s steadily decreased with time from a value of 1460 J m^{-2} $°C^{-1}$ $s^{-\frac{1}{2}}$ on May 30 to 1140 J m^{-2} $°C^{-1}$ $s^{-\frac{1}{2}}$ on June 5. The ~ 30% lower admittance at site 2 compared with site 1 for the wet days is perhaps somewhat unexpected since the 0 - 10 cm layer bulk densities differed by only 10 - 20%. This larger difference in μ_s reflected the fact that some surface drying had occurred on these days at both sites (especially at site 2 on July 12) so that the calculated soil admittances were not the maximum possible values. An estimate of the maximum effective soil admittance at site 1 can be made from the maximum values of k and C presented in Table 1.3. Using the 5 cm values at site 1 (C = 2.6 MJ m^{-3} $°C^{-1}$, k = 0.9 W m^{-1} $°C^{-1}$) yields $(\mu_s)_{max}$ = 1530 J m^{-2} $°C^{-1}$ $s^{-\frac{1}{2}}$ at this site and $(\mu_s)_{max}$ = 1300 J m^{-2} $°C^{-1}$ $s^{-\frac{1}{2}}$, i.e. ~ 15% less at site 2. The reason for choosing the 5 cm depth will become clear below.

Effective atmospheric admittances at both sites increased considerably with drying. Since wind regimes were similar on most of the wet and dry days this was mainly attributed to greater atmospheric instability

	WET		DRY	
	SITE 1	SITE 2	SITE 1	SITE 2
SOIL ADMITTANCE - $\mu_{s\,\frac{1}{2}}$ ($J\ m^{-2}\ °C^{-1}\ s^{-\frac{1}{2}}$)	1330 ± 160	940	1190 ± 110	690 ± 100
ATMOSPHERIC ADMITTANCE - $\mu_{a\,\frac{1}{2}}$ ($J\ m^{-2}\ °C^{-1}\ s^{-\frac{1}{2}}$)	520 ± 170	650	880 ± 170	1000 ± 230
ATMOSPHERIC DIFFUSIVITY - κ_a ($m^2\ s^{-1}$)	0.19	0.29	0.54	0.69

TABLE 1.4: Effective daily soil and atmospheric admittances and atmospheric diffusivities calculated on the clear days of maximum and minimum soil moisture content for each site as indicated in the text.

under the resulting stronger daytime lapse rates. The difference in atmospheric admittance of the sites on the dry days was also mostly attributed to this effect. The sites appeared to be of similar surface roughness and daytime lapse rates at site 2 at the 70 cm height were about $1\frac{1}{2}$ times those at site 1 for these days. Direct comparison of the atmospheric admittances of the two sites on the wet days is difficult since for site 1 some of these days occurred before monitoring at site 2 began. On July 12, the only wet clear day at both sites during the site 2 study period, μ_a at site 1 was 640 J m^{-2} $°C^{-1}$ $s^{-\frac{1}{2}}$ which was only 2% less than the site 2 value shown in Table 1.4.

The effective clear-day atmospheric diffusivities were ~ 2-8 times greater than daily average diffusivities at 70 cm above the surfaces (calculated by averaging daytime and nighttime values weighted according to daylength, i.e. 2:1 respectively). Comparison with Staley's (1956) results suggests that the height at which the daily average diffusivity would have equalled the effective diffusivity was between 2 - 20 m. At these heights turbulent exchange is dominated by free convection (Oke, 1978, pg. 49), which further supports the conclusion that the increase in μ_a with tillage and drying was mainly due to greater atmospheric instability. The depth in the soil at which the effective admittance was equal to $\sqrt{kC}$ was calculated on the wet and dry clear days defined above. Both daytime and nighttime values were used in same manner as for κ_a above. The depths calculated were ~ 5 cm at site 1 and ~ 2.5 cm at site 2 for both the wet and the dry days.

Diurnal influences in temperature were observed in the soil to depths ~ 20 - 50 cm at both sites. Diurnal amplitudes of T in the soil at 20 cm on both wet and dry clear days showed little change with drying.

Furthermore it is presumed that diurnal influences were felt to heights ~ 100 - 500 m in the atmosphere (see Section 1.1). Consequently, the depths at which the effective daily admittance of both the soil and the atmosphere were equal to the daily average value of $\sqrt{kC}$ were relatively shallow compared with the depths of which the diurnal influences were felt. This is at variance with the remarks of Priestley (1959), pg. 105 who suggested that it is the admittances at "some distance from the surface, where these are more nearly constant" that exert "the main control of the sharing between the two media". The results suggest that the manner in which the thermal properties vary with depth near the earth's surface significantly affects the partitioning of the total sensible heat (R_N - LE) between the soil and the atmosphere.

E. Daily and Daytime Average Values of G_o

Soil surface heat flux densities from both sites were plotted versus solar irradiance on a 24-hour and daytime average basis as shown in Figures 1.7a and 1.7b, respectively. The data were separated into the indicated ranges according to the coefficient, a_{PT}, defined by Priestley and Taylor (1972) using the equation:

$$LE = a_{PT}\frac{s_v}{s_v + \gamma_v}(R_N - G_o) \qquad (9)$$

where s_v is the slope of the saturated vapour pressure function. The values of a_{PT} used were calculated on a 24-hour average basis with the highest value measured being 1.41. Evaporation was considered to be energy-limited for $a_{PT} > 1.15$ and soil-limited below this value. The lowest values of a_{PT} measured were 0.73 at site 1 and 0.32 at site 2. The coefficient a_{PT} was used since soil moisture contents were not measured every day.

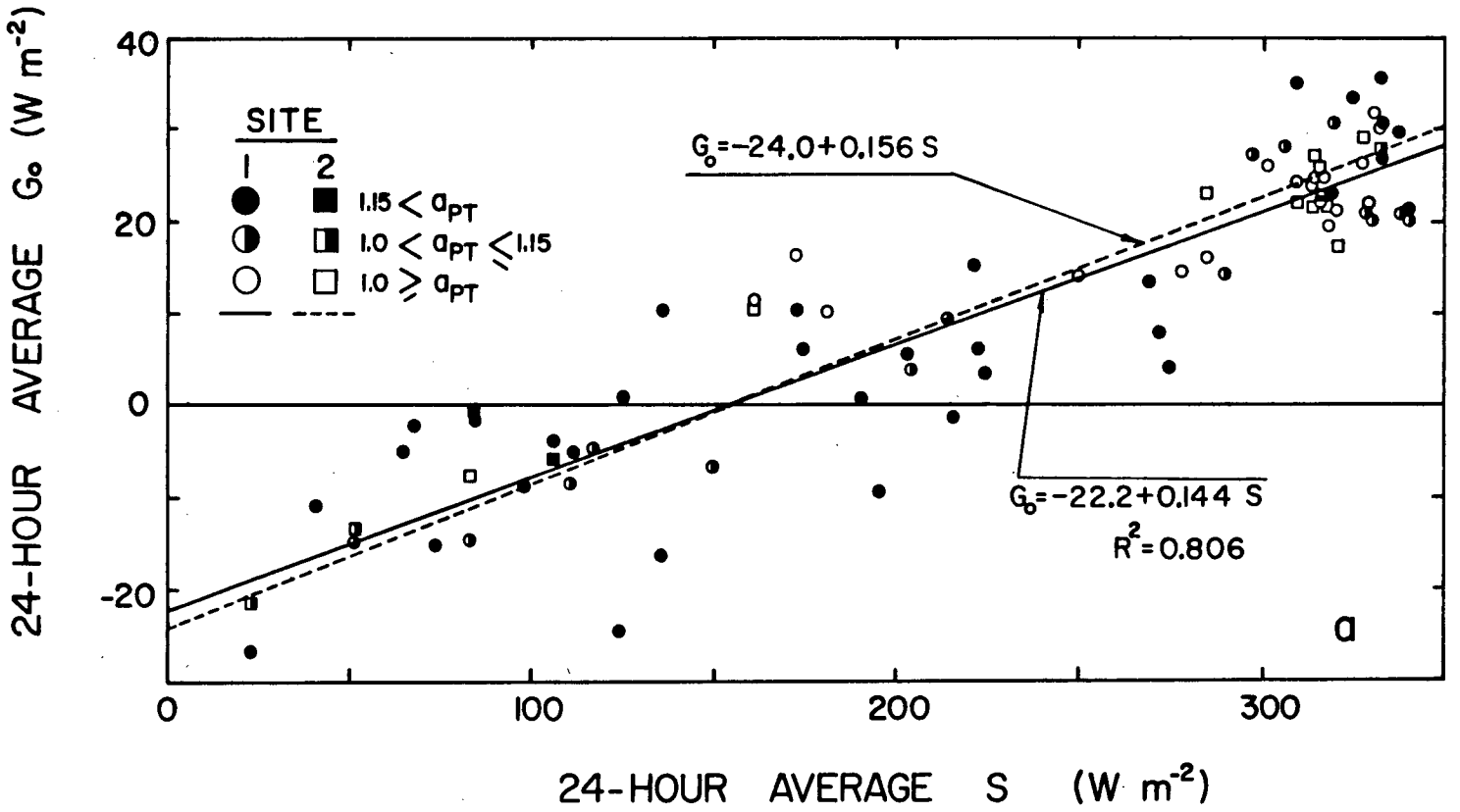

FIGURE 1.7a: Plot of daily average soil surface heat flux density versus daily average solar irradiance at both sites. The data have been separated into ranges according to the 24-hour average value of a_{PT}. The straight lines have been fit to the data as described in the text. The lines differ by a factor of 1.08 (site 2: site 1), which was not considered significant (see Figure 1.3a).

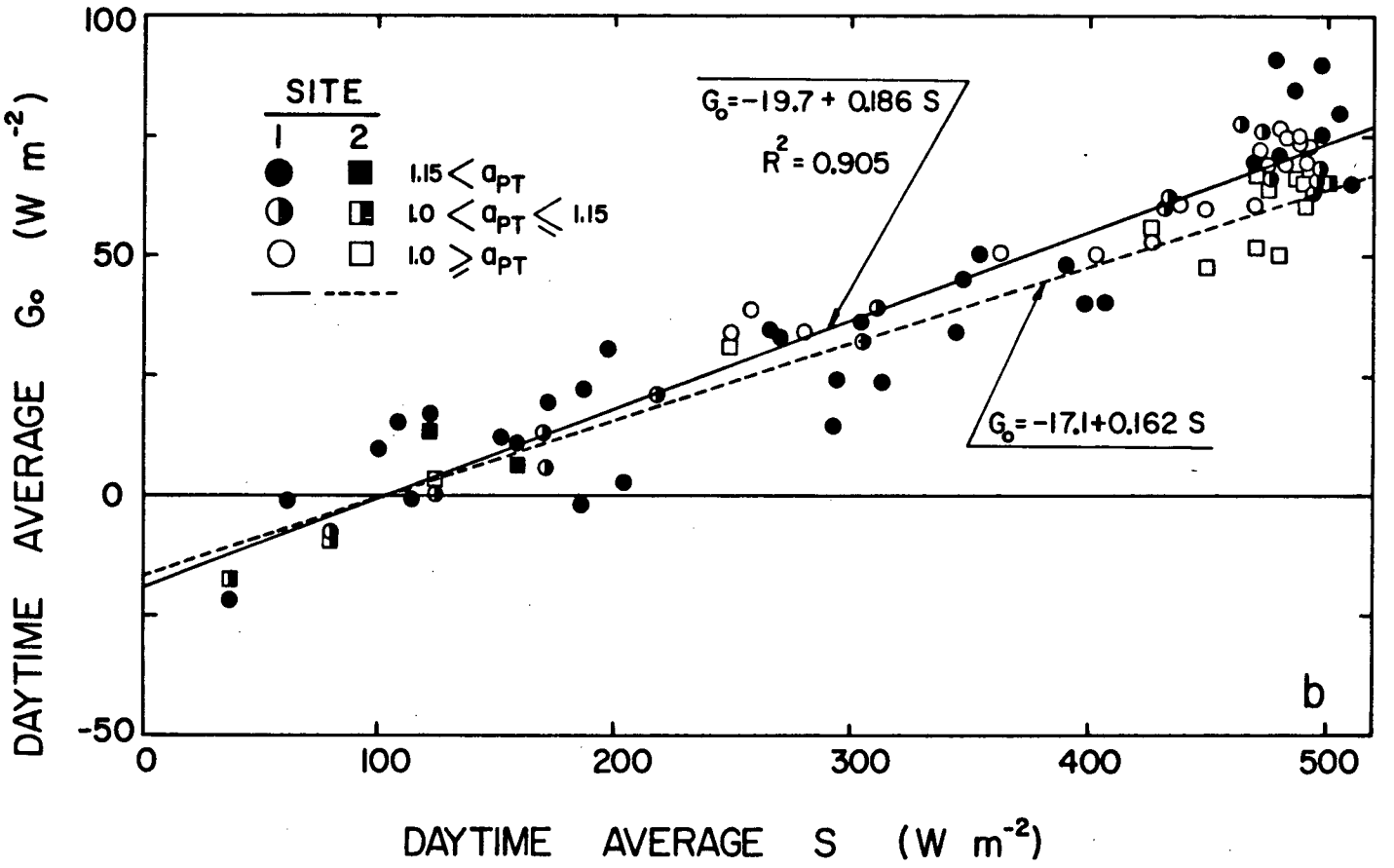

FIGURE 1.7b: As in Figure 1.7a except for daytime averages. The lines differ by a factor of 0.87 (site 2: site 1) which was considered significant (see Figure 1.3a).

Straight lines were fit by the standard least squares regression technique to the site 1 data in each figure, as indicated. The linear equations shown describing the site 2 data were found by multiplying the site 1 relationships by the ratio of the average site 2 surface heat flux density to the average site 1 surface heat flux density during the site 2 study period. This procedure was done for site 2 because of the smaller data set generated at this site and because of the scatter inherent in both sets of data.

The considerable scatter in Figure 1.7a is not unexpected since the 24-hour average value of G_o is equal to the relatively small difference between large positive daytime and negative nighttime flux densities. Relatively small percentage differences in either daytime or nighttime average soil heat flux densities on days of similar solar irradiance can lead to large percentage differences in the 24-hour average G_o. A 10 - 20% difference in the daytime average on clear days resulted in a 20 - 40% difference in 24-hour average G_o. Factors such as rainfall, nighttime cloud cover, sensible heat advection, and windspeed, as well as measurement difficulties, especially those associated with the sparseness of the gravimetric data set used to calculate soil heat capacities, contributed to the scatter. The reduction in scatter for daytime averages is shown in Figure 1.7b. Most of the scatter in this figure for the highest radiation days was due to the effects of advection and windspeed, both of which reached maximum observed levels on a few of the clear days (May 30 - June 3).

Both figures show that to within the scatter in each, the functional dependencies of G_o on S at each site were independent of whether evaporation was energy or soil-limited. This was not true for relationships between G_o and R_N (Figure 1.8) which were dependent upon a_{PT} due to the

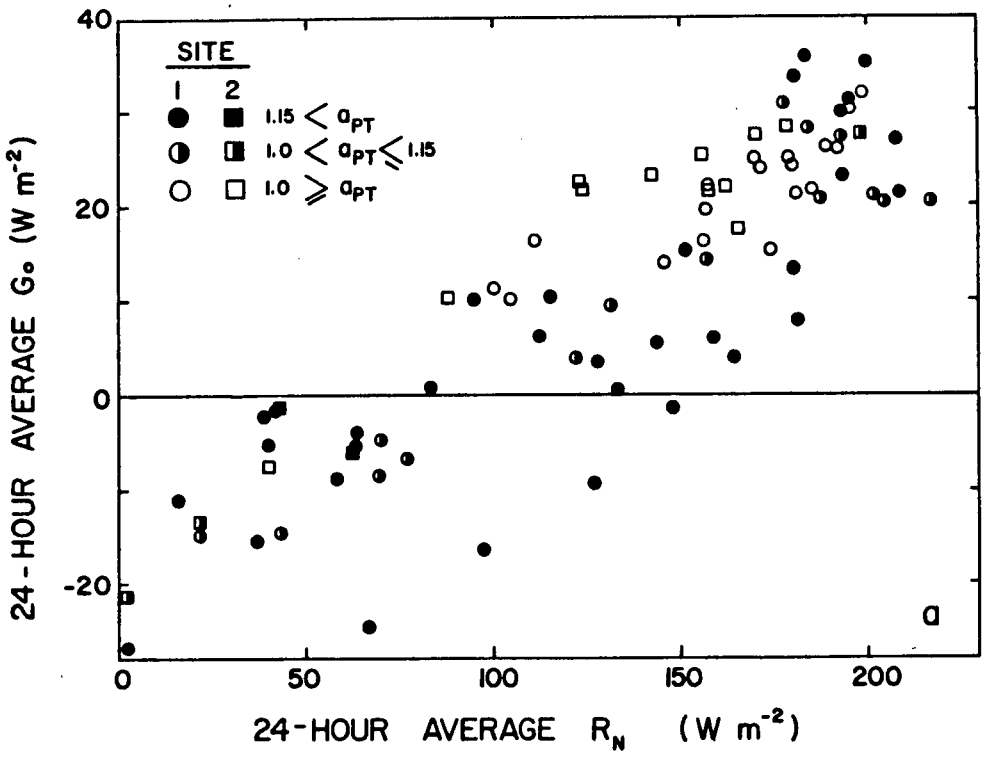

FIGURE 1.8a: Plot of daily average soil surface heat flux density versus daily average net radiation flux density at both sites. The data have been separated into ranges according to the 24-hour average value of a_{PT}.

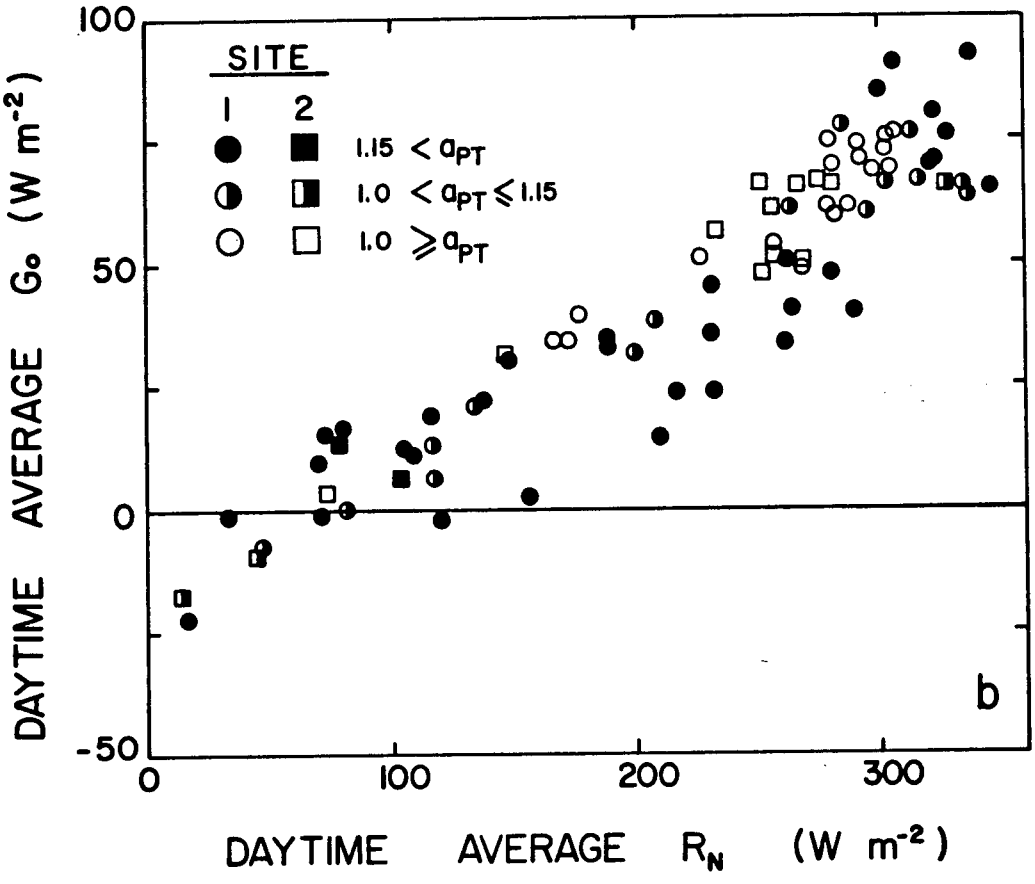

FIGURE 1.8b: As in Figure 1.8a except for daytime averages.

changes in albedo and surface temperature as the soil dried. Furthermore, the relationship between 24-hour average values of G_o and S was not site specific, although that between daytime values of these variables was. The values for $a_{PT} < 1.0$ in Figure 1.8b suggest that the relationship between daytime average values of G_o, R_N, and a_{PT} may not be quite as site specific as that between daytime average values of G_o and S.

Figure 1.7a demonstrates that below about 155 ± 50 W m^{-2} of solar irradiance, 24-hour average soil surface heat flux densities were negative and the soil was a net source in the daily surface energy balance. Similar remarks apply to the daytime average results in Figure 1.7b, for which the corresponding value of the daytime average solar irradiance was 105 ± 20 W m^{-2}. It is of interest to note that a monthly average S of 155 W m^{-2} occurs at about the beginning of April and in the middle of September at Vancouver (Hay, 1979), located 90 km west of Agassiz and the nearest station at which S is monitored routinely. Ouellet et al. (1975) used a multiple regression model requiring long-term local measurements of standard climatic variables to generate mean monthly soil temperatures under a short-grass surface at Agassiz. Their results show that the temperature difference between 1 and 10 cm, the two shallowest depths reported, changes sign at about the middle of March and the end of September, in good agreement with the dates above. This suggests that the relationships between 24-hour average G_o and S found in the spring and early summer for the two bare sites may have some applicability during other seasons.

F. Nighttime Average Values of G_o

Nighttime average soil surface heat flux densities are plotted versus nighttime average net radiation in Figure 1.9a and versus the daytime average cloudiness ratio, S/S_{max}, in Figure 1.9b. The data have been

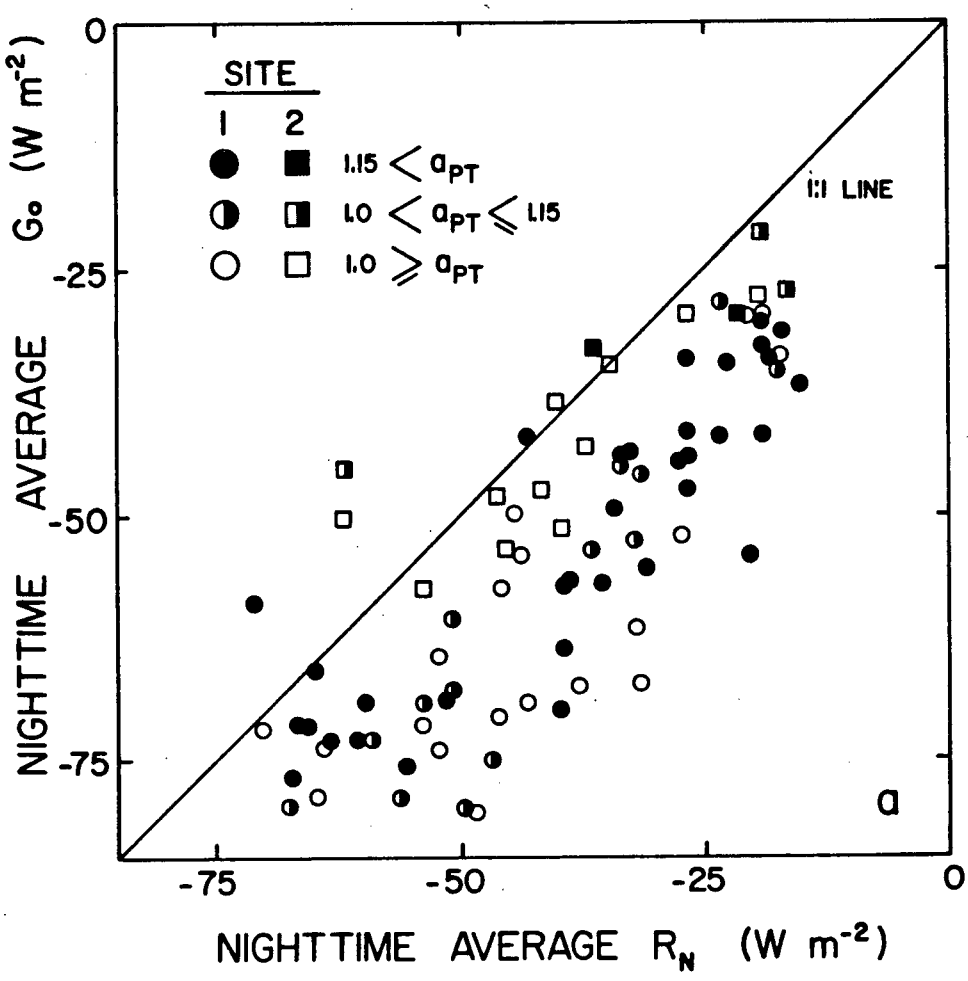

FIGURE 1.9a: Plot of nighttime average soil surface heat flux density versus nighttime average net radiation at both sites. The data have been separated into ranges according to the 24-hour average value of a_{PT}.

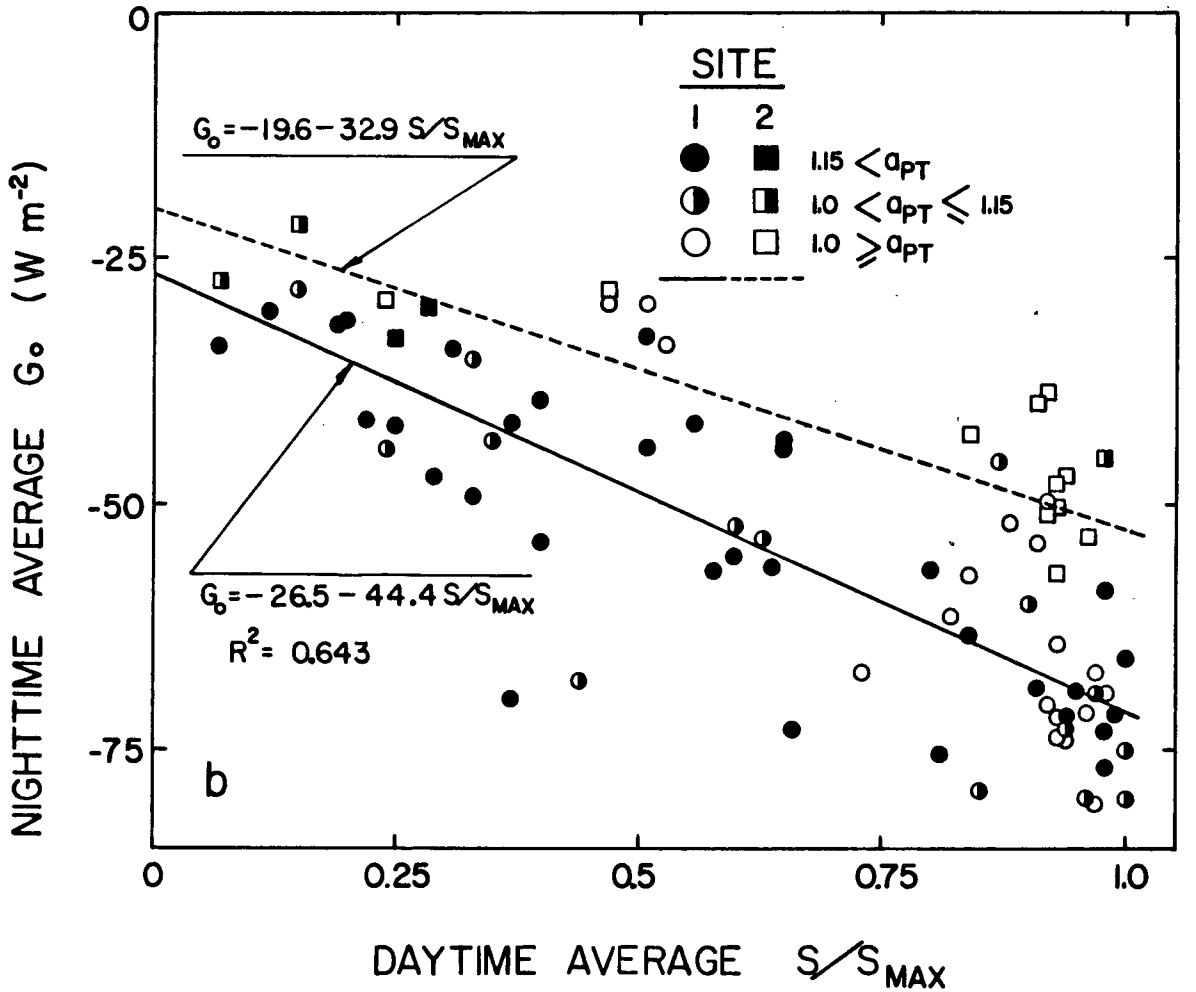

FIGURE 1.9b: Plot of nighttime average soil surface heat flux density versus daytime cloudiness ratio, S/S_{max}, at both sites. The data have been separated into ranges according to the 24-hour average value of a_{PT}. The straight lines have been fit to the data as described in the text. The lines differ by a factor of 0.74 (site 2: site 1) which was considered significant (see Figure 1.3a).

separated into ranges according to the coefficient a_{PT} (24-hour basis) as done previously. The straight lines shown in Figure 1.9b were fit to the data in the same manner as for the lines in Figures 1.7a and 1.7b.

Figure 1.9a demonstrates that at site 1 nighttime G_o was usually more negative than nighttime R_N, while at site 2 they were similar in magnitude. Most of this difference at site 1 was accounted for by evaporation. Since nighttime evaporation rates were considerably less than daytime rates, nighttime evaporation (at both sites) was considered to be energy-limited. Percent errors in nighttime measurements of latent and sensible heat flux density by the Bowen ratio method were considerably larger than for daytime measurements. This was mainly due to the smaller magnitudes of available energy flux density ($R_N - G_o$) and vertical temperature differences, Bowen ratios near -1 (measurements with $-1.5 < B < -0.5$ were neglected), and perhaps significant longwave radiation flux divergence (Oke, 1970). At site 1 the measured nighttime evaporation usually contributed about 5 - 10 percent of the daily total evaporation and only about 20% of the nights were characterized by significant sensible heat advection. The measurements appear to be consistent in that atmospheric diffusivities calculated from nighttime average latent heat flux densities and vapour pressure gradients were usually of the right order of magnitude (< 0.04 m^2 s^{-1} at 70 cm height) and positive in sign.

At site 2, however, calculated atmospheric diffusivities at night were often negative for clear-sky, dry-soil conditions, although for cloudy, wet-soil conditions they were positive and evaporation rates were of the same order of magnitude as at site 1. Vapour pressure gradients above site 2 for the clear-sky, dry-soil conditions were positive, which suggests that condensation occurred on these nights. As well temperature inversions

at site 2 were 2 - 5 times greater than at site 1 on these nights, consistent with the lower measured site 2 surface temperatures. The similar magnitudes of R_N and G_o as well as the fact that both temperature and vapour pressure gradients were of the same sign, demonstrate that both H and LE at site 2 on these nights were small compared with R_N and G_o and contributed insignificantly to daily totals.

Except for the few strongly advective nights, the soil was the major energy source in the nighttime surface energy balance. The disc-harrowing altered this surface energy balance mainly by reducing the energy that could be supplied to the surface from within the soil. This reduction was due to the differences in near-surface thermal properties of the soil at the two sites. While the soil was the major energy source at night, the major "driving force" for the flux densities was R_N. The lower nighttime surface temperatures at site 2 (1 - 2°C) resulted in less negative values of R_N (5 - 10 W m^{-2}) at this site.

Figure 1.9b shows that nighttime average values of G_o at each site could be expressed reasonably well as a linear function of a cloudiness ratio based upon the fraction of solar irradiance received during the daytime. This function was site specific. This suggests that nighttime cloud cover at Agassiz was well correlated with daytime cloudiness. Both Figures 1.9a and 1.9b show that near-surface soil moisture levels at both sites, expressed through the coefficient a_{PT}, had little effect on the relationships between G_o and R_N or S/S_{max}. This is not surprising in view of the considerable moisture movement to the surface that occurred at night at site 1, and the rapid surface drying and relatively little rewetting that occurred at site 2, i.e. site 1 remained relatively wet at night, and site 2 relatively dry. It may be that the relationship between nighttime G_o and

daytime cloudiness ratio S/S_{max} is applicable during other seasons. In that case the value of S_{max} appropriate to the time of year should be used.

1.4 Conclusions

Disc-harrowing to a depth of 10 cm significantly altered both the daytime and nighttime surface energy balances of a bare culti-packed soil. Evaporation after disc-harrowing was reduced on average by about 40% and net radiation by about 7% during a 16 day almost-rainless period in July.

Bulk densities and moisture contents in the upper 10 cm of soil were reduced after disc-harrowing. This resulted in lower values of volumetric heat capacity and thermal conductivity in this layer.

Neither the disc-harrowing nor the drying of the soil surface dramatically altered the 24-hour average value of G_o on days of similar solar irradiance. However clear-day diurnal amplitudes of G_o were reduced by about 20 - 25% by the disc-harrowing and only slightly, if at all, by the surface drying. These results were similar to those found by the author in a field study of heat transfer in an organic soil.

Daily average near-surface soil temperatures, as well as their diurnal amplitudes were greater following the disc-harrowing. Surface drying resulted in an increase in the diurnal amplitudes of near-surface soil temperatures, particularly after the disc-harrowing. In view of the variation of G_o with tillage and drying, these differences in temperature were attributable to the reductions in k and C in the upper layer of soil.

Effective daily soil admittance decreased and effective daily atmospheric admittance increased after disc-harrowing and drying. The effect on atmospheric admittance was attributed to greater atmospheric instability under the resulting stronger lapse rates. The effective daily admittance of each medium was dependent upon the thermal properties at

depths that were relatively shallow compared with the depth to which diurnal influences were felt.

Relationships between either 24-hour or daytime average values of G_o and S were not altered by surface drying. However those between G_o and R_N were affected. For daytime averages the relationship between G_o and S was altered by disc-harrowing, while that between G_o and R_N appeared to be less affected. For days on which S was less than about half the maximum observed value, daily average values of G_o were negative.

Nighttime average values of G_o could be related to the cloudiness ratio, S/S_{max}. This relationship was altered by the disc-harrowing, but not by surface drying. Before the disc-harrowing the value of nighttime G_o was generally more negative than that of nighttime R_N. After the disc-harrowing they were similar.

1.5 Literature Cited

Allmaras, R.R., E.A. Hallauer, W.W. Nelson, and S.D. Evans, Surface energy balance and soil thermal property modifications by tillage-induced soil structure, Minn. Agric. Exp. Stn. Tech. Bull. 306, 1977.

Black, T.A., and K.G. McNaughton, Psychrometric apparatus for Bowen-ratio determination over forests, Boundary-Layer Meteorol., 2, 246-254, 1971.

Carslaw, H.S., and J.C. Jaeger, Conduction of Heat in Solids, 2nd ed., Oxford University Press, London, 1959.

de Vries, D.A., On the integration of the heat-conduction equation with periodic variation of temperature, J. Meteorol., 14, 71-76, 1957.

de Vries, D.A., Heat transfer in soils, In: Heat and Mass Transfer in the Biosphere, Part 1 - Transfer Processes in the Plant Environment, D.A. de Vries and N.H. Afgan, Eds., Scripta Book Co., John Wiley and Sons, New York, pp. 5-28, 1975.

Dyer, A.J., The turbulent transport of heat and water vapour in an unstable atmosphere, Quart. J. Roy. Meteorol. Soc., 93, 501-508, 1967.

Fuchs, M., and A. Hadas, The heat flux density in a non-homogeneous bare loessial, soil, Boundary-Layer Meteorol., 3, 191-200, 1972.

Fuchs, M., and C.B. Tanner, Calibration and field test of soil heat flux plates, Soil Sci. Soc. Amer. Proc., 32, 326-328, 1968.

Fuchs, M., and C.B. Tanner, Error analysis of Bowen ratio measured by differential psychrometry, Agric. Meteorol., 7, 329-334, 1970.

Hanks, R.J., D.D. Austin, and W.T. Ondrechen, Soil temperature estimation by a numerical method, Soil Sci. Soc. Amer. Proc., 35, 665-667, 1971.

Hay, J.E., An analysis of solar radiation data for British Columbia, RAB Bulletin 14, Assessment and Planning Division, Victoria, B.C., 1979.

Hay, J.E., and Oke, T.R., The climate of Vancouver, B.C. Geographical Series, 23, 1976.

Idso, S.B., J.K. Aase, and R.D. Jackson, Net radiation - soil heat flux relations as influenced by soil water content variations, Boundary-Layer Meteorol., 9, 113-122, 1975a.

Idso, S.B., R.D. Jackson, and R.J. Reginato, Estimating evaporation: A technique adaptable to remote sensing, Science, 189, 991-992, 1975b.

Idso, S.B., T.J. Schmugge, R.D. Jackson, and R.J. Reginato, The utility of surface temperature measurements for the remote sensing of surface soil water status, J. Geophys. Res., 80, 3044-3049, 1975c.

Kimball, B.A., Smoothing data with cubic splines, Agron. J., 68, 126-129, 1976.

Kimball, B.A., and R.D. Jackson, Soil heat flux determination: a null-alignment method, Agric. Meteorol., 15, 1 - 9, 1975.

Lee, C.M., UBC CURVE: Curve fitting techniques, Computing Centre, University of British Columbia, 1978.

Lee, C.M., UBC NLE: Zeros of non-linear equations, Computing Centre, University of British Columbia, 1979.

Lettau, H., Theory of surface-temperature and heat-transfer oscillations near a level ground surface, Trans. Amer. Geophys. Union, 32, 189-200, 1951.

Lettau, H., Improved models of thermal diffusion in the soil, Trans. Amer. Geophys. Union, 35, 121-132, 1954.

Madderom, P., UBC INTEGRATION: Integration (Quadrature) Routines, Computing Centre, University of British Columbia, 1978.

Motha, R.P., S.B. Verma, and N.J. Rosenberg, Exchange coefficients under sensible heat advection determined by eddy correlation, Agric. Meteorol., 20, 273-280, 1979.

Novak, M.D., and T.A. Black, The effects of drainage and tillage on the thermal regime of a bare muck soil in early spring, presented at the 51st Annual Meeting of the Northwest Scientific Association, Washington State University, Pullman, Wash., Mar. 30, 31 and April 1, 1978.

Oke, T.R., Turbulent transport near the ground in stable conditions, J. Appl. Meteorol., 9, 778-786, 1970.

Oke, T.R., Boundary Layer Climates, Methuen & Co. Ltd., New York, 1978.

Ouellet, C.E., R. Sharp, and D. Chaput, Estimated monthly normals of soil temperature in Canada, Tech. Bull. 85, Canadian Department of Agriculture, Ottawa, 1975.

Parikh, R.J., J.A. Havens, and H.D. Scott, Thermal diffusivity and conductivity of moist porous media, Soil Sci. Soc. Amer. J., 43, 1050-1052, 1979.

Philip, J.R., The theory of heat flux meters, J. Geophys. Res., 66, 571-579, 1961.

Poppendiek, H.F., A periodic heat-transfer analysis for an atmosphere in which the eddy diffusivity varies sinusoidally with time and linearly with height, J. Meteorol., 9, 368-370, 1952.

Priestley, C.H.B., Turbulent Transfer in the Lower Atmosphere, Univ. Chicago Press, Chicago, 1959.

Reinsch, C.H., Smoothing by spline functions, Numer. Math., 10, 177-183, 1967.

Riha, S.J., K.J. McInnes, S.W. Childs, and G.S. Campbell, A finite element calculation for determining thermal conductivity, Soil Sci. Soc. Amer. J., 44, 1323-1325, 1980.

Sepaskhah, A.R., and L. Boersma, Thermal conductivity of soils as a function of temperature and water content, Soil Sci. Soc. Amer. J., 43, 439-444, 1979.

Staley, D.O., The Diurnal temperature wave for bounded eddy conductivity, J. Meteorol., 13, 13-20, 1956.

Stearns, C.R., Micrometeorological Studies in the Coastal Desert of Southern Peru, Ph.D. Thesis, Univ. Wisconsin, Madison, Wis., 1966.

Tang, P.A., Electronic data acquisition system for the energy balance/Bowen ratio measurement of evaporation, M.Sc. thesis, Univ. British Columbia, 1976.

Tang, P.A., K.G. McNaughton, and T.A. Black, Inexpensive diode thermometry using integrated circuit components, Can. J. For. Res., 4, 250-254, 1974.

Tang, P.A., K.G. McNaughton, and T.A. Black, Precision electronic integrator for environmental measurement, Trans. Amer. Soc. Agric. Eng., 19, 550-552, 1976.

Tanner, C.B., Basic instrumentation and measurements for plant environment and micrometeorology, Dept. Soil Sci., Bull. 6, Coll. Agric. Univ. Wisconsin, Madison, Wis., 1963.

van Duin, R.H.A., Influence of tilth on soil and air temperature, Neth. J. Agric. Sci., 2, 229-241, 1954.

van Wijk, W.R., and W.J. Derksen, Sinusoidal temperature variation in a layered soil, In: Physics of Plant Environment, W.R. van Wijk, Ed., North-Holland Publ. Co., Amsterdam, pp. 171-209, 1966.

van Wijk, W.R., and D.A. de Vries, Periodic temperature variations in a homogeneous soil, In: Physics of Plant Environment, W.R. van Wijk, Ed., North-Holland Publ. Co., Amsterdam, pp. 102-143, 1966.

Verma, S.B., N.J. Rosenberg, and B.L. Blad, Turbulent exchange coefficients for sensible heat and water vapour under advective conditions, J. Appl. Meteorol., 17, 330-338, 1978.

Wierenga, P.J., and C.T. de Wit, Simulation of heat transfer in soils, Soil Sci. Soc. Amer. Proc., 34, 845-848, 1970.

CHAPTER 2

THE USE OF SOIL SURFACE HEAT FLUX DENSITY IN PREDICTING SOIL TEMPERATURE

THE USE OF SOIL SURFACE HEAT FLUX DENSITY IN PREDICTING SOIL TEMPERATURE

2.1 Introduction

One of the major physical factors to be considered in the management of agronomic systems is soil temperature. This is especially true at higher latitudes. For example, throughout most of Canada soil temperatures play a major role in determining the length of the growing season (Baier and Mack, 1973). For annual crop systems, the soil thermal regime during the germination and seedling establishment phases is usually of major and even critical importance (Walker, 1969; Fairbourn, 1973; Hegarty, 1973; Phipps and Cochrane, 1975, Boatwright et al., 1976). During these early phases of a crop's development, the soil surface is often bare and near surface soil temperatures are greatly influenced by the degree to which the surface dries out by evaporation and by the tillage treatment used to prepare the soil for planting (Papendick et al., 1973; Idso et al., 1975a; Allmaras et al., 1977). The existence of a surface mulch, either natural or artificial, also affects the soil thermal regime (Army and Hudspeth, 1960; Moody et al., 1963; Kohnke and Werkhoven, 1963). Soil temperature is a function of the soil thermal conductivity and volumetric heat capacity, and the variation of these with depth and time (Wierenga and de Wit, 1970; Hanks et al., 1971). It is also a function of the amount of heat transferred to the soil, as determined by the surface energy balance (Chapter 1).

Soil temperatures can be predicted using a statistical approach

based upon regression relationships developed between soil temperatures of interest and standard meteorological and soil variables (Ouellet, 1973; Cruse et al. 1980). However, in assessing the effects of drying, tillage, and various surface treatments this approach lacks flexibility since the regressions are usually site specific, require many seasons of observation to establish, and often are inapplicable when thermal properties vary with depth and time. A physically based approach requires solution of the partial differential equation governing heat transfer in the soil (Carslaw and Jaeger, 1959; de Vries, 1975). Often the surface temperature, T_o, is specified (empirically) as the upper boundary condition (Reimer and Shaykewich, 1980; Gupta et al., 1981). However for management purposes, assessing the effects of drying, tillage and various surface treatments on (near) surface soil temperatures is usually the objective. The soil surface heat flux density, G_o, may equivalently be used as the upper boundary condition. In Chapter 1 it was seen that daily and daytime averages of G_o at bare soil sites at Agassiz, B.C. could be expressed as simple functions of solar irradiance, S. The results suggested that G_o may be a more conservative quantity than T_o when considering the effects of drying and tillage of bare soils, so that using it may be particularly advantageous.

The effect of tillage and drying on bare soil thermal regimes has been considered by van Duin (1954) and van Wijk and Derksen (1966). In their treatments the tilled soil was represented as a layer of depth d, homogeneous in its thermal properties, overlying a semi-infinite layer, also homogeneous and with thermal properties different from the first, as shown in Figure 2.1. These authors derived the periodic solutions to the equations of heat conduction:

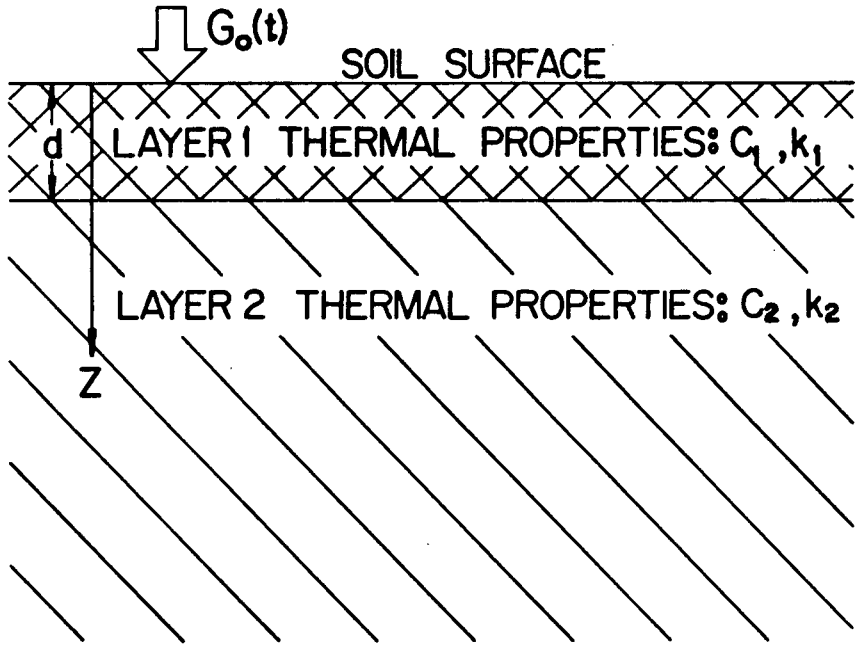

FIGURE 2.1: Simple two-layered model of a drying or tilled bare soil.

$$C_1\frac{\partial T_1}{\partial t} = k_1\frac{\partial^2 T_1}{\partial z^2} \; ; \; 0 \leq z < d$$

$$C_2\frac{\partial T_2}{\partial t} = k_2\frac{\partial^2 T_2}{\partial z^2} \; ; \; z > d \qquad (1)$$

for which either the surface soil heat flux density or temperature is given as a harmonic function of time. These solutions, while perhaps adequate for describing annual and clear-sky diurnal fluctuations, are inapplicable to problems in which the surface boundary conditions are more general functions of time. For example, the problem of determining daily average temperature profiles under highly variable synoptic conditions requires another approach. Similar remarks apply to the problem of assessing the effects of daylength, cloudiness, and nocturnal conditions on diurnal fluctuations.

In this chapter, the exact solution to (1) with the surface heat flux density given as an arbitrary function of time, and with a zero initial temperature distribution, is derived. This solution is then tested with the daily average surface heat flux densities and temperatures measured at Agassiz. The effect of a non-zero initial temperature distribution is approximated by the exact solution for a semi-infinite homogeneous medium insulated at its surface. As well the possibility of using the solution to (1) for a harmonic surface heat flux density (with an effective amplitude $||G_o||$ calculated from the 24-hour and daytime averages of G_o) to predict daily maximum and minimum temperatures is assessed.

2.2 Theory

A. Boundary-Value Problem

It is required to solve (1) subject to the following conditions:

$$-k_1 \frac{\partial T_1}{\partial z}(0,t) = G_o(t) \tag{2a}$$

$$T_1(d,t) = T_2(d,t) \tag{2b}$$

$$-k_1 \frac{\partial T_1}{\partial z}(d,t) = -k_2 \frac{\partial T_2}{\partial z}(d,t) \tag{2c}$$

$$T_2(z,t) \text{ is bounded as } z \to \infty \tag{2d}$$

$$T_1(z,0) = T_2(z,0) = 0 \tag{2e}$$

The solution will be carried out by the method of Laplace transforms (Spiegel, 1965). Applying this transform to (1) and (2a) to (2d) yields respectively:

$$\kappa_1 \frac{d^2 y_1}{dz^2} - s y_1 = -T_1(z,0) \; ; \; 0 \leq z < d \tag{3a}$$

$$\kappa_2 \frac{d^2 y_2}{dz^2} - s y_2 = -T_2(z,0) \; ; \; z > d \tag{3b}$$

$$-k_1 \frac{dy_1}{dz}(0,s) = g_o(s) \tag{3c}$$

$$y_1(d,s) = y_2(d,s) \tag{3d}$$

$$-k_1 \frac{dy_1}{dz}(d,s) = -k_2 \frac{dy_2}{dz}(d,s) \tag{3e}$$

$$y_2(z,s) \text{ is bounded as } z \to \infty \tag{3f}$$

where κ_1, κ_2 are the diffusivities given by $k_1 C_1^{-1}$, $k_2 C_2^{-1}$ respectively, and y_1, y_2, g_o are the Laplace transforms of T_1, T_2, G_o respectively. General solutions to (3a) and (3b), after using condition (2e), are as follows:

$$y_1 = A_1 e^{-z\sqrt{\frac{s}{\kappa_1}}} + A_2 e^{z\sqrt{\frac{s}{\kappa_1}}} \quad ; \; 0 \leq z < d$$

$$y_2 = B_1 e^{-z\sqrt{\frac{s}{\kappa_2}}} + B_2 e^{z\sqrt{\frac{s}{\kappa_2}}} \quad ; \; z > d \tag{4}$$

where A_1, A_2, B_1, B_2 are arbitrary constants. Using the four conditions (3c) to (3f) to determine these constants yields y_1 and y_2 as follows:

$$y_1 = \frac{g_o(s)\left[r_a e^{(z-2d)\sqrt{\frac{s}{\kappa_1}}} + e^{-z\sqrt{\frac{s}{\kappa_1}}}\right]}{\sqrt{k_1 C_1}\,\sqrt{s}\,\left(1 - r_a e^{-2d\sqrt{\frac{s}{\kappa_1}}}\right)} \; ; \; 0 \leq z < d$$

$$y_2 = \frac{2 g_o(s)\, r_b\, e^{-\left\{z - d\left(1-\sqrt{\frac{\kappa_2}{\kappa_1}}\right)\right\}\sqrt{\frac{s}{\kappa_2}}}}{\sqrt{k_1 C_1}\,\sqrt{s}\,\left(1 - r_a e^{-2d\sqrt{\frac{s}{\kappa_1}}}\right)} \; ; \; z > d \tag{5}$$

where $r_a = \dfrac{\sqrt{k_1 C_1} - \sqrt{k_2 C_2}}{\sqrt{k_1 C_1} + \sqrt{k_2 C_2}}$ and $r_b = \dfrac{\sqrt{k_1 C_1}}{\sqrt{k_1 C_1} + \sqrt{k_2 C_2}}$.

The desired solution is determined by finding the inverse Laplace transforms of y_1 and y_2. To do this it is first noted that y_1 and y_2 can both be written as sums of terms (two for y_1 and one for y_2) of the form

$$y = \frac{g_o(s)\; a\; e^{-b\sqrt{s}}}{\sqrt{s}\,\left(1 - r_a e^{-c\sqrt{s}}\right)} = g_o(s) \cdot \bar{x}(s) \tag{6}$$

where a, b, and c are constants and both b, c > 0. There are two complementary approaches to finding the inverse Laplace transform of $\bar{x}$ (Carslaw and Jaeger, 1959, pg. 309). The first, and simplest, consists of expanding

the term in brackets in the denominator of (6) in a binomial expansion so that,

$$x = a \sum_{j=0}^{\infty} \frac{(r_a)^j \, e^{-(jc+b)\sqrt{s}}}{\sqrt{s}} \tag{7}$$

Now the inverse Laplace transform ($L_t^{-1}\{\}$) of $\frac{e^{-(jc+b)\sqrt{s}}}{\sqrt{s}}$ is available in standard tables, as follows:

$$L_t^{-1}\{\frac{e^{-(jc+b)\sqrt{s}}}{\sqrt{s}}\} = \frac{e^{-\frac{(jc+b)^2}{4t}}}{\sqrt{\pi t}} \tag{8}$$

so that

$$L_t^{-1}\{x\} = a \sum_{j=0}^{\infty} \frac{(r_a)^j \, e^{-\frac{(jc+b)^2}{4t}}}{\sqrt{\pi t}} \tag{9}$$

which converges uniformly for $t \geq 0$ when $|r_a| < 1$. The convolution theorem for the product of Laplace transforms states that

$$L_t^{-1}\{g_o \cdot x\} = \int_o^t G_o(t-\lambda) \, L_\lambda^{-1}\{x\} \, d\lambda. \tag{10}$$

Combining (9) and (10) yields

$$L_t^{-1}\{y\} = \frac{a}{\sqrt{\pi}} \sum_{j=0}^{\infty} (r_a)^j \int_o^t \frac{G_o(t-\lambda) \, e^{-\frac{(jc+b)^2}{4\lambda}}}{\sqrt{\lambda}} d\lambda \tag{11}$$

The constants a, b, c in the expressions for y_1 and y_2 are:

$$a = \frac{r_a}{\sqrt{k_1 C_1}}; \quad b = \frac{2d-z}{\sqrt{\kappa_1}}; \quad c = \frac{2d}{\sqrt{\kappa_1}} \tag{12a}$$

$$a = \frac{1}{\sqrt{k_1 C_1}};\ b = \frac{z}{\sqrt{\kappa_1}};\ c = \frac{2d}{\sqrt{\kappa_1}} \tag{12b}$$

for the first and second term respectively of y_1, and

$$a = \frac{2r_b}{\sqrt{k_1 C_1}};\ b = \frac{z-d(1-\sqrt{\frac{\kappa_2}{\kappa_1}})}{\sqrt{\kappa_2}};\ c = \frac{2d}{\sqrt{\kappa_1}} \tag{12c}$$

for the single term of y_2.

Hence

$$T_1(z,t) = \frac{r_a}{\sqrt{\pi k_1 C_1}} \sum_{j=0}^{\infty} (r_a)^j \int_0^t \frac{G_o(t-\lambda)\ e^{-\frac{[(j+1)2d-z]^2}{4\kappa_1\lambda}}}{\sqrt{\lambda}}\, d\lambda +$$

$$\frac{1}{\sqrt{\pi k_1 C_1}} \sum_{j=0}^{\infty} (r_a)^j \int_0^t \frac{G_o(t-\lambda)\ e^{-\frac{[2jd+z]^2}{4\kappa_1\lambda}}}{\sqrt{\lambda}}\, d\lambda \tag{13a}$$

and

$$T_2(z,t) = \frac{2r_b}{\sqrt{\pi k_1 C_1}} \sum_{j=0}^{\infty} (r_a)^j \int_0^t \frac{G_o(t-\lambda)\ e^{-\frac{[(2j+1)d\sqrt{\frac{\kappa_1}{\kappa_1}}+z-d]^2}{4\kappa_2\lambda}}}{\sqrt{\lambda}}\, d\lambda \tag{13b}$$

These series expressions for T_1 and T_2 converge quite rapidly for small values (i.e. < 1) of the parameter $P_1 = \kappa_1 t d^{-2}$.

Since κ_1 for soils is typically ~ 200 - 500 $cm^2\ d^{-1}$, d is ~ 1 - 15 cm, z is ~ 1 - 100 cm, and times of interest are ~ 1 - 100 days, this leads to P_1 ~ 1 - 50,000. It is evident then that (13a) and (13b) are not computationally convenient for most cases of interest.

The solution convenient for P_1 > 1 is determined by the complex inversion theorem, i.e.

$$L_t^{-1}\{\bar{x}\} = \frac{1}{2\pi i}\int_{\gamma-i\infty}^{\gamma+i\infty} e^{st}\,\bar{x}(s)\,ds \tag{14}$$

where γ lies to the right of the singularities of $\bar{x}(s)$. The integral in (14) is usually evaluated by closing the contour in the s-plane and using the residue theorem. Since $\bar{x}$ in (6) has a branch point at s = 0, the appropriate closed contour is that shown in Figure 2.2 where the branch of $\sqrt{s}$ chosen is such that the real part of $\sqrt{s} > 0$. According to the residue theorem

$$L_t^{-1}\{\bar{x}\} = \Sigma\left(\begin{matrix}\text{residues of } e^{st}\,\bar{x}(s)\\ \text{at poles of } \bar{x}(s)\end{matrix}\right) - \frac{1}{2\pi i}\int_{1+2+3+4+5} e^{st}\,\bar{x}(s)\,ds \tag{15}$$

The poles of $\bar{x}(s)$ are given by $1 - r_a e^{-c\sqrt{s}} = 0$, or

$$\sqrt{s_p} = \frac{\ln(|r_a|^{-1}) + (2j + n_s)\,\pi i}{-c};\quad j = 0, \pm 1, \pm 2, \ldots.$$

where $n_s = 0$ for $r_a > 0$ and $n_s = 1$ for $r_a < 0$. Since $c > 0$, the real part of $\sqrt{s_p} < 0$, which demonstrates that the poles of $\bar{x}(s)$ are not located on the branch on which the contour integration is performed and so the contribution from the residue term in (15) is zero. As well, since $|\bar{x}(Re^{i\theta})| << a(1-|r_a|^{-1})(\sqrt{R})^{-1}$, the contributions as $R \to \infty$ from sections 1 and 5 of the contour integral are zero for $|r_a| < 1$. Furthermore by setting $s = \varepsilon e^{i\theta}$ and taking the limits as $\varepsilon \to 0$, it can be shown that the contribution from section 3 of the contour integral is zero as well. The contributions from sections 2 and 4 are evaluated by setting $s = \xi e^{i\pi}$ along 2 and $s = \xi e^{-i\pi}$ along 4 and taking the limits as $\varepsilon \to 0$ and $R \to \infty$. This yields,

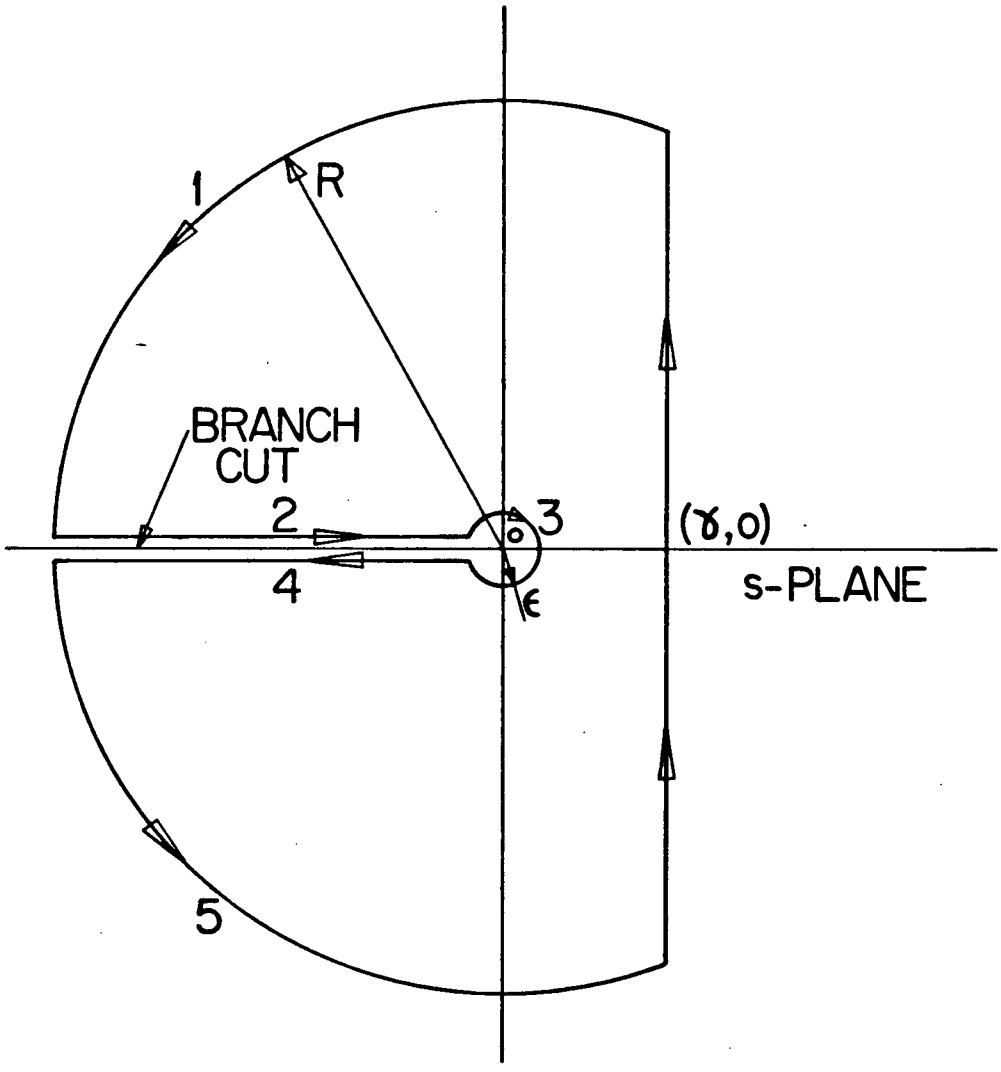

FIGURE 2.2: Contour in the s-plane for finding the inverse Laplace transform of x(s).

$$L_t^{-1}\{\bar{x}\} = \frac{a}{\pi}\int_0^\infty \frac{e^{-\xi t}}{\sqrt{\xi}}\left\{\frac{\cos[b\sqrt{\xi}] - r_a\cos[(c-b)\sqrt{\xi}]}{(1 + r_a^2 - 2r_a\cos[c\sqrt{\xi}])}\right\} d\xi \tag{16}$$

Setting a, b, and c to the appropriate values given in (12) and using (10) and (16) yields the following expressions for T_1 and T_2:

$$T_1(z,t) = \frac{(1-r_a{}^2)}{\pi\sqrt{k_1C_1}}\int_0^t G_o(t-\lambda)\int_0^\infty \frac{e^{-\lambda\xi}\cos[z\sqrt{\frac{\xi}{\kappa_1}}]d\xi\, d\lambda}{\sqrt{\xi}(1+r_a^2 - 2r_a\cos[2d\sqrt{\frac{\xi}{\kappa_1}}])} \tag{17a}$$

and

$$T_2(z,t) = \frac{2r_b}{\pi\sqrt{k_1C_1}}\int_0^t G_o(t-\lambda)\int_0^\infty \frac{e^{-\xi\lambda}\{\cos[(z-d+d\sqrt{\frac{\kappa_2}{\kappa_1}})\sqrt{\frac{\xi}{\kappa_2}}] - r_a\cos[(z-d-d\sqrt{\frac{\kappa_2}{\kappa_1}})\sqrt{\frac{\xi}{\kappa_2}}]\}d\xi d\lambda}{\sqrt{\xi}(1+r_a^2-2r_a\cos[2d\sqrt{\frac{\xi}{\kappa_1}}])} \tag{17b}$$

It was found that letting $\xi = \nu^2$ and interchanging the order of the integrals in (17) (allowable since the inner integrals are uniformly convergent for $0 < \lambda \leqslant t$) yielded expressions more convenient for computation, i.e.

$$T_1(z,t) = \frac{2(1-r_a^2)}{\pi\sqrt{k_1C_1}}\int_0^\infty\{\int_0^t G_o(t-\lambda)e^{-\nu^2\lambda}\, d\lambda\}\frac{\cos[\frac{z\nu}{\sqrt{\kappa_i}}]d\nu}{1 + r_a^2 - 2r_a\cos[\frac{2d\nu}{\sqrt{\kappa_1}}]} \tag{18a}$$

$$T_2(z,t) = \frac{4r_b}{\pi\sqrt{k_1C_1}}\int_0^\infty\{\int_0^t G_o(t-\lambda)e^{-\nu^2\lambda}d\lambda\}\frac{\{\cos[(z-d+d\sqrt{\frac{\kappa_2}{\kappa_1}})\frac{\nu}{\sqrt{\kappa_2}}] - r_a\cos[(z-d-d\sqrt{\frac{\kappa_2}{\kappa_1}})\frac{\nu}{\sqrt{\kappa_2}}]\}d\nu}{1 + r_a^2 - 2r_a\cos[\frac{2d\nu}{\sqrt{\kappa_1}}]} \tag{18b}$$

It is noted that when $k_1 = k_2 = k$ and $C_1 = C_2 = C$ ($r_a = 0$ and $r_b = \frac{1}{2}$) then both (18a) and (18b) reduce to the solution given by Carslaw and

Jaeger (1959), pg. 76, for a homogenous semi-infinite medium, i.e.

$$T(z,t) = \frac{1}{\sqrt{\pi kC}} \int_0^t \frac{G_o(t-\lambda)}{\sqrt{\lambda}} e^{\frac{-z^2C}{4k\lambda}} d\lambda \qquad (19)$$

B. Initial-Value Problem

Since equations (1) are linear, the influence of an initial temperature distribution (f(z)) can be accounted for separately by finding the solution such that

$$T_1(z,0) = f(z) \; ; \; 0 \leq z < d \qquad (20a)$$

$$T_2(z,0) = f(z) \; ; \; z > d \qquad (20b)$$

$$-k_1 \frac{\partial T_1}{\partial z} (0,t) = 0 \qquad (20c)$$

along with conditions (2b) to (2d). This solution, which is then added to equations (18) to yield the complete solution, can be found by the Laplace transform technique in a manner similar to that outlined above for the boundary-value problem, although the algebra is extremely cumbersome. However due to the isothermal nature of the initial-value solution at $z = 0$, the presence of the upper layer is of little consequence when P_1 is large enough. Hence for $P_1 >> 1$ the effect of the initial condition is well represented by the solution for a homogeneous semi-infinite medium, insulated at its surface, with thermal properties C_2, k_2 and initial temperature distribution f(z). The solution to this problem can be found by setting $f(\lambda) = f(-\lambda)$ in the solution for the infinite medium given by Carslaw and Jaeger (1959), pg. 53, i.e.

$$T(z,t) = \frac{1}{\sqrt{4\pi\kappa_2 t}} \left\{ \int_0^\infty f(\lambda) \, e^{-\frac{(z+\lambda)^2}{4\kappa_2 t}} d\lambda + \int_0^\infty f(\lambda) \, e^{-\frac{(z-\lambda)^2}{4\kappa_2 t}} d\lambda \right\} \qquad (21)$$

Letting $\lambda = -z + \xi\sqrt{4\kappa_2 t}$ in the first integral of (21) and $\lambda = z + \xi\sqrt{4\kappa_2 t}$ in the second, and rearranging yields

$$T(z,t) = \frac{1}{\sqrt{\pi}} \int_0^\infty e^{-\xi^2} \{f(-z + \xi\sqrt{4\kappa_2 t}) + f(z + \xi\sqrt{4\kappa_2 t})\}\, d\xi +$$

$$\frac{1}{\sqrt{\pi}} \int_0^{\frac{z}{\sqrt{4\kappa_2 t}}} e^{-\xi^2} \{f(z - \xi\sqrt{4\kappa_2 t}) - f(-z + \xi\sqrt{4\kappa_2 t})\}\, d\xi \qquad (22)$$

which is a convenient form for computation.

It is recognised that for $P_1 >> 1$, the boundary-value solution given by (18) can be simplified as well. To first order the heat stored in the upper layer can be neglected. All of the surface heat flux then enters the semi-infinite layer ((19) can be used to calculate T_2) and the temperature in the finite layer is a linear function of depth with $\frac{dT_1}{dz} = -G_o(t)\, k_1^{-1}$. The theoretical calculations presented in this chapter were carried out using the exact solution (18).

C. Diurnal Fluctuations

Assuming $G_o(t)$ is known well enough, i.e. over time intervals of at most 1 - 2 hours, then (18) and (22) can be used to evaluate daily maximum and minimum temperatures. However since this short-interval G_o data is often unavailable and the calculations would require a large amount of computer time, it was decided to see whether the harmonic solutions of (1) developed by van Duin (1954) and van Wijk and Derksen (1966) could be used to predict the amplitudes of diurnal temperature fluctuations in the field. According to their solutions these amplitudes are given by the following equations:

$$||T_1|| = \frac{||G_o||}{\sqrt{\omega_d k_1 C_1}} \left\{ \frac{e^{-\frac{2z}{D_{1d}}} + 2r_a e^{-\frac{2d}{D_{1d}}} \cos[\frac{2(d-z)}{D_{1d}}] + r_a^2 e^{-\frac{2}{D_{1d}}(2d-z)}}{1 - 2r_a e^{-\frac{2d}{D_{1d}}} \cos[\frac{2d}{D_{1d}}] + r_a^2 e^{-\frac{4d}{D_{1d}}}} \right\}^{\frac{1}{2}} \quad (23a)$$

for $0 \leq z < d$, and

$$||T_2|| = ||T_1||_{z=d} \, e^{-\frac{(z-d)}{D_{2d}}} \quad (23b)$$

for $z > d$, where $\omega_d = (2\pi/24)\ h^{-1}$, and D_{1d} and D_{2d} are the daily damping depths given by $(2k_1 C_1^{-1} \omega_d^{-1})^{\frac{1}{2}}$ and $(2k_2 C_2^{-1} \omega_d^{-1})^{\frac{1}{2}}$ respectively. This approach neglects day to day transient effects and the effects due to non-sinusoidal behaviour, especially on days of variable cloudiness. The procedure for calculating an effective $||G_o||$, even on such days, is outlined in the next section.

2.3 Procedures

A. Temperature Measurements in the Field

Soil temperatures were measured at half-hour intervals at 30 depths ranging from 0.2 to 100 cm in a culti-packed area (site 1) and a disc-harrowed area (site 2). The bulk densities of the upper 10 cm of soil were 1030 kg m^{-3} at site 1 and 870 kg m^{-3} at site 2. The soil was a Monroe series loam/silt-loam. The study period at site 1 lasted from May 19 to July 21, 1978 and at site 2 from July 5 to July 21, 1978. Temperature differences between depths were measured with copper-constantan thermocouples to ± 0.03°C while the required absolute temperature was measured to ±0.1°C by an FD-300 silicon diode placed at the 105 cm depth. The temperatures were smoothed in time and depth by fitting with cubic spline polynomials (Reinsch, 1967; Kimball, 1976).

Surface temperatures calculated with these polynomials are compared with those measured with a hand-held Barnes PRT-10-L infrared thermometer in Figure 2.3a. Also shown are surface temperatures calculated in a similar manner from a backup profile of 6 FD-300 silicon diodes at site 1. The overestimates (~5-8°C) by the thermocouple system at both sites occurred for high-radiation dry-soil conditions. The bolometer reference thermometer was calibrated to ± 0.3°C in the laboratory. The fact that the bolometric temperatures were not corrected for soil emissivities different from 1 could only account for ~ 1-2°C. The errors may have been due to distortion of the temperature profiles by the framework, consisting of acrylic and stainless steel tubing (Appendix I, Figure 3), used to position the thermocouples at the desired depths, although the possibility of some site disturbance during installation cannot be ruled out. Comparison with the FD-300 profile at site 1 showed that the errors were negligible below 2.5 cm. Figure 2.3b demonstrates that the differences in surface temperature between the sites measured by the thermocouple systems were in reasonable agreement with those measured by the bolometer as well as those inferred from radiation and sensible heat flux measurements also carried out at both sites (full details about these latter measurements are in Chapter 1). The differences from the radiometer measurements were calculated using

$$(T_o)_2 - (T_o)_1 = [(L_N)_1 - (L_N)_2]\ [4\sigma(T_o + 273)^3]^{-1} \qquad (24)$$

where the subscripts $_1$ and $_2$ refer to sites 1 and 2 respectively, T_o is the average of $(T_o)_2$, $(T_o)_1$ measured by the bolometer, $L_N = R_N - S(1-\alpha)$, i.e. it was assumed that $(L\downarrow)_1 = (L\downarrow)_2$ and $(\varepsilon_s)_1 = (\varepsilon_s)_2 = 1$, and $\sigma = 5.67 \times 10^{-8}$ W m^{-2} °C^{-4}. The differences from the sensible heat flux density measurements (H_1 and H_2 at sites 1 and 2 respectively) were calculated according to

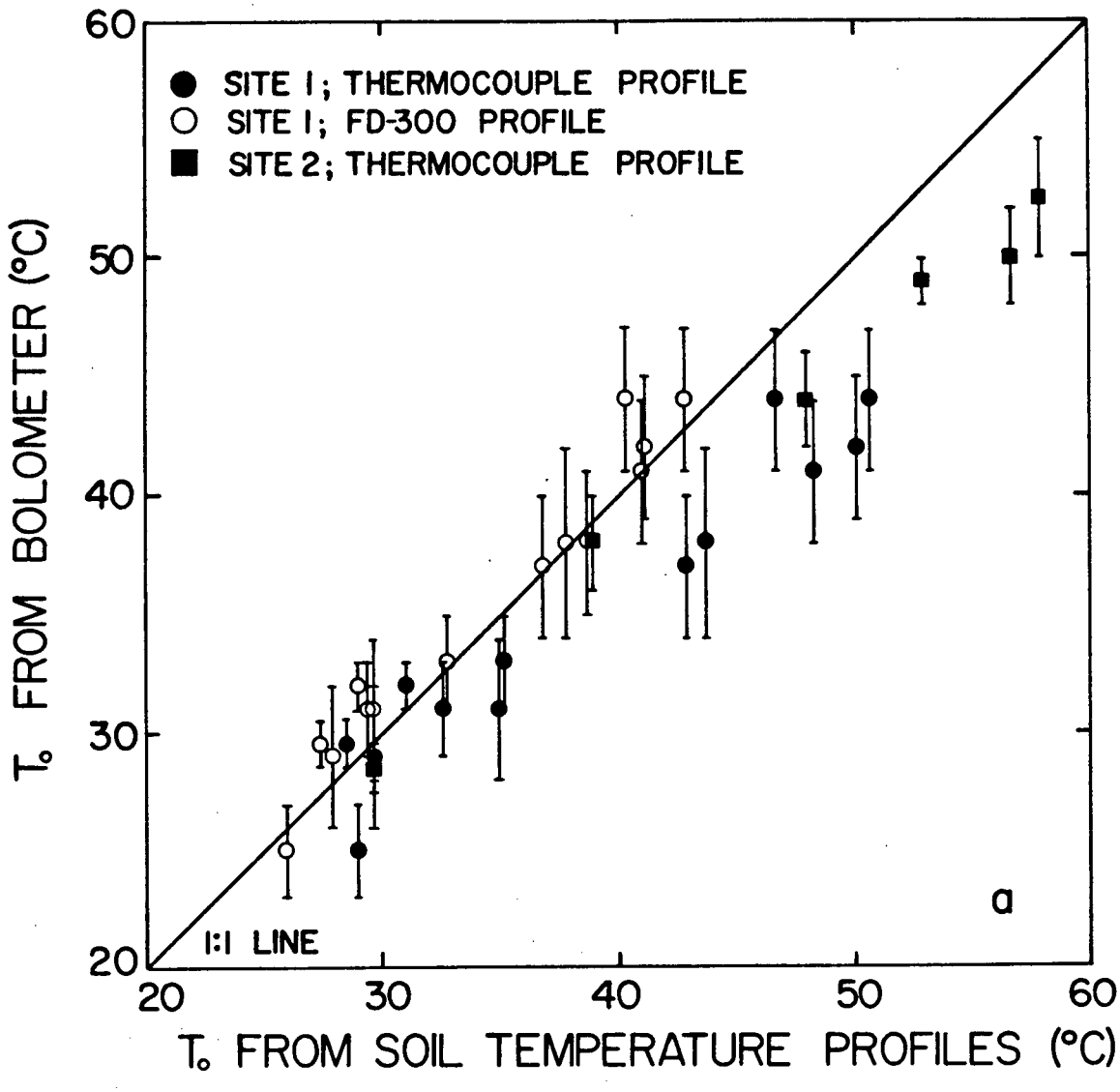

FIGURE 2.3a: Comparison of surface temperatures measured with a hand-held Barnes PRT-10-L infrared thermometer (bolometer) and half-hourly surface temperatures calculated from thermocouple and FD-300 diode profiles at site 1 and thermocouple profiles at site 2. The bars indicate the range of values measured by the bolometer.

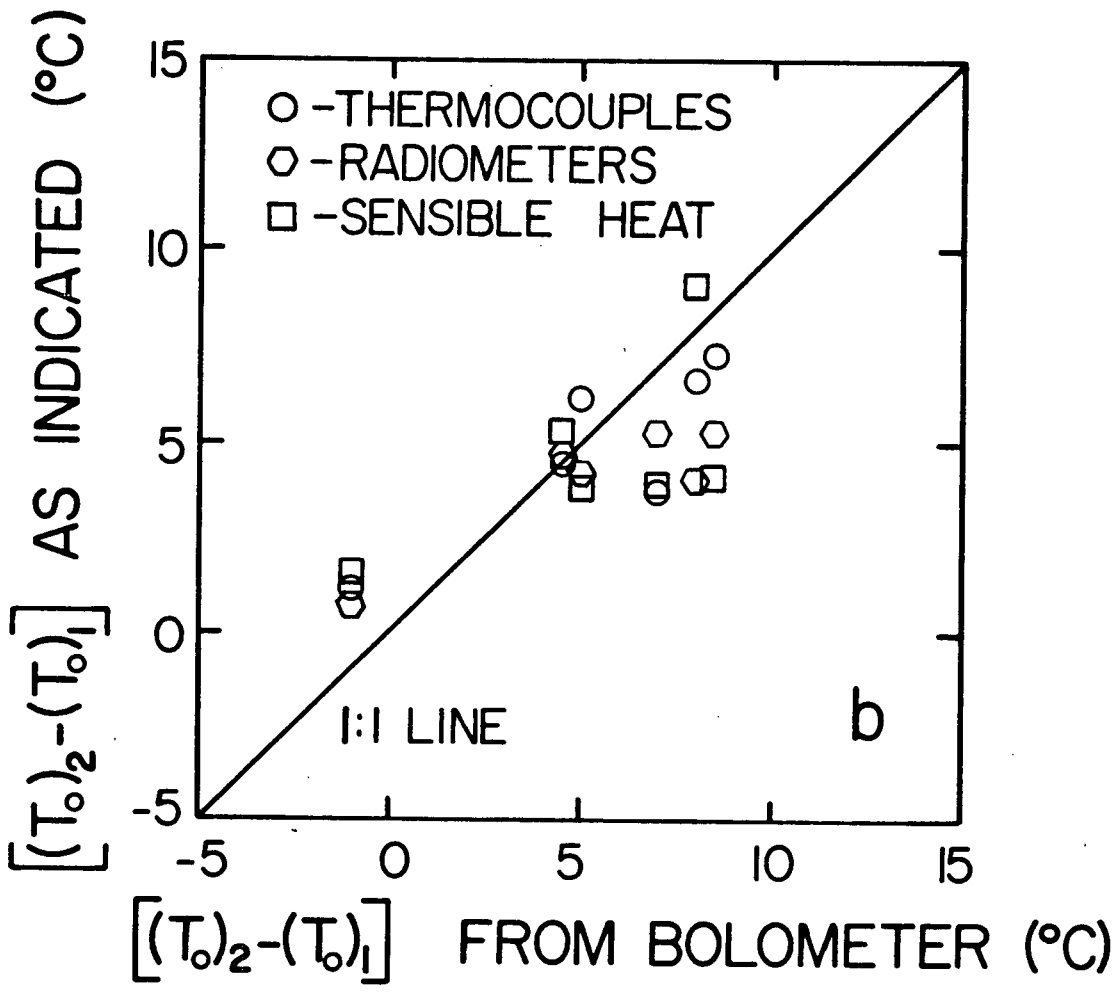

FIGURE 2.3b: Comparison of measured and inferred differences in half-hourly surface temperature between sites 1 and 2.

$$(T_o)_2 - (T_o)_1 = [(T_a)_2-(T_o)_1] + H_2H_1^{-1}\,[(T_o)_1 - (T_a)_1] \quad (25)$$

where the $(T_o)_i$ from the FD-300 profile was used, while $(T_a)_1$ and $(T_a)_2$ were measured at 70 cm above the surfaces, i.e. it was assumed that the atmospheric diffusivities between 0 and 70 cm were the same at both sites. All surface temperature measurements and thermal conductivities (i.e. temperature gradients) calculated from them presented in this chapter have been corrected in accordance with Figure 2.3a; the corrections in 24-hour average T_o were < 1.8°C at site 1 and < 1.4°C at site 2. The overestimate in G_o implied by the errors in T_o was not corrected for since calculations showed that the overestimate was < 2 W m^{-2} for 24-hour averages.

B. Programming the Solutions

The surface heat flux density, $G_o(t)$, required to numerically evaluate (18a) and (18b) was represented as a series of square pulses of width τ as shown in Figure 2.4. The temperature calculated at the midpoint of each pulse was assumed to be the average temperature for the pulse period. The inner integral in (18a) and (18b) for each time t(j) was evaluated exactly for this representation of G_o, as follows:

$$\int_0^{t(j)} G_o(t-\lambda)e^{-\nu^2\lambda}\,d\lambda = \frac{G_o(j)}{\nu^2}\left(1-e^{-\frac{\nu^2\tau}{2}}\right) + \frac{(1-e^{-\nu^2\tau})}{\nu^2}\sum_{n=2}^{j} G_o(j-n+1)e^{-\nu^2(2n-3)\frac{\tau}{2}} \quad (26)$$

This led to a considerable saving in computation time compared with numerical evaluations. A similar procedure could be readily carried out for other simple representations of $G_o(t)$, e.g. as a series of continuous ramping functions.

Comparison with the Agassiz field measurements was made on a

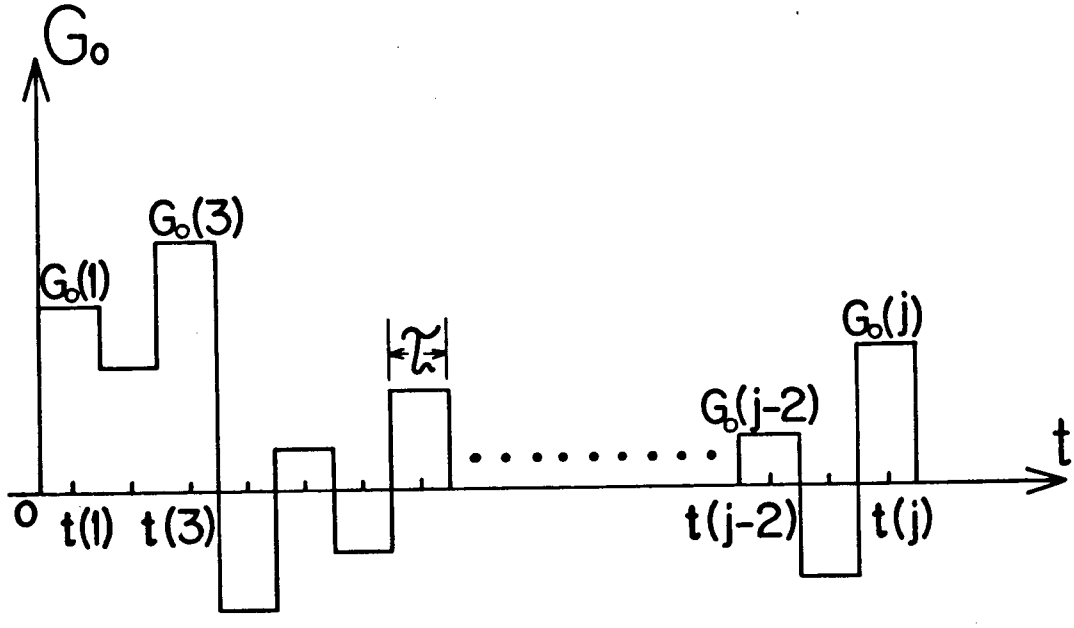

FIGURE 2.4: Representation of $G_o(t)$ as a series of square pulses of width τ.

24-hour basis (τ = 1 d) at eight depths - 0.0, 1.0, 2.5, 5.0, 10.0, 20.0, 50.0, and 100.0 cm. Soil surface heat flux densities were computed half-hourly at both sites from measured soil temperature and volumetric heat capacity profiles using the Kimball and Jackson (1975) null-alignment procedure with slight modifications, and then simply averaged over each day. The time course of 24-hour average G_o at site 1 is presented in Figure 2.5; values at site 2 were similar (see Chapter 1). The thermal properties of the two layers and the depth, d, of the upper layer at both the culti-packed and disc-harrowed sites were chosen from the measured profiles of k and C at maximum and minimum surface soil moisture contents, as shown in Figure 2.6. The volumetric soil heat capacities were calculated from measured bulk densities, organic matter fractions, and gravimetric moisture contents while the thermal conductivities were calculated from calculated profiles of soil heat flux density (the null-alignment method yields the soil heat flux density at any depth of interest) and measured temperature gradients using Fourier's law. These measured thermal properties were in good agreement with those reported in the literature for loam and silt-loam soils of similar porosities and moisture contents (de Vries, 1966; Riha et al., 1980).

The thermal properties of the semi-infinite layer at each site were chosen from the measured values at depths of 10-20 cm. The depth, d, and maximum and minimum values of the properties of the upper layer at each site were chosen so that both $\int_0^{20\ cm} C\ dx$ and $\int_0^{20\ cm} k\ dx$ of the actual and layered maximum and minimum profiles respectively were about equal. The theoretical calculations of the temperatures were performed with C_2, k_2, and d fixed while C_1 and k_1 varied from day to day depending upon the daytime average albedo at each site. Both k_1 and C_1 were assumed to linearly

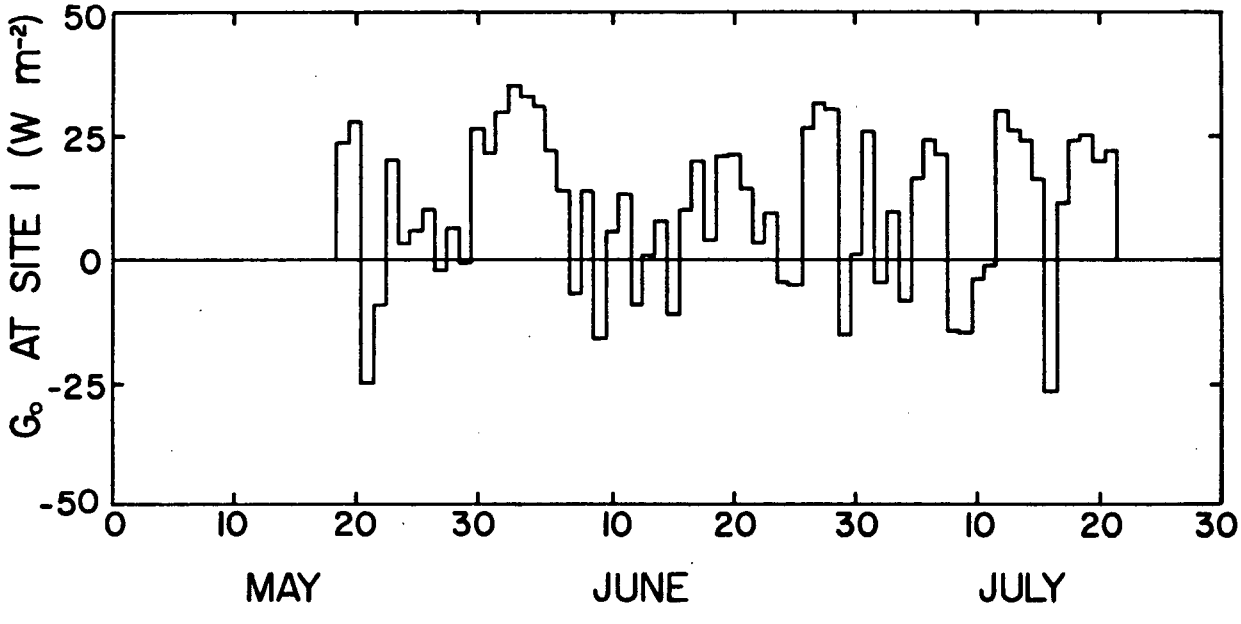

FIGURE 2.5: Time course of 24-hour average G_o at the culti-packed site.

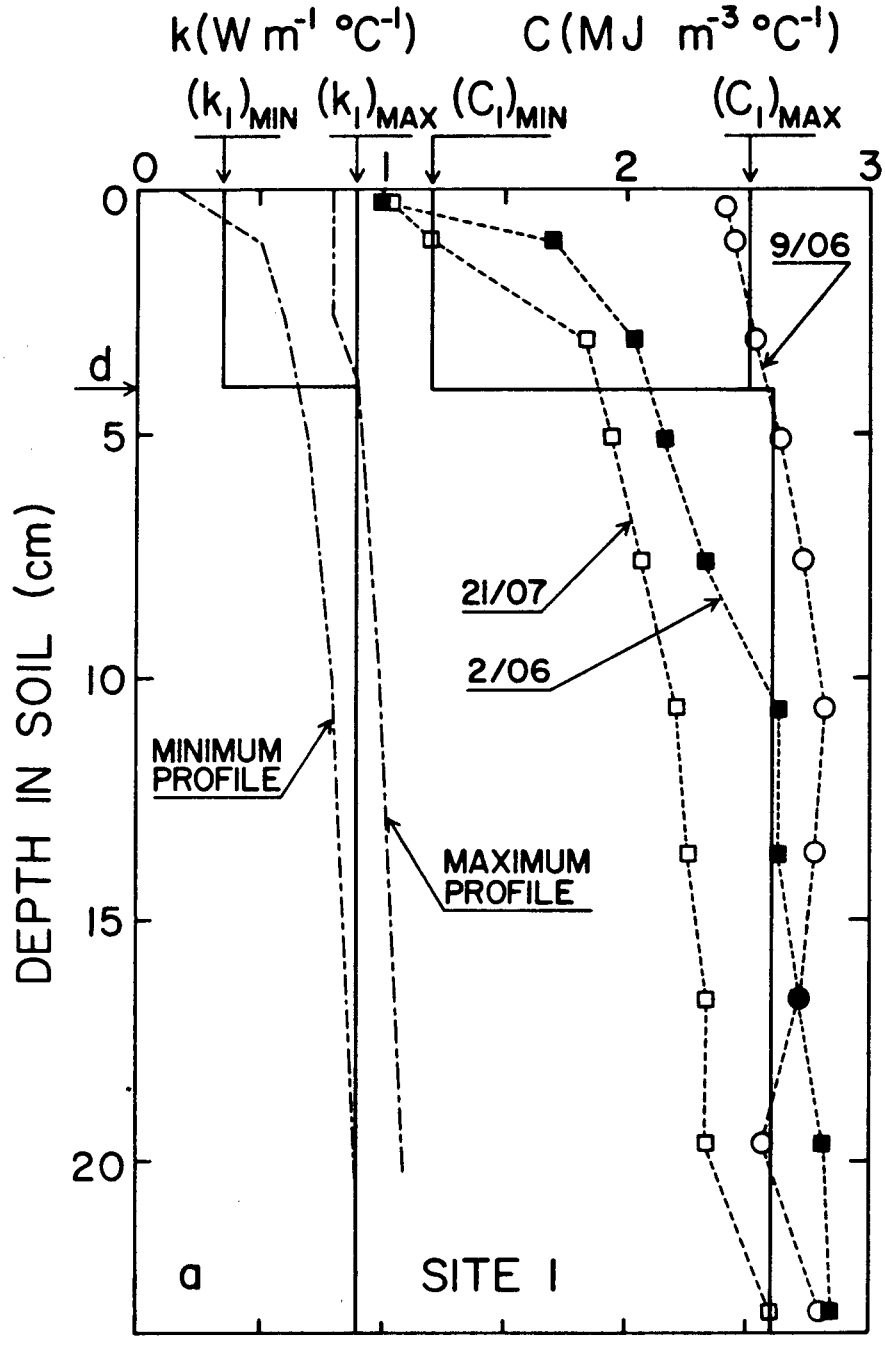

FIGURE 2.6a: Measured and modelled profiles of k and C at site 1. The maximum and minimum profiles of k were computed from daytime and nighttime averages (see Table 1.3). The measured profiles of C (unsmoothed) are representative of maximum and minimum soil moisture conditions. Daytime average albedos on June 2, June 9, and July 21 were 0.166, 0.078, and 0.156 respectively.

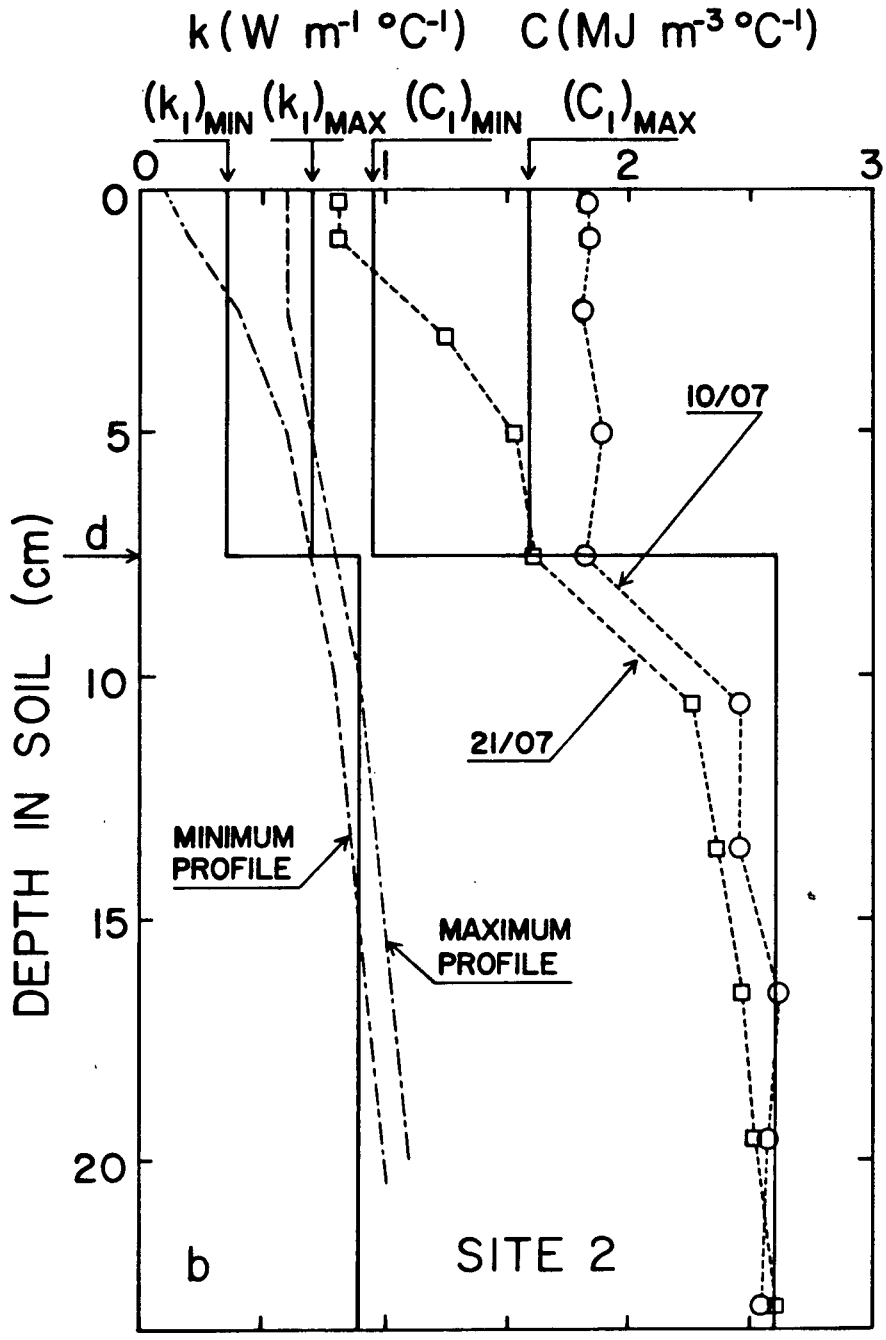

FIGURE 2.6b: As in Figure 2.6a except for site 2. Daytime average albedos on July 10 and 21 were 0.066 and 0.156 respectively.

decrease with albedo within the indicated ranges as the daytime average albedos increased from minimum to maximum observed values, which were 0.065 ± 0.01 and 0.165 ± 0.01 respectively for both sites. This was done for simplicity and also because soil moisture data were not available every day. The results of Idso et al. (1975b) suggested that near-surface soil moisture content, and hence k and C, could be determined in this manner. While the solution given by (18a) and (18b) was derived with the assumption that k_1 and C_1 were constant, the temperatures calculated by this procedure, along with those calculated with k_1 and C_1 constant and equal to the maximum values in their respective indicated ranges, should at least bracket the more appropriate theoretical solution in which k_1 and C_1 are given as explicit functions of time.

The initial temperature profile, f(z), was represented by the function

$$f(z) = T_{aa} + \frac{(T_o - T_{aa})}{\sin[\eta_a]} e^{-\frac{z}{D_{2a}}} \sin[\eta_a - \frac{z}{D_{2a}}] \qquad (27)$$

with the annual damping depth of the semi-infinite layer, $D_{2a} = (2k_2 C_2^{-1} \omega_a^{-1})^{\frac{1}{2}}$, and $\omega_a = (2\pi/365)\ d^{-1}$. The annual average soil temperature, T_{aa} = 11.5°C, was determined from the results of Ouellet et al. (1975), who generated monthly average soil temperatures under a short-grass surface at Agassiz using a multiple regression model based on long-term local measurements of standard climatic variables. The parameters T_o and η_a were chosen so that the temperatures on the first day of a run at all eight output depths agreed with observed temperatures on that day to within 1.0°C (but usually within 0.5°C).

To compute the diurnal amplitudes of soil temperature using (23), an effective surface amplitude $||G_o||$ was calculated using G_o^{24} and G_o^d, the

measured 24-hour and daytime average soil surface heat flux densities respectively, by first representing G_o on each day as

$$G_o = G_o^{24} + ||G_o|| \sin[\omega_d t + \eta_o] \tag{28}$$

where t varies from 0 to 24 h. The phase parameter $\eta_o = -1.178$ was chosen so that G_o reached a maximum at 10.5 h, in accordance with the clear-day observations at both sites. Integrating (28) from the average time of sunrise, t_1, to the average time of sunset, t_2, yielded

$$G_o^d = \frac{1}{(t_2-t_1)} \int_{t_1}^{t_2} G_o dt = G_o^{24} + \frac{||G_o||}{(t_2-t_1)\omega_d} \{\cos[\omega_d t_1+\eta_o]-\cos[\omega_d t_2+\eta_o]\} \tag{29}$$

from which $||G_o||$ was computed. The maximum and minimum soil temperatures were then calculated by respectively adding and subtracting the amplitudes computed using (23) to the 24-hour average temperatures computed from (18) and (22). The values of t_1 and t_2 used were 4.5 and 20.5 h respectively.

The integrals over the semi-infinite ranges in (18) and (22) as well as the proper integral in (22) were evaluated numerically using packaged routines (QINF and CADRE respectively) available through the University of B.C. Computing Centre (Madderom, 1978). The final program was tested by comparison with results presented in Carslaw and Jaeger (1959), pp. 55 and 75 for homogeneous media in which (i) the surface heat flux density was constant and the temperature profile was initially isothermal, (ii) the surface was insulated and the temperature initially was constant above a certain depth and zero below that depth. The program required about 50 s of CPU time on the university's Amdahl 470 V/8 computer to compute the temperatures at the 8 output depths for 75 days with an error of at most 0.2°C. A sample listing of this program is presented in Appendix II.

2.4 Results and Discussion

A. Daily Averages

Comparison between the calculated (solid lines) and measured 24-hour average soil temperatures at 0, 10, and 50 cm depths is shown in Figures 2.7 and 2.8 for the site 2 and site 1 study periods respectively. The effect of maintaining k_1 and C_1 at their respective maximum values for each site is demonstrated in Figure 2.7 (dashed lines). Accounting for the drying of the 4.0 cm layer at site 1 changed the calculated 24-hour average surface temperatures by less than 1.6°C, although at site 2, which was modelled with a 7.5 cm layer, this resulted in differences as large as 3°C. Furthermore, accounting for the drying of the upper layers resulted in higher calculated temperatures at depths below these layers, although the differences were small (< 0.5°C at 10 cm). Thus it is apparent that the calculation of 24-hour average soil temperatures at both sites (but especially at site 1) did not constitute a particularly strong test of the layering aspects of the theory. The minimal near-surface drying that occurred over the longer study period at site 1 was largely attributed to upward movement of moisture from the water table located between 1 and 2 m below the surface.

Both figures demonstrate that the theoretical calculations reproduced the measured day to day fluctuations fairly well at both sites, although a systematic overestimate of all the temperatures occurred for later times at all 3 depths, particularly at the deeper depths. Figure 2.7 shows that the measured daily average surface temperatures on July 19-21 were 2.3 - 2.6°C higher at site 2 than at site 1, compared with the 2.8 - 3.7°C and 1.9 - 2.2°C by the theory, with and without the drying of the upper layer accounted for, respectively. For July 13-15 these values

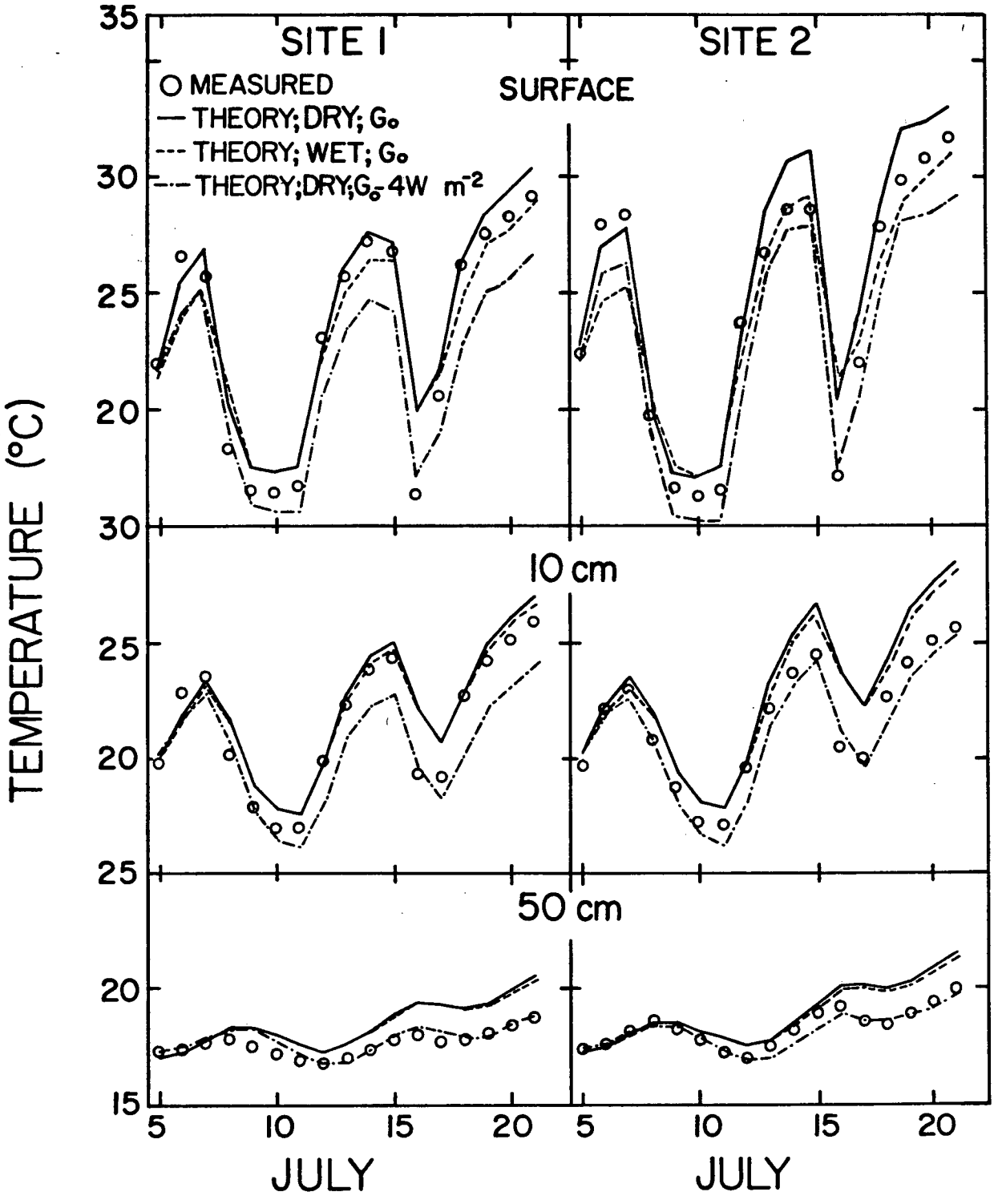

FIGURE 2.7: Measured and theoretically calculated daily average temperatures at the 0, 10, and 50 cm depths at sites 1 and 2 during the site 2 study period. The thermal properties of the upper layer were either maintained at maximum values (WET) or allowed to change according to surface albedo as described in the text (DRY). Either the measured (G_o) or modified (G_o minus 4 W m^{-2}) 24-hour average values of surface heat flux density were used in the calculations.

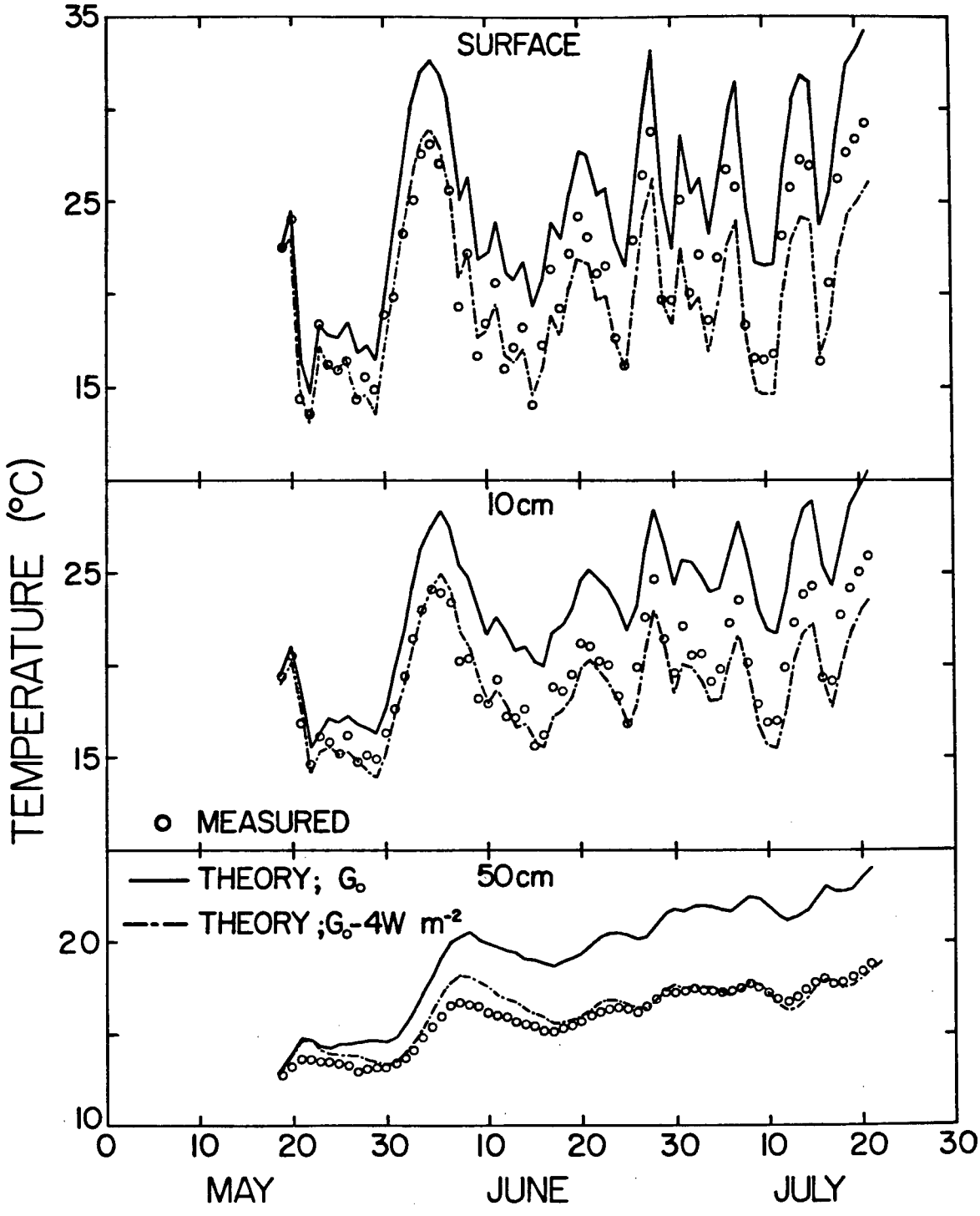

FIGURE 2.8: Measured and theoretically calculated daily average temperatures at the 0, 10, and 50 cm depths at site 1. Either the measured (G_o) or modified (G_o minus 4 W m^{-2}) values of surface heat flux density were used in the calculations.

were 1.0 - 1.8°C, 2.8 - 3.8°C, and 1.7 - 2.7°C respectively. At the 10 and 50 cm depths, the theory predicted that temperatures at site 2 would exceed those at site 1 by 1.3 - 1.5°C and 0.9°C respectively on July 19-21. The measured values (site 2 minus site 1) were -0.2°C and 0.8 - 1.1°C respectively. In view of the similar temperatures at 10 (and 20) cm at both sites, the higher measured temperatures at site 2 at 50 cm were attributed to differences in texture between the sites at about that depth, noted upon installation of the thermocouples.

It was difficult to identify exactly the source of all the discrepencies between the theory and measurements. Figure 2.6 demonstrates that the simple two-layered model represented the variation with depth of the measured profiles of k and C only marginally well for the driest soil conditions at both sites, especially at site 1 and at depths near z=d. The profiles of C measured on June 2 and July 21 differed greatly, despite the similar indicated surface albedos on these days. The time dependence of C_1 and k_1 was not accounted for explicitly in the theory. Despite these drawbacks the theory did correctly indicate the orders of magnitude of the effects of tillage and drying. It would be expected that at sites with deeper water tables and longer drying periods the theory would perform better. Furthermore it would be appropriate when considering the effects of surface mulches and plant cover, since the thermal properties of these change slowly with time and usually differ greatly from the underlying soil (Watson, 1973).

The calculations of the initial-value solution given by (22) showed that except for the first 2 days of each run, the daily average temperature profile in the first 10 cm of soil was isothermal to within 0.05°C. This confirmed that neglecting the layering for this part of the complete

solution was valid.

The dashed lines in Figure 2.7 demonstrate that the systematic overestimate by the theory (which as shown in Figure 2.8 was ~ 5°C at 50 cm by the end of the complete site 1 study period) was not related to the manner in which the near-surface soil drying was accounted for. Neither uncertainties in the initial conditions below 100 cm nor in the thermal properties used for the semi-infinite layer could account for all of the overestimate. Changing the annual average temperature, T_{aa}, to 4°C only reduced the overestimate by 1.5 - 1.7°C for all three depths by the end of the site 1 experimental period, i.e. after about 65 days. Increasing C_2 to 2.8 MJ m^{-3} $°C^{-1}$ and k_2 to 1.1 W m^{-1} $°C^{-1}$ decreased the overestimate at 50 cm depth by ~ 2°C by the end of the site 1 study period.

To test the sensitivity of the theory to errors in 24-hour average G_o, the calculations were carried out with G_o reduced by 4 W m^{-2}, as shown in both figures (dot-dashed lines). This reduction in G_o considerably improved the agreement between the theoretical calculations and the observations, especially at the 50 cm depth. However temperatures near the surface were then underestimated on the final days of both study periods; this may have been due to differences between actual and modelled profiles of k and C on these days, particularly at site 1 (Figure 2.6). Since the measurement of half-hour average soil surface heat flux densities to better than ± 10 W m^{-2} is difficult, the theory is sensitive to small systematic errors in G_o. The reason for this sensitivity is evident upon examination of the monthly averages of measured G_o, which were 11 ± 1 W m^{-2} at both sites for the measurement days in each of May, June, and July where appropriate. Thus 4 W m^{-2} represented almost a 40%

error in these monthly averages.

The sources of this apparent bias in the reported (in Chapter 1) measurements of surface heat flux density for the two sites are difficult to identify considering the accuracy, mentioned above, of the half-hour measurements. An error of 4 $W m^{-2}$ represented only about a 5-10% error in maximum daytime and nighttime average G_o and about a 15-20% error in maximum 24-hour average G_o, so that the major conclusions derived from the originally measured G_o remain essentially unchanged. One source of the systematic overestimate may have been the neglect of diurnal changes in C arising from the upward movement of moisture at night; calculations show that this could have resulted in an overestimate of 24-hour average G_o ~ 2-3 W m^{-2}. It was indicated earlier that the errors in measured near-surface temperature resulted in an overestimate of 24-hour average G_o of < 2 $W m^{-2}$. Thus determining monthly or even 2-week averages of G_o from half-hour measurements is fraught with difficulty. The results suggest that the theory presented herein can be used to determine these averages with greater accuracy.

B. Convective Heat Transfer

Since the monthly averages of G_o were so small (as is typical in soils) it was of interest to investigate the significance of convective heat flow due to moisture movement, which was assumed to be negligible in both the theoretical and measurement calculations. The partial differential equation governing heat transfer in a homogenous medium in which a steady movement of fluid is occurring with velocity v (positive downward) is given by

$$C\frac{\partial T}{\partial t} = -\frac{\partial G}{\partial z} - C_f v\frac{\partial T}{\partial z} = k\frac{\partial^2 T}{\partial z^2} - C_f v\frac{\partial T}{\partial z} \qquad (30)$$

where C_f is the volumetric heat capacity of the fluid. Integrating this equation between o and z yields:

$$\int_o^z C\frac{\partial T}{\partial t}\,dz = (G_o - G_z) - C_f v(T_z - T_o) \qquad (31)$$

It has been inferred (Chapter 1) that the average upward liquid moisture flow rate at site 1 was ~ 0.001 - 0.002 m d^{-1}. With C_f = 4.2 MJ m^{-3} $°C^{-1}$ and $|T_z - T_o|$ ~ 10 - 20°C for z ~ 1-2 m, the convective term in (31) is then ~ -1 W m^{-2}. Since $(G_o - G_z)$ < 5-10 W m^{-2}, the convective term was at least 10-20% of the conductive term on a monthly time scale. The solution to (30) with G_o a given function of time and the initial temperature distribution f(z) = 0 was derived by the method of Laplace transforms and is as follows:

$$T(z,t) = \int_o^t G_o(t-\lambda)\left\{\frac{e^{-pz-\frac{p^2k\lambda}{C}-\frac{z^2C}{4k\lambda}}}{(\pi kC\lambda)^{\frac{1}{2}}} + \frac{p}{C}\,\mathrm{erfc}\left[\frac{z}{2}\sqrt{\frac{C}{k\lambda}} - p\sqrt{\frac{k\lambda}{C}}\right]\right\} d\lambda \qquad (32)$$

where $p = C_f v(2k)^{-1}$. Evaluating (32) with G_o = 10 W m^{-2}, v = -0.002 m d^{-1}, C_f = 4.2 MJ m^{-3} $°C^{-1}$, k = 0.9 W m^{-1} $°C^{-1}$, and C = 2.6 MJ m^{-3} $°C^{-1}$ shows that after 65 days temperatures in the upper 100 cm of soil were all reduced by 0.9 - 1.3 °C compared with the v = 0 case. Thus this mode of heat transfer may have partially contributed to the disagreement between theory and observations. Examination of (31) shows that formally neglecting the convective term would lead to an underestimate of 24-hour average G_o by the null-alignment method, although the error is small compared with the "noise" inherent in the G_o measurement.

Convective heat transfer by vapour movement may be analyzed in a manner similar to that for liquid flow. Generally this is significant only in the near-surface soil layers in which adequate drying has occurred.

In this case C_f = 1.85 MJ m^{-3} $°C^{-1}$ (per m^3 of equivalent liquid water), $|v| < 0.002$ m d^{-1}, and $|T_z - T_o| < 4°C$ for z ~ 10-20 cm, so that the convective term in (31) is < 0.2 W m^{-2}. However vapour movement also transports latent heat according to the relation $G_{vL} = \rho_w L_w v$ with L_w = 2.5 MJ kg^{-1} and ρ_w = 1000 kg m^{-3}. Some of this heat flux is accounted for implicitly in the apparent (measured) thermal conductivities, while some is due to gradients in volumetric moisture content, θ_v, according to the expression

$$G_{vL}^{\theta} = - \rho_w L_w \kappa_{\theta v} \frac{d\theta_v}{dz} \qquad (33)$$

in which $\kappa_{\theta v}$ is negligible for $\theta_v > 0.15$ (Philip, 1957; Jackson et al. 1975). According to these authors, $\kappa_{\theta v}$ is ~ 10^{-10} - 5 x 10^{-9} m^2 s^{-1}, so that with $d\theta/dz$ ~ 1-10 m^{-1} the magnitude of this term is ~ 0.2 - 130 W m^{-2}. This is the energy used in evaporation at sites below the soil surface, so that (33) is only of importance in the upper few cm of soil for the driest soil conditions, and does not affect the heat transfer at greater depths. According to Philip (1957) surface temperatures would be underestimated by < 1°C if heat transfer by (33) were neglected. It was pointed out in Chapter 1 that the minimum near-surface thermal conductivities measured at both sites may have been underestimated due to neglecting (33), and so some compensation would have occurred in the tests of the theory presented earlier.

C. Diurnal Fluctuations

Measured values of $(T_{max} + T_{min})/2$ are plotted versus measurements of 24-hour average temperature at the 0 and 10 cm depths (Figure 2.9). The diurnal variations at the 50 cm depth were generally < 0.5°C and so were not considered. The arithmetic average of the maximum and minimum

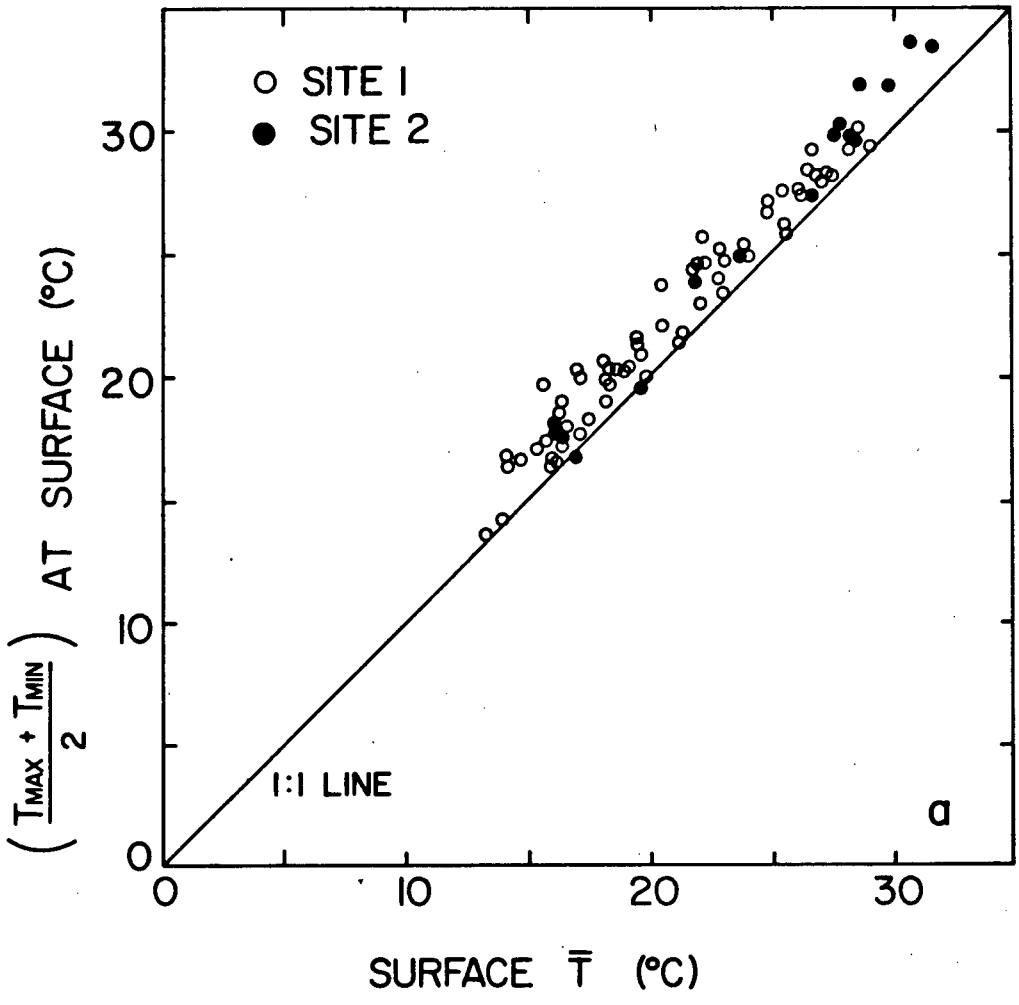

FIGURE 2.9a: Comparison of measured values of $(T_{max} + T_{min})/2$ with measured 24-hour average temperatures ($\bar{T}$) at the surface of both sites.

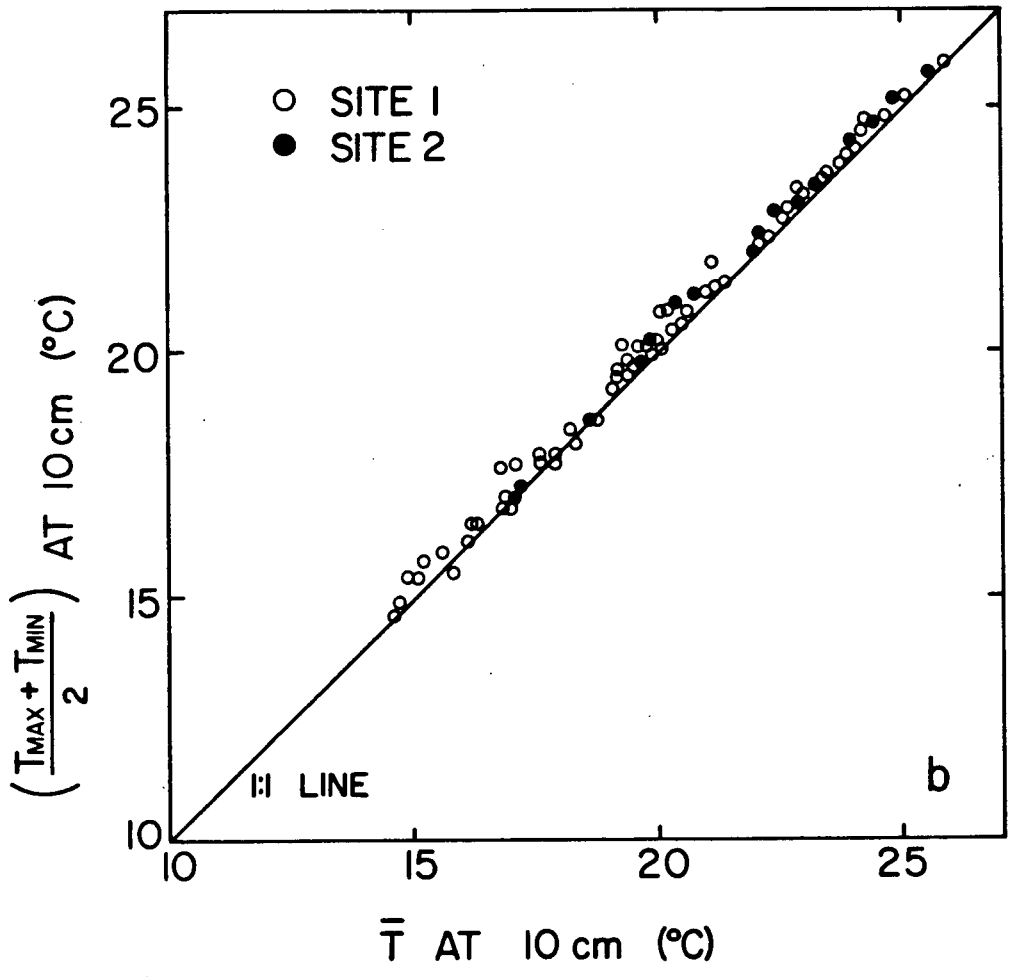

FIGURE 2.9b: As in Figure 2.9a except for the 10 cm depth.

temperatures represented the 24-hour average temperature quite well, especially at 10 cm. The improvement with depth is not unexpected since it can be shown from (1) that the higher frequency (Fourier) components of a surface disturbance are filtered out with increasing depth. This justified calculating maximum and minimum temperatures from 24-hour average temperatures and diurnal amplitudes, as was presented in the procedures section. Clear-day values of $||G_o||$ calculated from G_o^{24} and G_o^d using (28) and (29) were on average 0.86 ± 0.15 and 0.91 ± 0.15 of measured values at sites 1 and 2 respectively (Figure 2.10). The measured values were calculated by halving the difference between maximum and minimum values. Clear days were defined as those with S > 90% of the maximum observed (24-hour average) value (340 W m^{-2}). The underestimate reflected the deviation from exact sinusoidal behaviour by the observed diurnal time courses of G_o on these days (Chapter 1).

The calculated values of $(T_{max} - T_{min})$ i.e. twice the diurnal amplitudes at 0 and 10 cm depths, both with the drying of the upper layer accounted for and with k_1 and C_1 maintained at their respective maximum values, are plotted versus measured values in Figure 2.11. The importance of accounting for the drying of the upper layer is evident. The calculated values were generally less than the measured values at 10 cm and at the surface for measured $(T_{max} - T_{min}) < 25°C$ (even when the drying of upper layer was accounted for). This was in large part due to transient effects arising from the change in 24-hour average temperature between successive days as well as the underestimate of calculated $||G_o||$ mentioned above. The former would have led to an underestimate regardless of whether the soil was warming or cooling (for small enough diurnal amplitudes). For surface measurements of $(T_{max} - T_{min}) > 25°C$ the agreement is better, especially

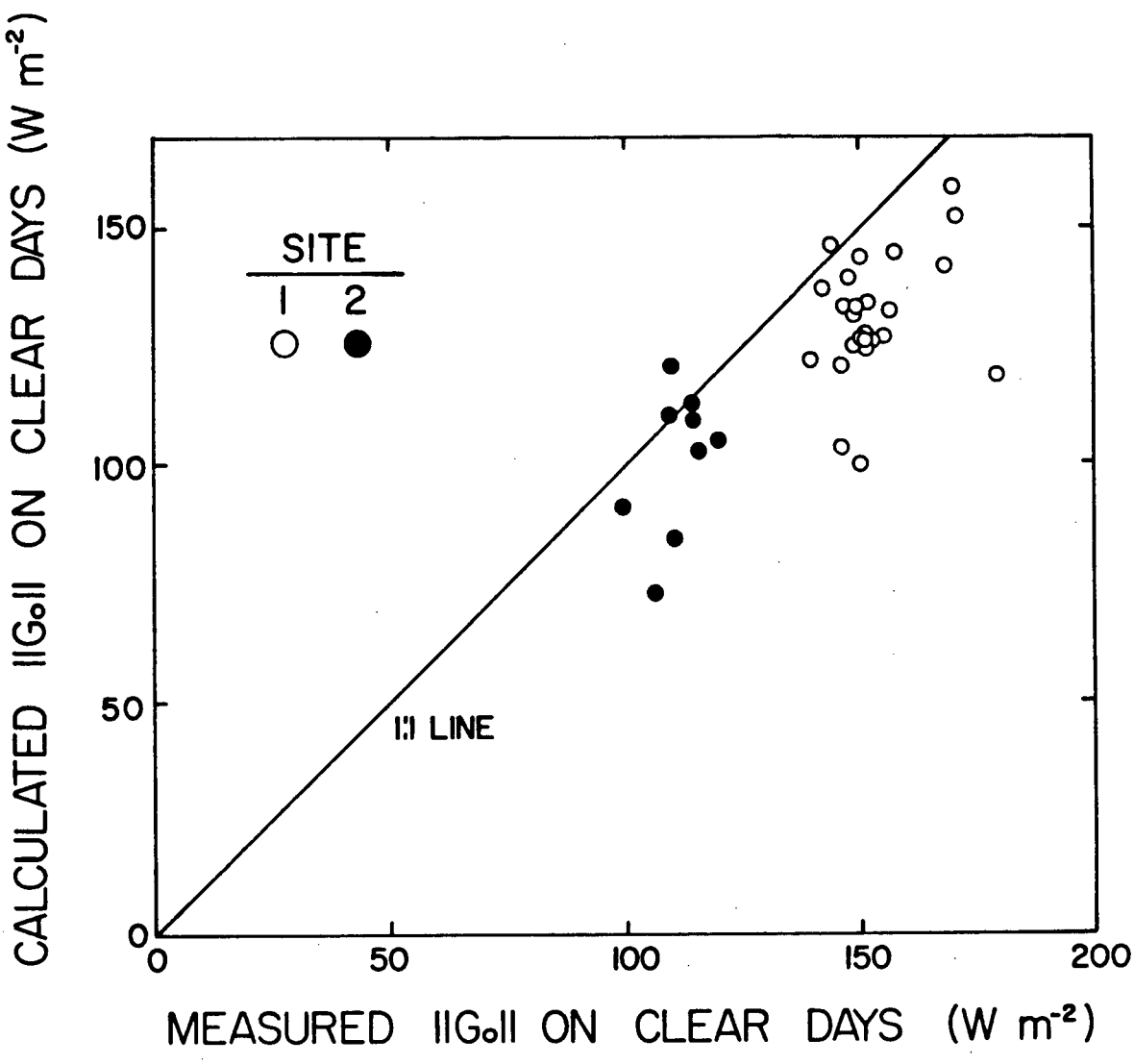

FIGURE 2.10: Comparison of calculated and measured values of $||G_o||$ on clear days at both sites.

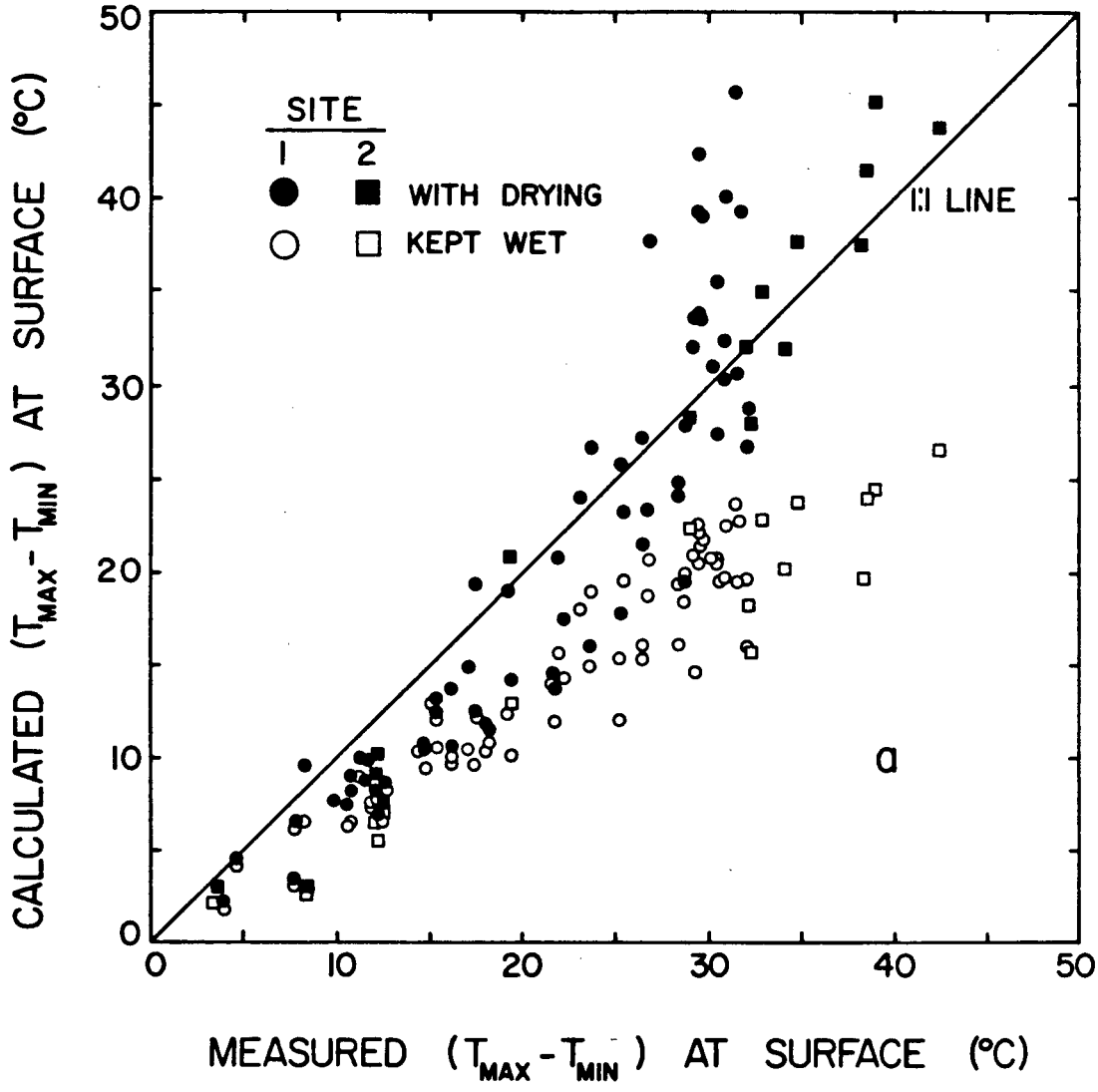

FIGURE 2.11a: Comparison of calculated and measured values of (T_{max} - T_{min}) at the surface of both sites, with and without the drying of the upper layer accounted for as described in the text.

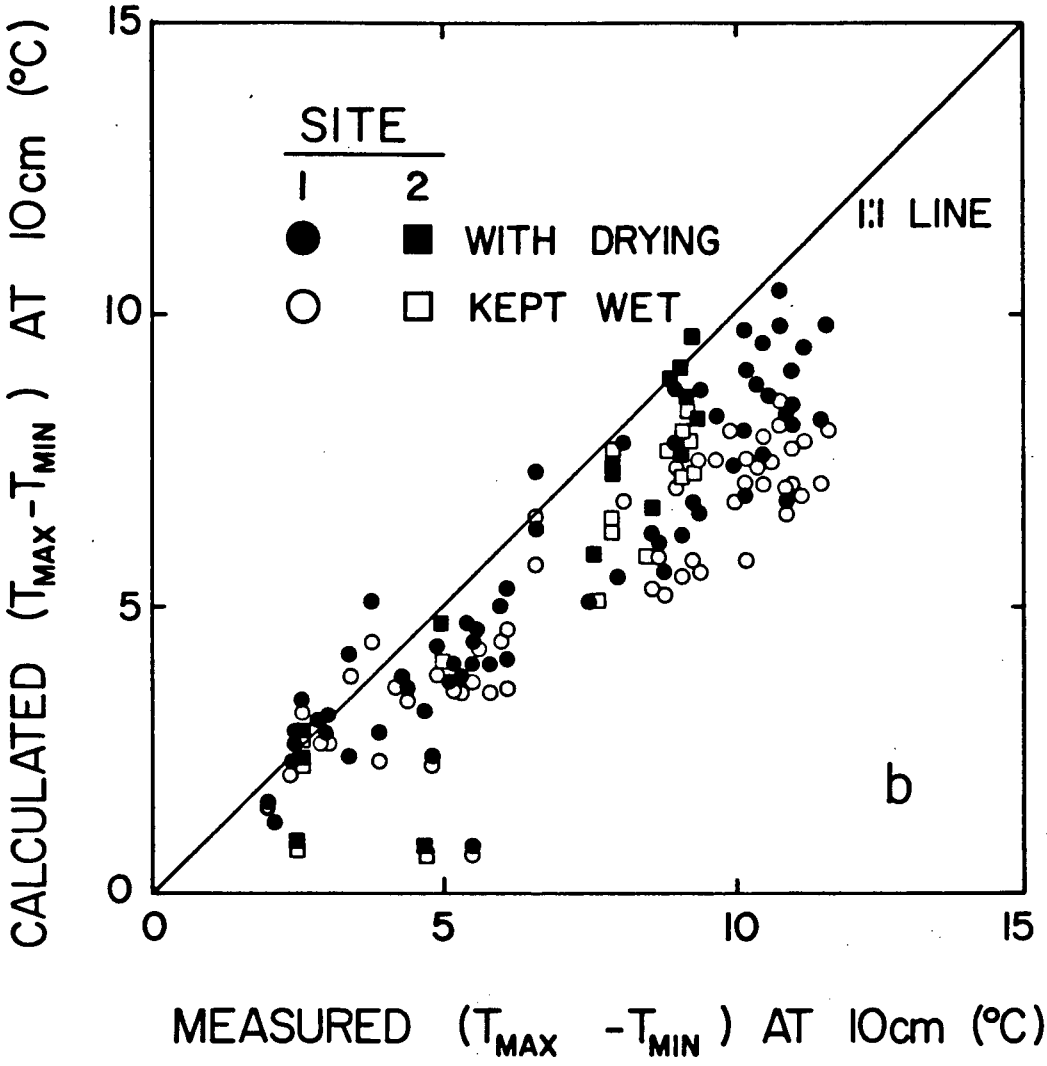

FIGURE 2.11b: As in Figure 2.11a except at the 10 cm depth.

at site 2 and despite the underestimate of $||G_o||$. For site 1, the results showed that differences between the modelled and measured profiles of k and C for dry-soil conditions were critical in determining the diurnal surface variations (thus the scatter for measured surface values of ($T_{max} - T_{min} >$ 28°C). According to Chapter 1, effective soil admittances can be defined as

$$\mu_s = \frac{||G_o||}{||\dot{T}_o|| \sqrt{\omega}} \tag{34}$$

Using (34) and taking into account the respective underestimates of $||G_o||$ mentioned above, the layered model with drying underestimated μ_s by as much as 40% at site 1 and as much as 15% at site 2 on the clear days for dry-soil conditions. The better agreement at site 2 may have been related to the greater surface drying that occurred there.

2.5 Concluding Remarks

The exact solution to (1), with the surface heat flux density given as an arbitrary function of time and with a zero initial temperature distribution, was derived. This solution, combined with the solution to the initial-value problem for a homogeneous semi-infinite medium insulated at its surface, is useful in assessing the effects of tillage and drying on 24-hour average soil temperatures, except at depths near z = d at which some distortion occurs. For sites where the surface drying or tillage is deeper and the climate hotter and drier, use of this solution to determine daily average near-surface temperatures would be even more appropriate than for the relatively wet sites at Agassiz. For sites of the latter type, the derivation of a solution in which the variation of C and k with depth and time is better represented than by the simple two-layered model is desirable. The layered solution should be useful in evaluating the effects on soil temperature due to surface residues, plant cover, or artificial

mulches such as polyethylene plastic sheets placed above the surface. Transient effects and deviations from sinusoidal behaviour did not greatly affect the calculation of daily maximum and minimum temperatures using a simple procedure based upon the harmonic solution of (1). However the layered model, with drying, did underestimate effective daily soil admittances for dry-soil conditions, particularly at site 1.

The calculations require specification of the initial temperature distribution f(z), 24-hour and daytime average G_o, and C, k, and d of the layers. The latter three quantities can be estimated from bulk density, organic matter fraction, soil texture, and daily moisture content data. Near-surface moisture contents may either be estimated empirically or predicted by solution of the equation governing soil-moisture movement. The calculated daily average temperatures were relatively insensitive to uncertainties in initial temperatures and thermal properties at depth but were sensitive to small systematic errors in 24-hour average G_o over periods > 10 days. Consequently determining averages of G_o for such periods from half-hourly or 24-hour averages of G_o is difficult. The results suggested that the theory could be used with measured temperature profiles to improve the estimation of these averages of surface heat flux density. Calculations showed that convective heat transfer by liquid moisture movement had a < 20% effect on soil temperature change for periods < 70 days, and that convective heat transfer by vapour movement was negligible except in the upper few cm of soil for the driest soil conditions. The sensitivity of the theoretical calculations to small systematic errors in G_o as well as the relative importance of convective heat transfer applies to other solutions, including numerical, of the one-dimensional soil heat transfer equations in which G_o is used as an upper

boundary condition. In many management applications it is the difference in temperatures between treatments that is of greatest interest. In these cases the approach based upon using G_o as an upper boundary condition will be most useful. For applications in which the prediction of absolute temperature is required for periods > 10 days, an approach based upon specifying T_o as the upper boundary condition would probably produce better results. In basic studies that attempt to correctly partition the energy received at the earth's surface among the various energy balance components the approach based upon using G_o is potentially more useful.

2.6 Literature Cited

Allmaras, R.R., E.A. Hallauer, W.W. Nelson, and S.D. Evans, Surface energy balance and soil thermal property modifications by tillage-induced soil structure, Minn. Agric. Exp. Stn. Tech. Bull. 306, 1977.

Army, T.J., and E.B. Hudspeth, Jr., Alteration of the microclimate of the seed zone, Agron. J., 52, 17-22, 1960.

Baier, W., and A.R. Mack, Development of soil temperature and soil water criteria for characterizing soil climates in Canada, In: Field Soil Water Regime, R.R. Bruce et al., Eds., Spec. Publ. 5, pp. 195-212, Soil Sci. Soc. Amer., Madison, Wis., 1973.

Boatwright, G.O., H. Ferguson, and J.R. Sims, Soil temperature around the crown node influences early growth, nutrient uptake, and nutrient translocation of spring wheat, Agron. J., 68, 227-231, 1976.

Carslaw, H.S., and J.C. Jaeger, Conduction of Heat in Solids, 2nd ed., Oxford University Press, London, 1959.

Cruse, R.M., D.R. Linden, J.K. Radke, W.E. Larson, and K. Larntz, A model to predict tillage effects on soil temperature, Soil Sci. Soc. Amer. J., 44, 378-383, 1980.

de Vries, D.A., Thermal properties of soils, In: Physics of Plant Environment, W.R. van Wijk, Ed., North-Holland Publ. Co., Amsterdam, pp. 210-235, 1966.

de Vries, D.A., Heat transfer in soils, In: Heat and Mass Transfer in the Biosphere, Part 1 - Transfer Processes in the Plant Environment, D.A. de Vries and N.H. Afgan, Eds., Scripta Book Co., John Wiley and Sons, New York, pp. 5-28, 1975.

Fairbourn, M.L., Effect of gravel mulch on crop yields, Agron. J., 65, 925-928, 1973.

Gupta, S.C., J.K. Radke, and W.E. Larson, Predicting temperatures of bare and residue covered soils with and without a corn crop, Soil Sci. Soc. Am. J., 45, 405-412, 1981.

Hanks, R.J., D.D. Austin, and W.T. Ondrechen, Soil temperature estimation by a numerical method, Soil Sci. Soc. Amer. Proc., 35, 665-667, 1971.

Hegarty, T.W., Temperature relations of germination in the field, In: Seed Ecology - Proceedings of the Nineteenth Easter School in Agricultural Science, University of Nottingham, 1972, W. Heydecker, Ed., London, Butterworths, 1973.

Idso, S.B., T.J. Schmugge, R.D. Jackson, and R.J. Reginato, The utility of surface temperature measurements for the remote sensing of surface soil water status., J. Geophys. Res., 80, 3044-3049, 1975a.

Idso, S.B., R.D. Jackson, R.J. Reginato, B.A., Kimball, and F.S. Nakayama, The dependence of bare soil albedo on soil water content, J. Appl. Meteorol., 14, 109-113, 1975b.

Jackson, R.D., B.A. Kimball, R.J. Reginato, S.B. Idso, and F.S. Nakayama, Heat and water transfer in a natural environment, In: Heat and Mass Transfer in the Biosphere, Part 1 - Transfer Processes in the Plant Environment, D.A. de Vries and N.H. Afgan, Eds., Scripta Book Co., John Wiley and Sons, New York, pp. 67-76, 1975.

Kimball, B.A., Smoothing data with cubic splines, Agron. J., 68, 126-129, 1976.

Kimball, B.A., and R.D. Jackson, Soil heat flux determination: a null-alignment method, Agric. Meteorol., 15, 1-9, 1975.

Kohnke, H., and C.H. Werkhoven, Soil temperature and soil freezing as affected by an organic mulch, Soil Sci. Soc. Proc., 27, 13-17, 1963.

Madderom, P., UBC INTEGRATION: Integration (Quadrature) Routines, Computing Centre, Univ. British Columbia, 1978.

Moody, J.E., J.N. Jones, Jr., and J.H. Lillard, Influence of straw mulch on soil moisture, soil temperature and the growth of corn, Soil Sci. Soc. Proc., 27, 700-703, 1963.

Ouellet, C.E., Macroclimate model for estimating monthly soil temperatures under short-grass cover in Canada, Can. J. Soil Sci., 53, 263-274, 1973.

Ouellet, C.E., R. Sharp, and D. Chaput, Estimated monthly normals of soil temperature in Canada, Tech. Bull. 85, Canadian Department of Agriculture, Ottawa, 1975.

Papendick, R.I., M.J. Lindstrom, and V.L. Cochran, Soil mulch effects on seedbed temperature and water during fallow in eastern Washington, Soil Sci. Soc. Amer. Proc., 37, 307-314, 1973.

Philip, J.R., Evaporation, and moisture and heat fields in the soil, J. Meteorol., 14, 354-366, 1957.

Phipps, R.H., and J. Cochrane, The production of forage maize and the effect of bitumen mulch on soil temperature, Agric. Meteorol., 14, 399-404, 1975.

Reimer, A., and C.F. Shaykewich, Estimation of Manitoba soil temperatures from atmospheric meteorological measurements, Can. J. Soil Sci., 60, 299-309, 1980.

Reinsch, C.H., Smoothing by spline functions, Numer. Math., 10, 177-183, 1967.

Riha, S.J., K.J. McInnes, S.W. Childs, and G.S. Campbell, A finite element calculation for determining thermal conductivity, Soil Sci. Soc. Amer. J., 44, 1323-1325, 1980.

Spiegel, M.R., Schaum's Outline of Theory and Problems of Laplace Transforms, Schaum Publ. Co., New York, 1965.

van Duin, R.H.A., Influence of tilth on soil and air temperature, Neth. J. Agric. Sci., 2, 229-241, 1954.

van Wijk, W.R., and W.J. Derksen, Sinusoidal temperature variation in a layered soil, In: Physics of Plant Environment, W.R. van Wijk, Ed., North-Holland Publ. Co., Amsterdam, pp. 171-209, 1966.

Walker, J.M., One-degree increments in soil temperatures affect maize seedling behaviour, Soil Sci. Soc. Amer. Proc., 33, 729-736, 1969.

Watson, K., Periodic heating of a layer over a semi-infinite solid, J. Geophys. Res., 78, 5904-5910, 1973.

Wierenga, P.J., and C.T. de Wit, Simulation of heat transfer in soils, Soil Sci. Soc. Amer. Proc., 34, 845-848, 1970.

CHAPTER 3

TEST OF AN EQUATION FOR EVAPORATION FROM BARE SOIL

TEST OF AN EQUATION FOR EVAPORATION FROM BARE SOIL

3.1 Introduction

Since evaporation is a major component of the spring and summer soil water balance, and latent heat flux a major component of the surface energy balance, investigation of evaporation relationships was considered a major part of the Agassiz study. There are few practical formulae reported in the literature for calculating the evaporation from bare soil. Recently, Idso et al. (1979) presented a simple empirical formula, well adapted to remote sensing, for the 24-hour average latent heat flux density from bare Avondale loam soil, as follows:

$$LE_{I,II,III} = (\frac{3}{8} + \frac{5}{8}\beta)(S_N + 1.56\ L_N + 76) \qquad (1)$$

where S_N and L_N are the 24-hour average net solar and net longwave radiation flux densities respectively, β is the soil surface wetness partitioning factor, and all energy flux densities are in W m^{-2}. The factor β was originally defined in Jackson et al. (1976) as

$$\beta = (\alpha_d - \alpha)/(\alpha_d - \alpha_w) \qquad (2)$$

where α_d is the dry soil albedo, α_w is the wet soil albedo and α is the daytime average albedo on any given day. β varies from 1 to 0 as the soil surface changes from wet to dry. The Roman numeral subscripts indicate that (1) applies to all three stages of soil drying, as defined in Idso

---

Parts of this chapter were presented at the 15th Conference on Agriculture and Forest Meteorology and Fifth Conference on Biometeorology, April 1-3, 1981, Anaheim, California.

et al. (1974).

Stage I, or potential, evaporation occurs for $\beta = 1$ and at a rate given by

$$LE_I = PLE = S_N + 1.56\ L_N + 76 \qquad (3)$$

The development of (3) from the Avondale loam evaporation and climate data was described by Idso et al. (1975). Its validity was shown to extend over all four seasons in Phoenix, Arizona. Idso et al. (1977) further extended its validity to crop, soil, and water surfaces in both Arizona and California.

Stage III, or soil moisture limited, evaporation occurs for $\beta = 0$. From (1) it is seen that it takes place at a rate equal to 3/8 times the potential rate expression (3). Idso et al. (1979) showed that expressing the stage III evaporation in this manner absorbed the seasonal variation in this rate. They speculated that this expression might account for variations due to soil type as well. They also noted that modelling stage III in this manner represents a considerable simplification over a more complete procedure, such as that described in Jackson et al. (1976).

Stage II, or the transition stage, evaporation occurs for $0 < \beta < 1$. Their model for this stage is a soil surface partitioned into patches evaporating at either stage I or stage III rates, with the partitioning determined by β.

The purpose of this chapter is primarily to report on the evaluation of equation (1) using the data set obtained in the Agassiz study described in the previous chapters. In addition, the Priestley-Taylor (1972) method of describing stage I evaporation, which has received a good deal of attention in the last 8 years, is evaluated. The Idso et al.

(1979) approach, described above, is discussed on the basis of available evaporation theory. Since the cool, wet, and cloudy climatic conditions at Agassiz contrasted sharply with the mostly clear-sky conditions of Phoenix, and since two contrasting tillage treatments were studied (culti-packed versus disc-harrowed), this was felt to be an opportunity for a demanding test of equation (1).

3.2 Theoretical Considerations

Numerous expressions have been presented in the literature to calculate potential evaporation; these have been reviewed by McNaughton et al. (1979), Sellers (1965), Tanner and Richie (1974). Perhaps the most basic of them is that given by Penman (1948):

$$PLE = \frac{s_v}{s_v + \gamma_v}(R_N - G_o) + \frac{\rho_a c_p}{s_v + \gamma_v} h_z(e_z^* - e_z) \qquad (4)$$

where R_N is the net radiation flux density, G_o is the soil surface heat flux density, h_z is the bulk vapour and heat transfer coefficient (similarity assumed), e_z^* and e_z are the saturated and actual vapour pressures at height z above the soil surface, s_v is the slope of the saturated vapour pressure function, γ_v is the psychrometric constant, and ρ_a and c_p are the density and specific heat of the atmosphere respectively. In deriving (4) it is assumed that the vapour pressure at the soil surface is equal to the saturated vapour pressure at the soil surface temperature. Equation (4) contains a large number of variables, some of which are quite difficult to evaluate routinely or remotely, especially the transfer coefficient h_z. Furthermore, despite its physical basis, the Penman equation is limited in theoretical applications since the variables it contains are not independent. For example, a change in windspeed will

affect every variable in (4) in a manner that, except perhaps for h_z, cannot be directly predicted other than by more fundamental analyses, such as McNaughton (1976a and b) and Lettau (1951). In essence Idso et al. (1975) are postulating that the interdependence of the parameters in (4) is such that the potential evaporation rate can be related solely to net solar and net longwave radiation flux densities as given in (3).

Another equation that has received prominence more recently is that presented by Priestley and Taylor (1972):

$$PLE = a_{PT} \frac{s_v}{s_v + \gamma_v} (R_N - G_o) \tag{5}$$

with a_{PT} ranging from 1.2 to 1.3 in "advection-free" conditions. Except for the soil heat flux density term, which can usually be neglected for 24-hour averages, this equation is simple and well adapted to remote sensing. Jury and Tanner (1975) present a procedure to correct a_{PT} for advection; however, their method requires extensive local calibration and is restricted to relatively narrow ranges of advective effects. The arguments presented by Idso et al. (1975) suggest that (3) should describe potential evaporation rates throughout the complete range of possible advective conditions, i.e. in "windy, dry situations" as well as in "calm, humid situations".

Figure 3.1 schematically describes the theoretical and laboratory results concerning the evaporation from bare soil discussed in Gardner and Hillel (1962), Gardner and Fireman (1958), Gardner (1959), and Gardner (1962). The figure shows cumulative evaporation versus time from a homogeneous soil, initially uniformly wetted to near saturation, for a range of PLE values and during a single drying period. Figure 3.1a applies to a soil either wetted to or bounded by an impermeable layer at some

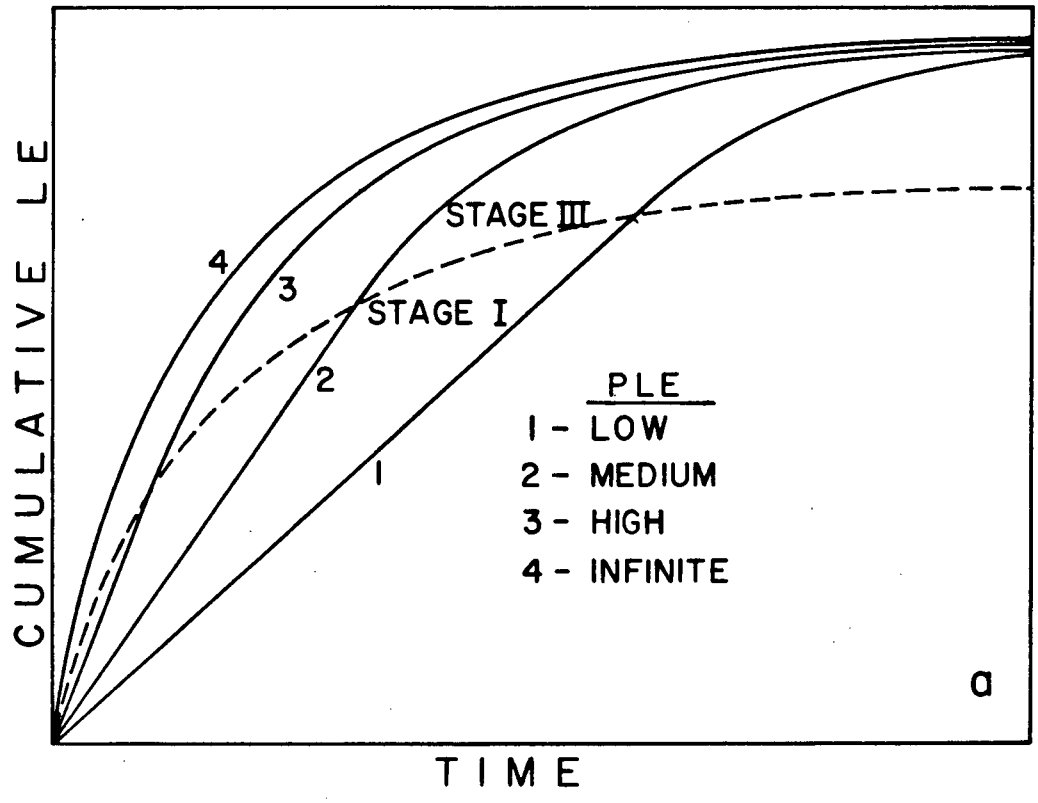

FIGURE 3.1a: Schematic plots of cumulative evaporation versus time from a homogeneous soil, initially uniformly wetted to near saturation, for a range of PLE values and during a single drying period. The soil is either wetted to or bounded by an impermeable layer at some depth.

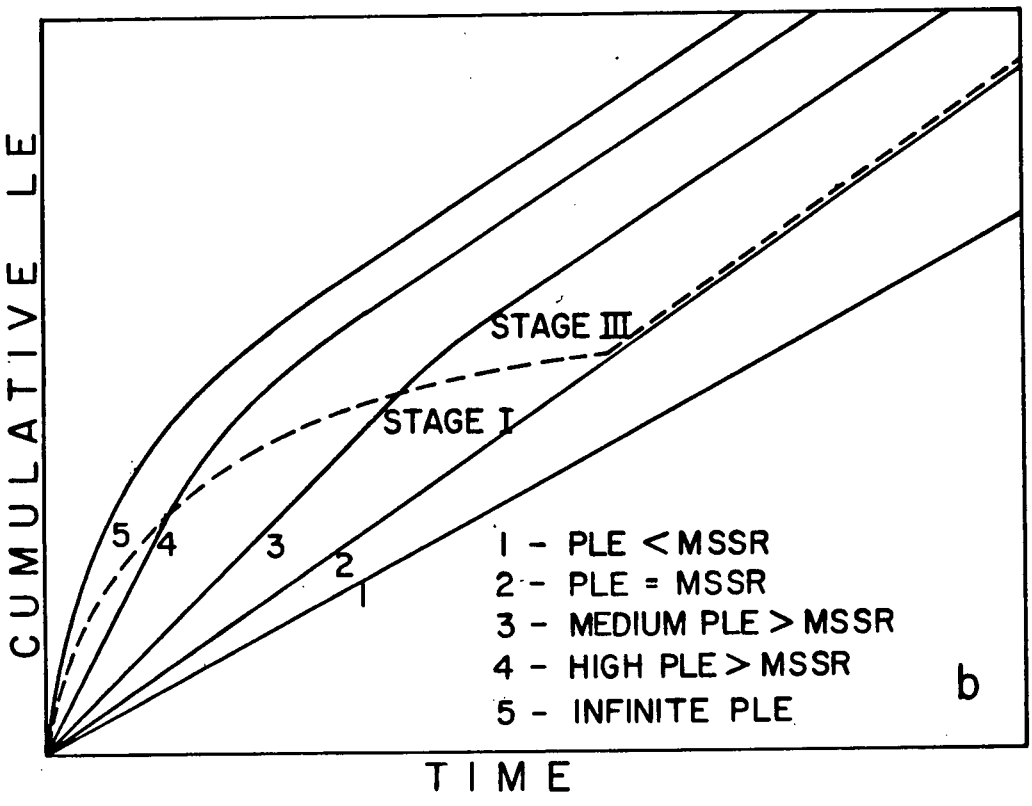

FIGURE 3.1b: As in Figure 3.1a except that the soil is bounded by a water table at some depth.

depth. Increasing this depth shifts the stage III parts of all of the curves and the dashed curve upward. The cumulative evaporation approached asymptotically in time by all of the curves is the same and the evaporation rate approached asymptotically is 0. Figure 3.1b applies to a soil bounded by a water table at some depth. The evaporation rate designated as MSSR is the maximum steady-state rate possible from the water table source, and is calculated by assuming an infinitely negative surface moisture potential. It is seen that for PLE > MSSR, the rate approached asymptotically in time is MSSR while for PLE < MSSR the soil maintains the potential rate. Increasing the depth to the water table shifts the stage III of all of the curves and the dashed curve downward, and decreases MSSR.

The dashed lines in the figure represent the transition from potential (stage I) rates to soil moisture limited (stage III) rates. Stage II of Idso et al. (1974) is not defined within Gardner's framework; it only has significance in field studies, where because of soil heterogeneity the time to this transition is spatially variable. During stage III, the evaporation rates are essentially only a function of soil moisture content. It is evident that the higher the potential evaporation rate, the sooner the transition to stage III and the higher the moisture content at this transition. Hence the initial stage III evaporation rates are higher for higher potential evaporation rates, which since PLE is a strong function of S_N implies that LE_{III} is seasonally dependent. According to Gardner and Hillel (1962), the stage III curve for any value of PLE in either figure can be found approximately by translating the infinite PLE curve in time by an amount equal to t_{III}, the number of days required to reach the transition to stage III. For values of depth of

wetting large enough or water tables deep enough, Gardner (1959) shows that that the infinite PLE curve can be described by the relation

$$(LE)_{PLE = \infty} = F\ t^{-\frac{1}{2}} \qquad (6)$$

where t is the time in days from the initial wetting and F is a constant related to the hydraulic diffusivity of the soil. This type of relationship has been verified in the field in several studies (Ritchie, 1972; Black et al., 1969). Jackson et al. (1976) found that F was a function of soil temperature and hence varied with season. This effect is not accounted for in the theoretical and laboratory results shown in Figure 3.1.

Figure 3.1 demonstrates that eventually the stage III evaporation rates of all the curves become independent of the potential evaporation rate. This result seems incompatible with the idea implicit in (1) that LE_{III} is proportional to the expression for potential evaporation, except perhaps for a period of time just after the transition to this stage. However, since L_N is generally a decreasing function of time during stage III due to increasing soil surface temperatures, it appears that (3) could simulate some of the square-root of time behaviour of (6).

3.3 Experimental Procedure

The study was carried out at the Agriculture Canada Research Station at Agassiz, British Columbia on a Monroe series loam/silt-loam soil (Degraded Eutric Brunisol) which developed from Fraser River deposits. Soil profiles showed little textural variability to depths of 50 to 100 cm, below which coarser textured layers were often encountered. The water table was located between 1 and 2 meters below the soil surface.

The experiments took place in a 145 x 175 meter level field, normally used for horticultural trials, but kept bare for this study. The surrounding fields were quite level and supported crops throughout the study periods. The tillage treatment at site 1 consisted of disc-harrowing followed by firm packing with a culti-packer and occurred in the first week of May. Data collection at this site was carried out from May 17 to July 21 (site 1 study period). The tillage treatment at site 2 consisted of disc-harrowing which loosened the upper 10 cm of soil. This took place on June 28 on about one third of the field, which consequently reduced the size of site 1 by this amount. Instrumentation at site 2 was almost identical to that of site 1 and data collection there was carried out from July 6 to July 21 (site 2 study period). The instruments were centrally located in both sites and the division of the field was done with due consideration to the prevailing wind directions and fetch requirements. The sites were maintained free of weeds with periodic applications of glyphosate, a broad spectrum herbicide. The bulk densities in the upper 10 cm of soil were 1030 and 870 kg m^{-3} at sites 1 and 2 respectively. Bulk densities below 10 cm were in the range 1000 to 1300 kg m^{-3} at both sites.

Half-hourly integrated evaporation rates were measured throughout the day by the energy balance/Bowen ratio technique, using the same instrumentation described in Black and McNaughton (1971). The reversing psychrometer units (50 cm separation) were mounted (one unit per site) within 1 meter of the soil surfaces, which led to a minimum fetch-height ratio of 80:1. Unit 1 was at site 2 and unit 2 at site 1. Windspeeds were generally quite low, usually falling in the range of 1 to 2 m s^{-1} at 0.95 m above site 1. Net radiation was measured by Swissteco S-1 net

radiometers (one per site) located 0.65 m above the soil surface. Soil surface heat flux densities were calculated half-hourly from soil temperatures measured at 30 depths down to 1 m (one profile per site in which the density of thermocouples decreased logarithmically with depth) and volumetric heat capacity profiles calculated from bulk densities and gravimetric moisture contents (sampled every two days) by using a slightly modified version of the null-alignment method described by Kimball and Jackson (1975). These soil heat flux densities were in good agreement with those measured with heat flux plates constructed in the laboratory in a manner similar to that of Fuchs and Tanner (1968b) after application of Philip's (1961) correction to account for the difference between soil and plate thermal conductivities. Evaporation calculated from gravimetric measurements of changes in soil moisture storage on May 30 and June 5 at site 1 agreed well with the evaporation measured by the energy balance/Bowen ratio instrumentation (Table 3.1). Furthermore the Bowen ratio units were compared by operating them together at site 1 on July 22. As indicated in Figure 3.2 the differences in the Bowen ratios measured by the two units were < 10%. These differences imply errors of < 5% in the half-hourly evaporation rates at Bowen ratios near unity. The differences are related to dissimilarities in the construction of the two units (Spittlehouse and Black, 1981). Further details pertaining to the energy balance and soil temperature instrumentation are found in Chapter 1.

Net longwave radiation flux densities were calculated from measured net and solar radiation flux densities using the relation, $L_N = R_N - S_N = R_N - S(1 - \alpha)$, where S is the 24-hour average solar irradiance. S was measured by a Kipp and Zonen CM5 pyranometer which was continuously integrated while the albedos were measured once every half-hour using inverted

DATE AND TIME PERIOD (ℏ P.S.T.)	CUMULATIVE EVAPORATION MEASURED BY THE BOWEN RATIO SYSTEMS (mm)	CHANGE IN SOIL MOISTURE IN 0-2 cm LAYER (mm)	CHANGE IN SOIL MOISTURE IN 0-9 cm LAYER (mm)	CHANGE IN SOIL MOISTURE IN 0-21 cm LAYER (mm)
May 30 12:00-17:00	2.7	0.9 ± 1	3 ± 1	3 ± 2
June 5 8:00-18:00	3.4	0.7 ± 1	2 ± 1	4 ± 2

TABLE 3.1: Comparison between the evaporation measured by the energy balance/Bowen ratio instrumentation and changes in soil moisture measured gravimetrically at site 1 on May 30 and June 5. The gravimetric results are the average of 9 profiles, taken within a 2-hour period centered on each time and from an area ~ 10 m^2 for each day.

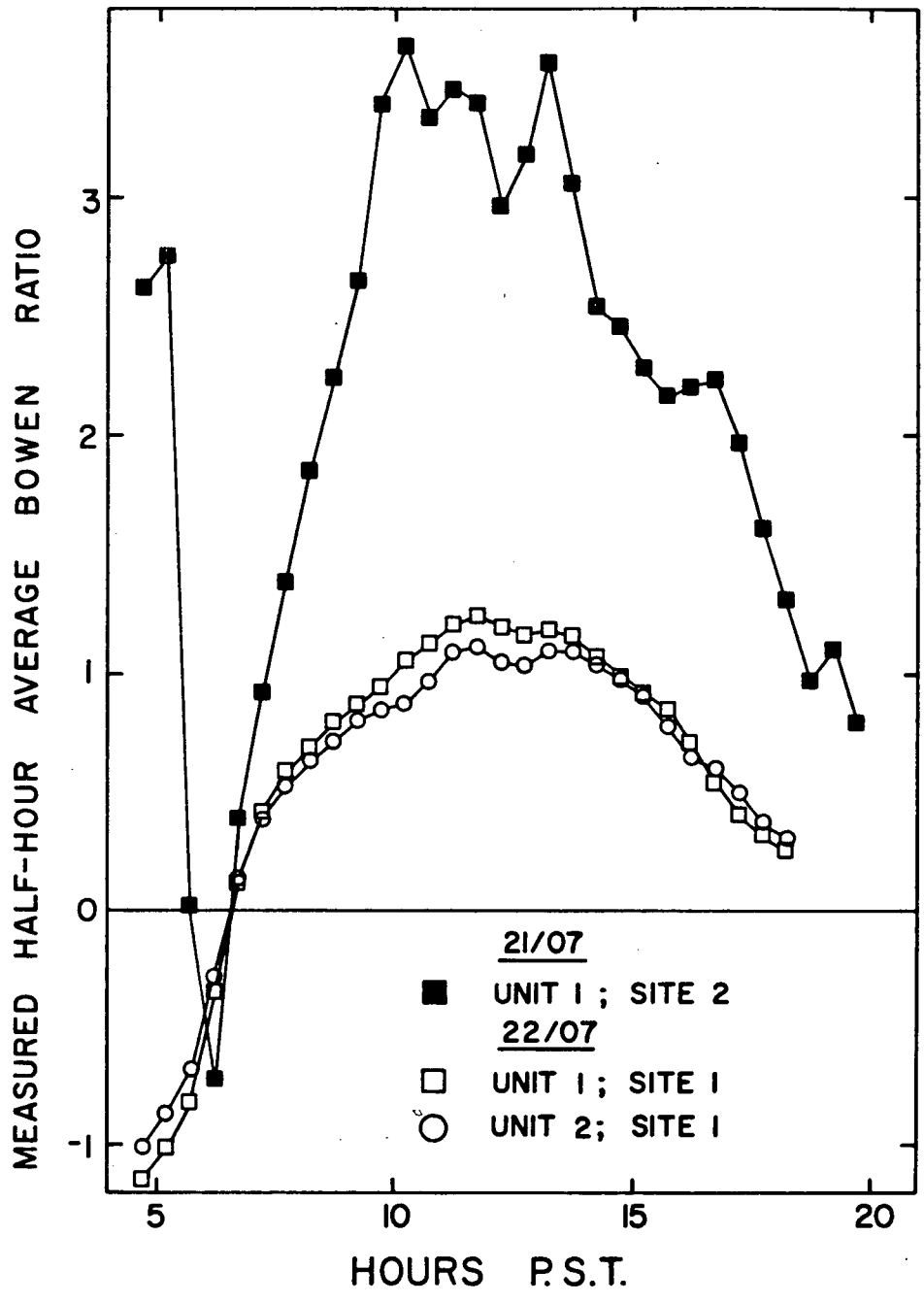

FIGURE 3.2: Half-hourly Bowen ratios measured by both reversing psychrometer units at site 1 on July 22. Also shown are the measurements taken at site 2 on July 21 by unit 1. Both days were clear with similar wind regimes and soil moisture conditions (the driest measured during the study).

Kipp and Zonen pyranometers (one per site) located 0.6 m above the soil surface. As a check on the above calculations, L_N was also calculated as follows:

$$L_N = \sigma[\varepsilon_s \varepsilon_a(T_a+273)^4 - \varepsilon_s(T_o+273)^4][0.1+0.9q] \quad (7)$$

where T_a and T_o are 24-hour average air (at 70 cm height) and soil surface (extrapolated from the profiles and corrected according to Chapter 2) temperatures (°C) respectively, the atmospheric emissivity was given by $\varepsilon_a = 1 - 0.261 \exp[-7.77 \times 10^{-4} T_a^2]$ (Idso and Jackson, 1969), the soil emissivity was given by $\varepsilon_s = 0.94 + 0.02\beta$ (inferred from Fuchs and Tanner, 1968a), and $\sigma = 5.67 \times 10^{-8}$ W m^{-2} °C^{-4}. Reflection by the soil of the incoming longwave radiation was accounted for in the first expression in square brackets. The second expression in square brackets (which accounted for cloudiness) was inferred from Linacre (1968) with $q = S/S_{max}$ and S_{max} = 340 W m^{-2} (the maximum observed value of S during the study). The good agreement between calculated and measured values of L_N (Figure 3.3) shows that it can be calculated accurately enough for use in (1) from data available by remote sensing techniques and standard meteorological measurements (Idso et al., 1975) even under cloudy conditions.

Calculation of the wetness partitioning factor β was carried out using (2) with α_w = 0.065 and α_d = 0.173. These were the extreme values of measured daytime average albedo from both sites. It will be shown below that stages I and III did not occur at precisely these respective albedos but were confined to narrow ranges near these values. Examination of Figure 2 in Idso et al. (1974) shows that both stages I and III were defined by narrow ranges of α. The exact manner in which α_d and α_w were defined by Jackson et al. (1976) and Idso et al. (1979) to calculate β from (2) was not specified.

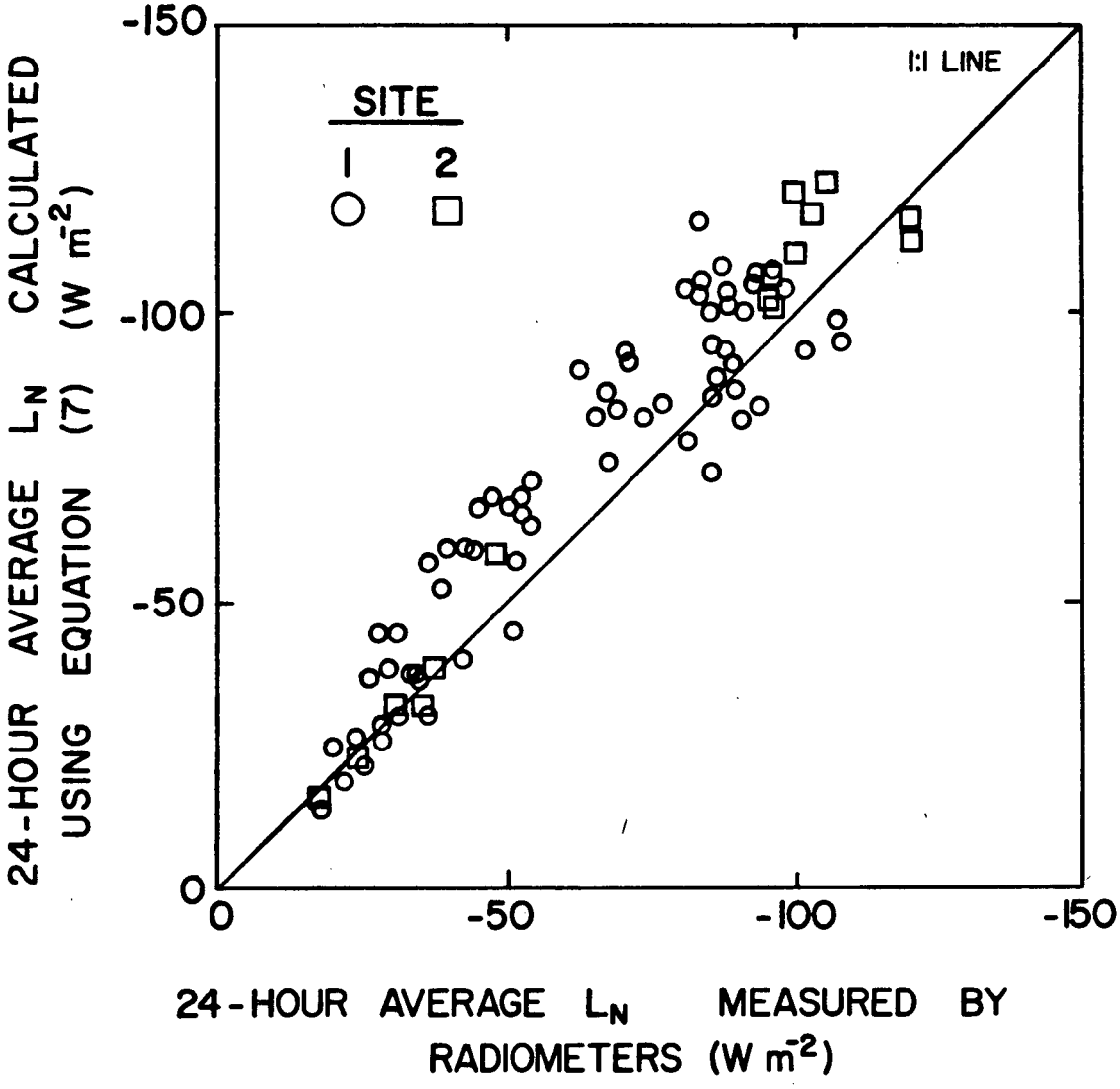

FIGURE 3.3: Comparison of 24-hour average values of L_N calculated using (7) with values measured by radiometers at sites 1 and 2.

3.4 Results and Discussion

It was mentioned in the previous section that during stage I the soil surface is saturated. Measured half-hourly Bowen ratios at 10:00 and 15:00 P.S.T. are compared in Figure 3.4 with values calculated according to

$$B = \frac{\gamma_v (T_o - T_a)}{(e_o^* - e_a)} \qquad (8)$$

where e_o^* is the saturation vapour pressure at T_o (corrected according to Chapter 2), e_a is the actual vapour pressure at 70 cm height and $\gamma_v = 0.066$ kPa $°C^{-1}$. Excellent agreement was obtained for half-hourly values of $\alpha < 0.09$ and was maintained at somewhat higher values of α on a few of the days. Consequently, half-hour evaporation rates fell below potential rates for $\beta < 0.77$. For 24-hour averages, a more conservative figure of $\beta = 0.8$, was chosen as defining the transition between stages I and II. Idso et al. (1974) decided that the transition to stage III occurred when diurnal plots of albedo versus time begin to "plateau" near the maximum values. In the present study this occurred approximately at $\alpha = 0.15 (\beta = 0.21)$, as indicated in Figure 3.5. As a result the data were separated into ranges corresponding to stages I, II, III according to whether $\beta \geq 0.8$, $0.8 > \beta > 0.2$, $\beta < 0.2$, respectively.

Daily average evaporation rates calculated from (1) are plotted against measured rates from both sites in Figure 3.6. It is evident that (1) did not agree with most of the measurements at site 1 and all of the measurements at site 2. Examination of the potential evaporation rate data ($\beta \geq 0.8$) shows clearly that (3) failed to described these. The dashed line drawn in Figure 3.6 was fit by eye to the potential rate data of both sites. The stage II points falling near this line were all

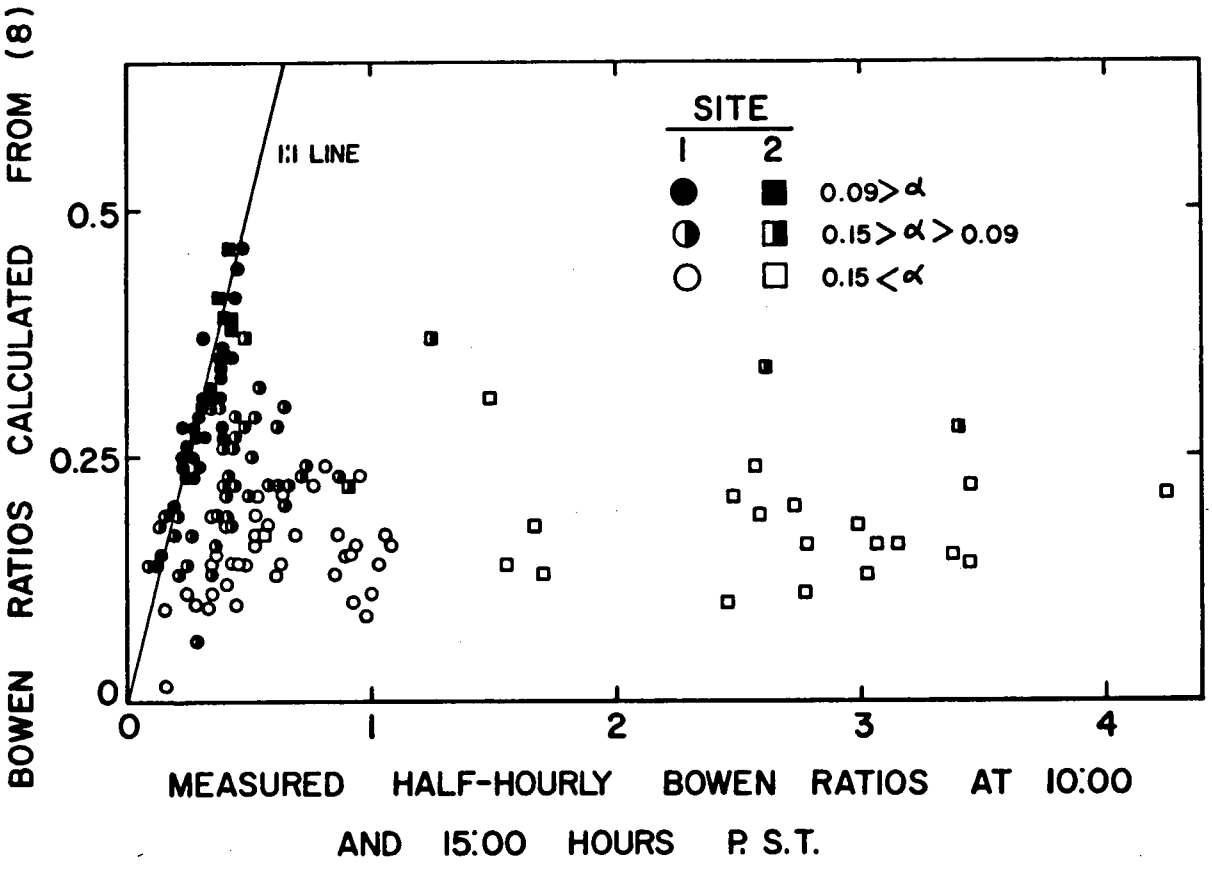

FIGURE 3.4: Comparison of half-hourly Bowen ratios calculated using (8) with measured values at sites 1 and 2. Only measurements at 10:00 and 15:00 h P.S.T. are plotted. The data have been separated into ranges according to measured half-hourly surface albedos as indicated.

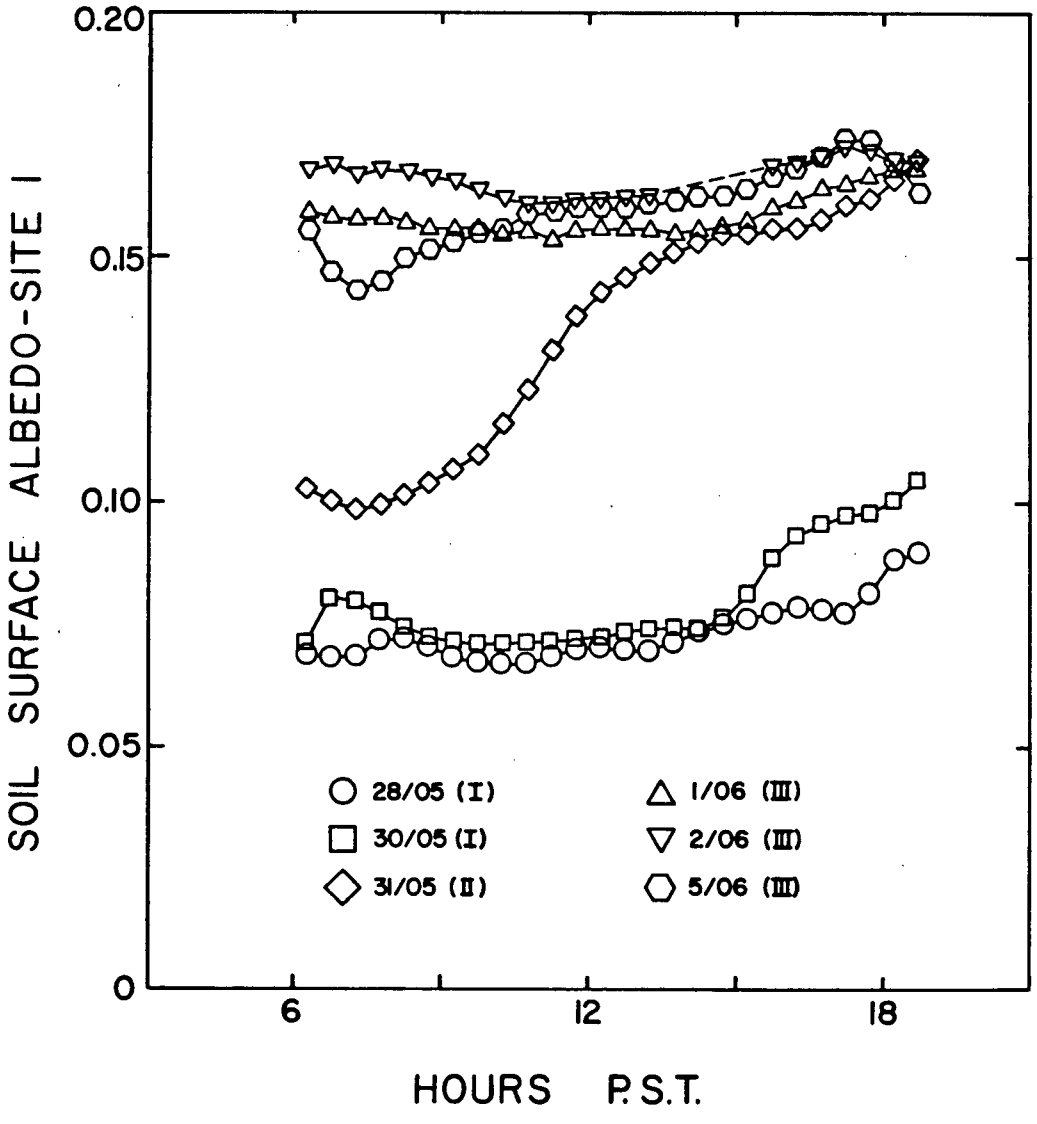

FIGURE 3.5: Daytime courses of surface albedo on selected days at site 1. The drying stage of each day, based upon the daytime average albedo, is also indicated. The dashed line on 2/06 indicates missing data due to a calibration of the solarimeters.

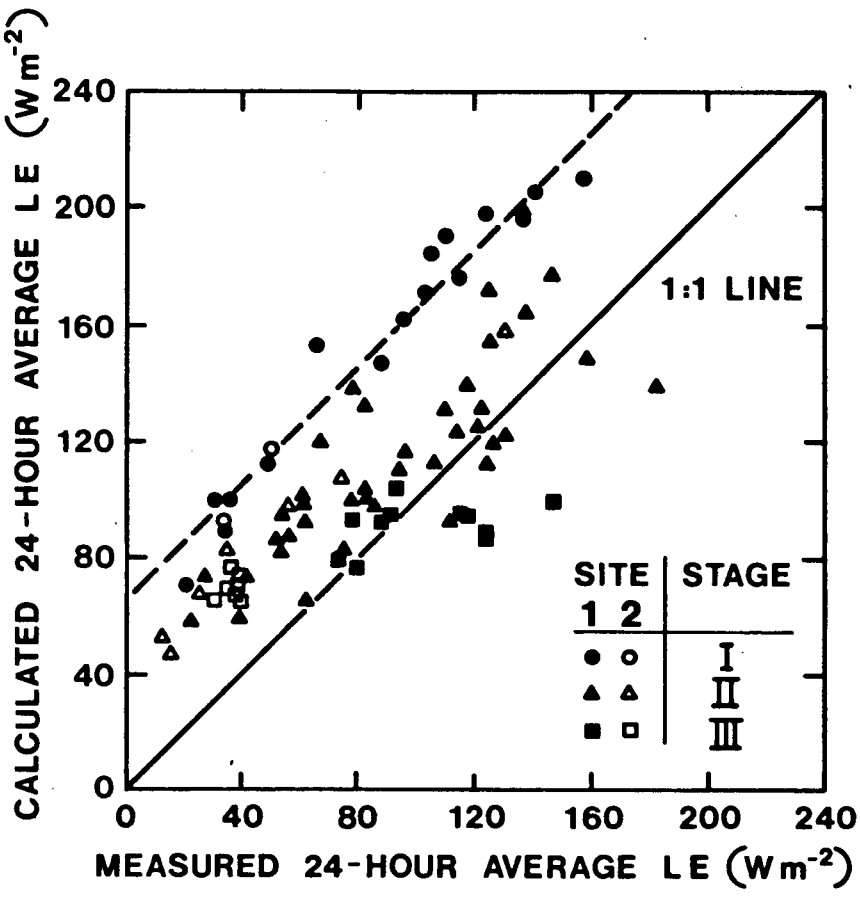

FIGURE 3.6: Plot of daily average evaporation rates calculated from (1) versus measured rates at sites 1 and 2. The drying stage of each day is indicated. The dashed line was fit by eye to the stage I data from both sites.

in the range $0.8 \geq \beta \geq 0.7$ and virtually satisfied the surface saturation criterion mentioned above. In view of the failure of (3) to represent the potential evaporation rate at Agassiz, as well as the agreement of (1) with some of the site 1 points (the stage III and near stage III points), it is evident that the factor 3/8 in (1) cannot apply to the site 1 data.

Since (1) did not adequately describe the measured data, it was decided to determine whether the concept of expressing the stage III rate as proportional to the expression for potential evaporation rate, as done in (1), would still work, i.e.

$$LE_{I,II,III} = [\delta + (1-\delta)\beta]PLE_{Ag} \tag{9}$$

where PLE_{Ag} is the expression describing potential evaporation rate at Agassiz, and δ is to be calculated from the stage III results as was done in Idso et al. (1979). The expression describing the potential evaporation rate at Agassiz can be determined from the dashed line in Figure 3.6 and is as follows:

$$PLE_{Ag} = S_N + 1.56\ L_N + 7 \tag{10}$$

The values of δ for both sites were calculated by substituting (10) into (9) and rearranging it into the following:

$$\delta = [\overline{LE_{III}/(S_N + 1.56\ L_N + 7)} - \bar{\beta}]/(1 - \bar{\beta}) \tag{11}$$

where the bars refer to arithmetic averages of the stage III days. There were 12 such days for site 1 and 7 for site 2. The ratio $\overline{LE_{III}/(S_N + 1.56L_N + 7)}$ took on values of 0.78 ± 0.2 and 0.4 ± 0.1 for sites 1 and 2 respectively. $\bar{\beta}$ was 0.137 and 0.092 for the two sites respectively. This led to the following two equations:

$$LE_{I,II,III} = (0.74 + 0.26\beta)(S_N + 1.56\ L_N + 7) \qquad (12a)$$

for site 1, and

$$LE_{I,II,III} = (0.34 + 0.66\beta)(S_N + 1.56\ L_N + 7) \qquad (12b)$$

for site 2. Since PLE_{Ag} at site 2 was at most 20% less than at site 1, stage III rates at site 2 were about half of those at site 1 (Figure 3.2). Comparison of these two formulas with the measurements is shown in Figure 3.7. The degree of scatter is similar for all three stages and is about ± 25 W m^{-2}.

Equation (10), which described the potential evaporation rate at Agassiz, differs from equation (3) for Phoenix by a constant, -69 W m^{-2}. Jackson et al. (1976) point out that the Priestley-Taylor coefficient a_{PT} in (5) varied from 1.41 for summer days to 2.41 for winter days when 24-hour totals of net radiation were used. Soil heat flux densities were assumed to be negligible, although it is seen that for spring and summer, including them would only increase these values. This indicates that considerable advective enhancement of evaporation occurred at the Phoenix site. At Agassiz the average 24-hour value of a_{PT} (G_o not neglected) for the stage I days was 1.27 ± 0.1, indicating minimal advection on these days. This is shown in Figure 3.8 in which the evaporation rate on stage I days is plotted versus "equilibrium evaporation rate", i.e. that given by (5) with $a_{PT} = 1$. This shows that (3) is inconsistent with (5) with a_{PT} in the range 1.2 to 1.3 and air and soil temperatures near 15°C, and so is not applicable over the full range of possible atmospheric advective effects, as conjectured in Idso et al. (1975). It is evident then that formulae such as (3) and (10) have no advantage over (5) except at a

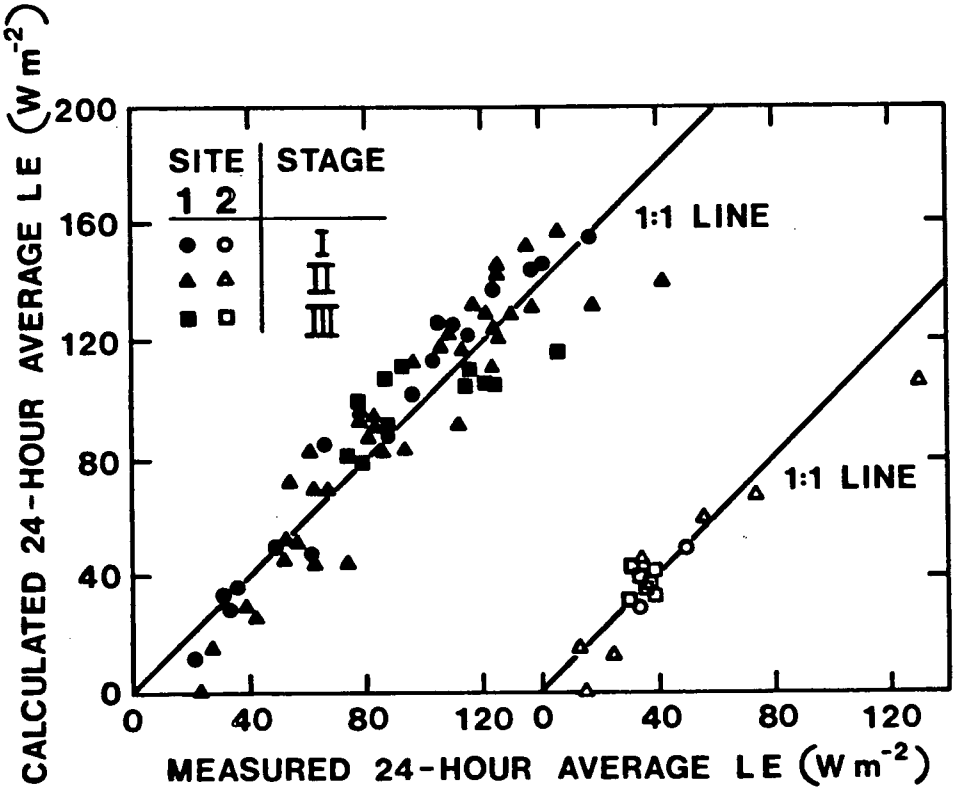

FIGURE 3.7: Comparison of daily average evaporation rates calculated using (12a) for site 1 and (12b) for site 2 with measured values. The drying stage of each day is indicated.

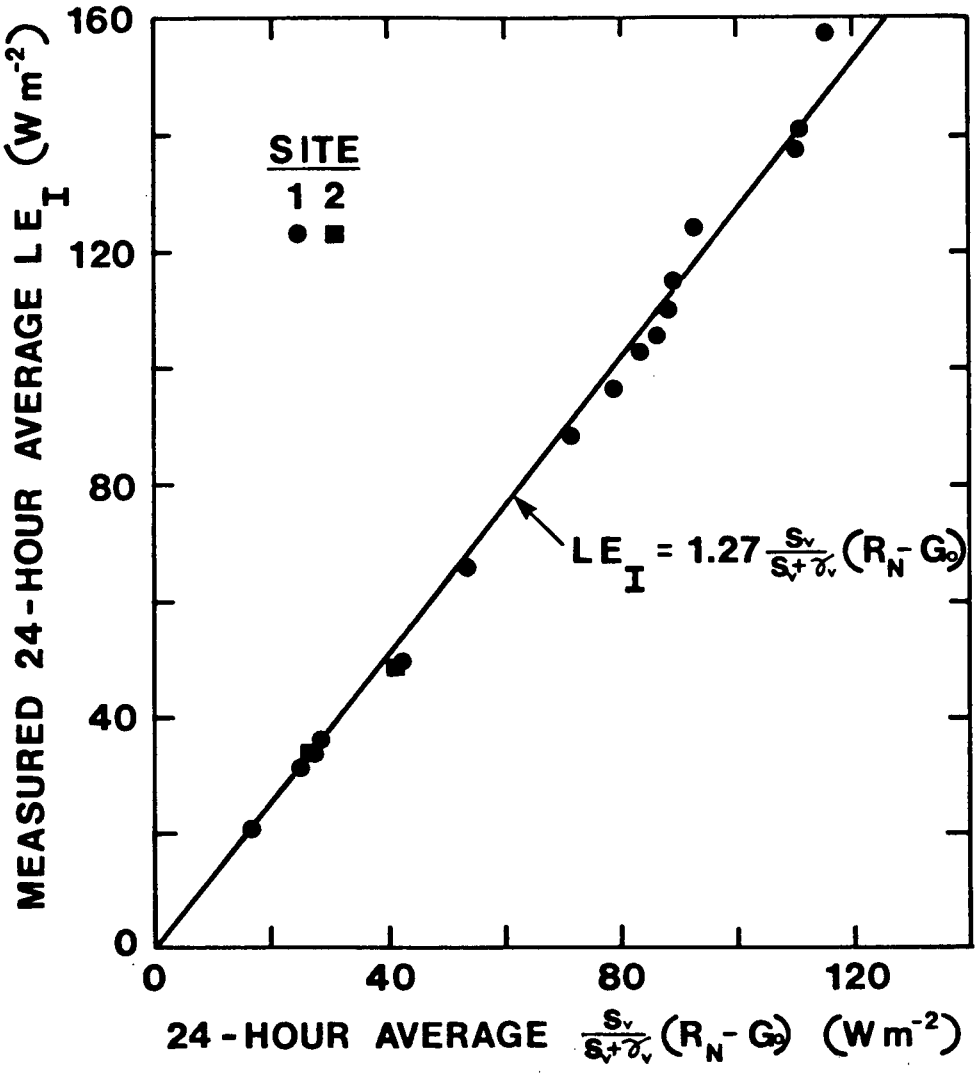

FIGURE 3.8: Plot of measured daily average evaporation rates on stage I days versus equilibrium evaporation rates. The solid line was fit by eye.

single site and after extensive calibration. Furthermore examination of diurnal trends during the stage I days at Agassiz shows that (5) with a_{PT} in the range 1.0 to 1.3 described the half-hourly daytime evaporation rates quite well while (10) failed to do so at all (overestimating by up to 120%).

The difference in δ for the two sites demonstrates that this factor is a strong function of near surface bulk density and/or structure, and is not only a function of soil type. No mention was made of the type of tillage used to prepare the Avondale loam site at Phoenix, although the 0.34 appropriate to the disc-harrowed site at Agassiz agrees quite well with the 3/8 found at Phoenix. The manner in which (12a) and (12b) simulated the day to day fluctuations of LE at sites 1 and 2 respectively is shown in Figure 3.9 for the site 2 study period.

The ± 30% variability in δ for each of the two Agassiz sites is not inconsistent with the scatter in Figure 1 of Idso et al. (1979); however for site 1 the variability is not random. Averaging the value of δ at site 1 for the stage III days in the first and last thirds of the site 1 study period (there were no stage III days in the middle third due to cloudy and rainy weather) shows that δ decreased from 0.84 ± 0.1 in the first third to 0.62 ± 0.1 in the last third, as indicated for the latter third in Figure 3.9a. The explanation of this decrease can be found by examining the soil moisture contents on the stage III days (Table 3.2). During the first third of the experiment the average volumetric soil moisture content in the upper 0.06 m of soil on the stage III days was 0.27 ± 0.01, whereas by the last third this value had dropped to 0.23 ± 0.01. The daily average stage III evaporation rates corresponding to these moisture contents were 119 ± 20 W m^{-2} and 82 ± 10 W m^{-2} respectively,

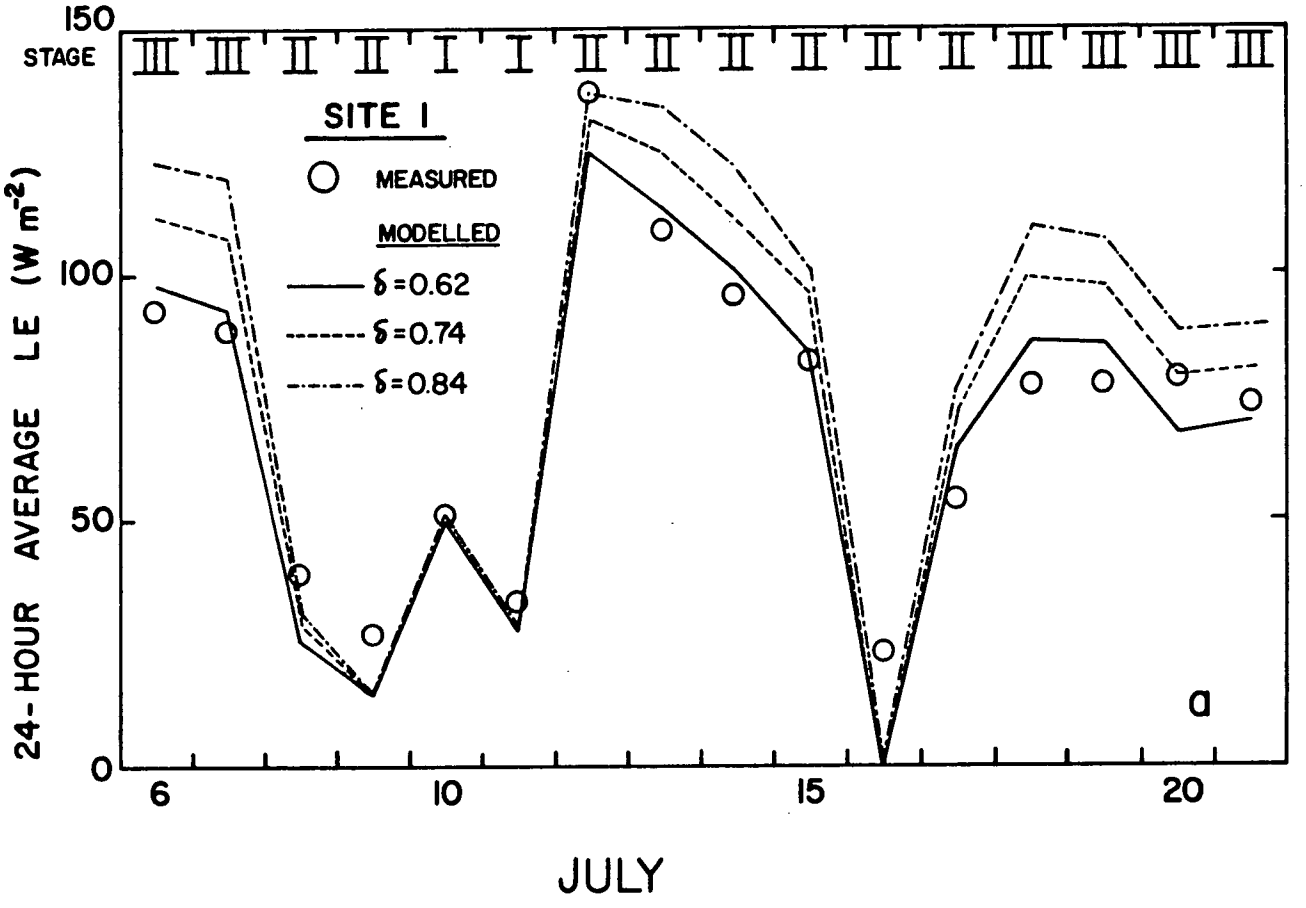

FIGURE 3.9a: Measured and calculated daily average evaporation rates at site 1 during the site 2 study period. The calculations were performed using (9) and (10) with the indicated values of δ. The drying stage of each day is also indicated.

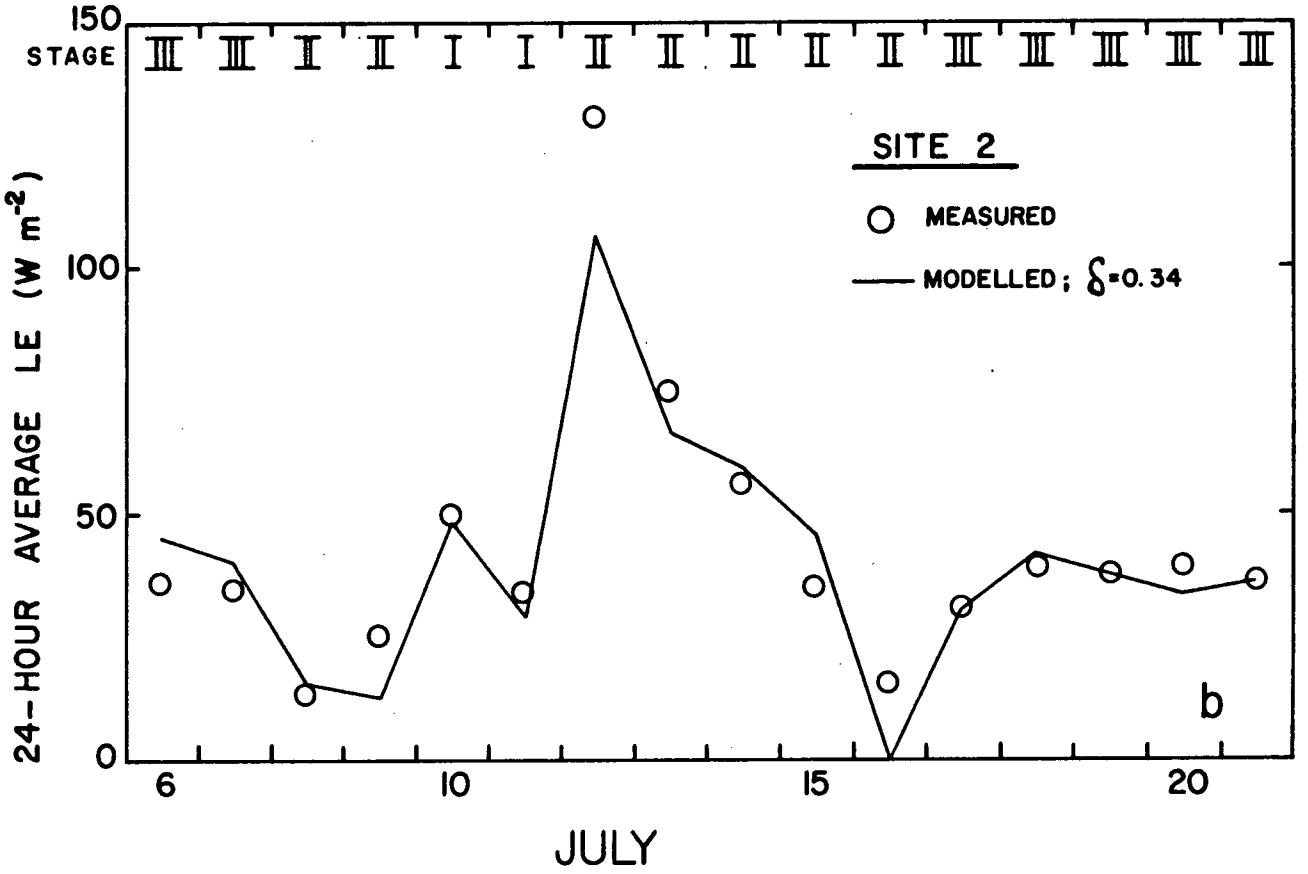

FIGURE 3.9b: As in Figure 3.9a except at site 2.

SITE	PERIOD	$\overline{\theta_v}$(0-0.06 m) ON STAGE III DAYS	$\overline{LE}$ (W m^{-2}) MEASURED	$\overline{PLE_{Ag}}$(W m^{-2}) FROM (10)	δ FROM (11)
1	17/05 - 8/06	0.27 ± 0.01	119 ± 20	137 ± 20	0.84
1	30/06 - 21/07	0.23 ± 0.01	82 ± 20	123 ± 20	0.62
2	6/07 - 21/07	0.15 ± 0.01	36 ± 10	97 ± 20	0.34

TABLE 3.2: Volumetric moisture content θ_v (0-0.06 m), measured 24-hour average LE, calculated PLE_{Ag} (from (10)), and calculated values of δ (from (11)) for the stage III days in the first and last thirds of the site 1 study period and for the site 2 study period. Bars refer to averages over the stage III days.

while the corresponding daily average values of PLE_{Ag} given by (10) were 137 $\pm$ 20 W m^{-2} and 123 $\pm$ 20 W m^{-2} respectively. Only about a half of the decrease in PLE_{Ag} was due to a decrease in L_N, the other half being due to a decrease in S. This 10% decrease in PLE_{Ag} could not compensate for the 31% decrease in stage III rate between the first and last thirds of the experiment. This suggests that had the experiment continued farther into the drier summer weather, the calculated site 1 δ would have decreased even more so and (12a) would not have described the data adequately. As to whether this would have been true for site 2 as well is difficult to assess since that site was monitored for only 16 days. The already low stage III rates observed at this site (30 to 40 W m^{-2} (Figure 3.9b) and ~ 25% of the potential rate) as well as the asymptotic nature of the schematic drying curves in Figure 3.1a at low stage III rates suggests that (12b) would have described site 2 evaporation adequately over a longer period of time. Hence for soils with stage III rates well in excess of 50% of potential rate, as was the case for site 1, equations of the form (9) will not work well over extended drying periods. In these cases, formulae such as (6) will have to be used to describe the stage III evaporation rates.

The success of (1) in describing the Phoenix stage III data during a drying period in any season appears to depend upon the fact that these rates were quite low (~ 30 to 60 W m^{-2}). Some of the square-root of time behaviour of (6) was probably absorbed as scatter in Figure 1 of Idso et al. (1979). With regard to the seasonal variations, Jackson et al. (1976) reported that the transition to stage III occurred 5 days after irrigation under the high PLE conditions in July, 1970 and 10 days after irrigation under the low PLE conditions in March, 1971, in agreement with

the schematic curves in Figure 3.1. However Figure 11 in Jackson (1973) shows that the volumetric moisture contents in the upper 0.09 m of soil immediately following the transition to stage III, were somewhat higher in March (0.23) than in July (0.21) in contradiction to Figure 3.1a. Despite this the stage III rates in July were about double those in March, i.e. ~ 60 W m^{-2} versus ~ 30 W m^{-2}, an effect attributed to the temperature dependence of the soil vapour diffusivity (Jackson et al., 1976).

3.5 Conclusions

Equation (3), developed in Idso et al. (1975) to describe potential evaporation at Phoenix, Arizona, did not work for Agassiz, British Columbia. However subtracting from it 69 W m^{-2} gave good agreement. This offset accounted for the difference in advection between the two locations and demonstrates that formulae such as (3) and (10) have no greater generality than the Priestley-Taylor formulation represented by (5). The Agassiz potential evaporation rate data was well represented by (5) with a_{PT} = 1.27 ± 0.1.

Expressing the stage III evaporation rate as proportional to the expression for potential evaporation, as suggested in Idso et al. (1979), worked only marginally well on the firmly packed site (δ = 0.74 ± 0.2) and quite well at the disc-harrowed site (δ = 0.34 ± 0.1). The results showed that this concept is applicable to soils with stage III rates much less than 50% of potential rate, but that on soils with stage III rates much greater than 50% of potential rate, the square-root of time approach used by several workers previously or diffusion theory should be used for extended drying periods.

3.6 Literature Cited

Black, T.A., W.R. Gardner, and G.W. Thurtell, The prediction of evaporation, drainage, and soil water storage for a bare soil, Soil Sci. Soc. Amer. Proc., 33, 655-660, 1969.

Black, T.A., and K.G. McNaughton, Psychrometric apparatus for Bowen-ratio determination over forests, Boundary-Layer Meteorol., 2, 246-254, 1971.

Fuchs, M., and C.B. Tanner, Surface temperature measurements of bare soils, J. Appl. Meteorol., 7, 303-305, 1968a.

Fuchs, M., and C.B. Tanner, Calibration and field test of soil heat flux plates, Soil Sci. Soc. Amer. Proc., 32, 326-328, 1968b.

Gardner, W.R., and M. Fireman, Laboratory studies of evaporation from soil columns in the presence of a water table, Soil Sci., 85, 244-249, 1958.

Gardner, W.R., Solutions of the flow equation for the drying of soils and other porous media, Soil Sci. Soc. Amer. Proc., 23, 183-187, 1959.

Gardner, W.R. Note on the separation and solution of diffusion type equations, Soil Sci. Soc. Amer. Proc., 26, 404, 1962.

Gardner, W.R., and D.I. Hillel, The relation of external evaporative conditions to the drying of soils, J. Geophys. Res., 67, 4319-4325, 1962.

Idso, S.B., and R.D. Jackson, Thermal radiation from the atmosphere, J. Geophys. Res., 74, 5397-5403, 1969.

Idso, S.B., R.J. Reginato, R.D. Jackson, B.A. Kimball, and F.S. Nakayama, The three stages of drying of a field soil, Soil Sci. Soc. Amer. Proc., 38, 831-837, 1974.

Idso, S.B., R.D. Jackson, and R.J. Reginato, Estimating evaporation: A technique adaptable to remote sensing, Science, 189, 991-992, 1975.

Idso, S.B., R.J. Reginato, and R.D. Jackson, An equation for potential evaporation from soil, water, and crop surfaces adatable to use by remote sensing, Geophys. Res. Lett., 4, 187-188, 1977.

Idso, S.B., R.J. Reginato, and R.D. Jackson, Calculation of evaporation during the three stages of soil drying, Water Resour. Res., 15, 487-488, 1979.

Jackson, R.D., Diurnal changes in soil water content during drying, Field Soil Water Regime, edited by R.R. Bruce et al., Spec. Publ. 5, pp. 37-55, Soil Sci. Soc. Amer., Madison, Wis., 1973.

Jackson, R.D., S.B. Idso, and R.J. Reginato, Calculation of evaporation rates during the transition from energy-limiting to soil-limiting phases using albedo data, Water Resour. Res., 12, 23-26, 1976.

Jury, W.A., and Tanner, C.B., Advection modification of the Priestley and Taylor evapotranspiration formula, Agron. J., 67, 840-842, 1975.

Kimball, B.A., and R.D. Jackson, Soil heat flux determination: A null-alignment method, Agric. Meteorol., 15, 1-9, 1975.

Lettau, H., Theory of surface - temperature and heat-transfer oscillations near a level ground surface, Trans. Amer. Geophys. Union, 32, 189-200, 1951.

Linacre, E.T., Estimating the net-radiation flux, Agric. Meteorol., 5, 49-63, 1968.

McNaughton, K.G., Evaporation and advection I: Evaporation from extensive homogeneous surfaces, Quart. J. Roy. Meteorol. Soc., 102, 181-191. 1976a.

McNaughton, K.G., Evaporation and advection II: Evaporation downwind of a boundary separating regions having different surface resistances and available energies, Quart. J. Roy. Meteorol. Soc., 102, 193-202. 1976b.

McNaughton, K.G., B.E. Clothier, and J.P. Kerr, Evaporation from land surfaces, Physical Hydrology, New Zealand Experience, edited by D.L. Murray and P. Ackroyd, pp. 97-119, N.Z. Hydrol. Soc., 1979.

Penman, H.L., Natural evaporation from open water, bare soil and grass, Proc. Roy. Soc. London, Ser. A., 193, 120-145, 1948.

Philip, J.R., The theory of heat flux meters, J. Geophys. Res., 66, 571-579, 1961.

Priestley, C.H.B., and R.J. Taylor, On the assessment of surface heat flux and evaporation using large-scale parameters, Mon. Weather Rev., 100, 81-92, 1972.

Ritchie, J.T., Model for predicting evaporation from a row crop with incomplete cover, Water Resour. Res., 8, 1204-1213, 1972.

Sellers, W.D., Physical Climatology, U. of Chicago Press, Chicago and London, 1965.

Spittlehouse, D.L., and T.A. Black, A comparison of reversing psychrometric Bowen ratio measurement systems, Atmosphere-Ocean (submitted), 1981.

Tanner, C.B., and J.T. Richie, Evapotranspiration: Empiricisms and modelling, paper presented at Annual meeting Amer. Soc. Agron., Chicago, Ill., Nov. 1974.

CONCLUDING REMARKS

For both daily averages and diurnal variations the large reduction in LE that accompanied the surface drying at both the culti-packed and disc-harrowed sites did not lead to an increase in G_o as speculated in the Introduction. Rather it remained approximately constant. This was because R_N decreased and H increased in a manner that exactly compensated for the reduction in LE. The decrease in R_N occurred because albedos and surface temperatures increased with drying. The ratio of H/G_o also increased with drying so that the partitioning of R_N - LE between the soil and the atmosphere was shifted in favour of the atmosphere. This was because of an increase in atmospheric admittance resulting from greater instability and a decrease in soil admittance resulting from the reduction in thermal properties with drying. Consequently a theory that correctly partitions R_N - LE between the soil and the atmosphere must account for the variation in time of the thermal properties of both media. Furthermore the variations of these properties with depth (near the surface) in both media must also be included in such a theory. It appears that the simple two-layered model will not always adequately describe this variation. Both R_N and LE can often be represented in a simplified semi-empirical manner although a more fundamental theory would determine them from radiation and moisture balances coupled to the energy balance.

APPENDIX I

PHOTOGRAPHS OF THE AGASSIZ SITES AND INSTRUMENTATION

PHOTOGRAPHS OF THE AGASSIZ SITES

AND INSTRUMENTATION

FIGURE 1: Overall view of the Agassiz study area (at ~ 13:00 P.S.T. on July 12). The culti-packed site is in the foreground and the disc-harrowed site with its instrumentation is in the background.

FIGURE 2: The two reversing psychrometer units operating together at site 1 on July 22. The horizontal white cylinders house the electric reversing motors.

FIGURE 3: The upper part of the framework consisting of stainless steel and acrylic tubing used to position the thermocouples in the soil at the desired depths. The thermocouples are located near the tip of each stainless steel tube (0.32 cm o.d.). Each stainless steel tube snugly fits into a hole drilled radially in an acrylic tube (1.3 or 1.9 cm o.d.). There were four acrylic tubes (sections) per profile. The section nearest the surface (the upper tube shown) was installed at an angle of 60° to the vertical with the stainless steel tubes horizontal. The second section (also shown) was installed at 45° to the vertical and the two lower sections were installed vertically. The acrylic tubes were filled with soil from the horizons in which they were installed.

FIGURE 1

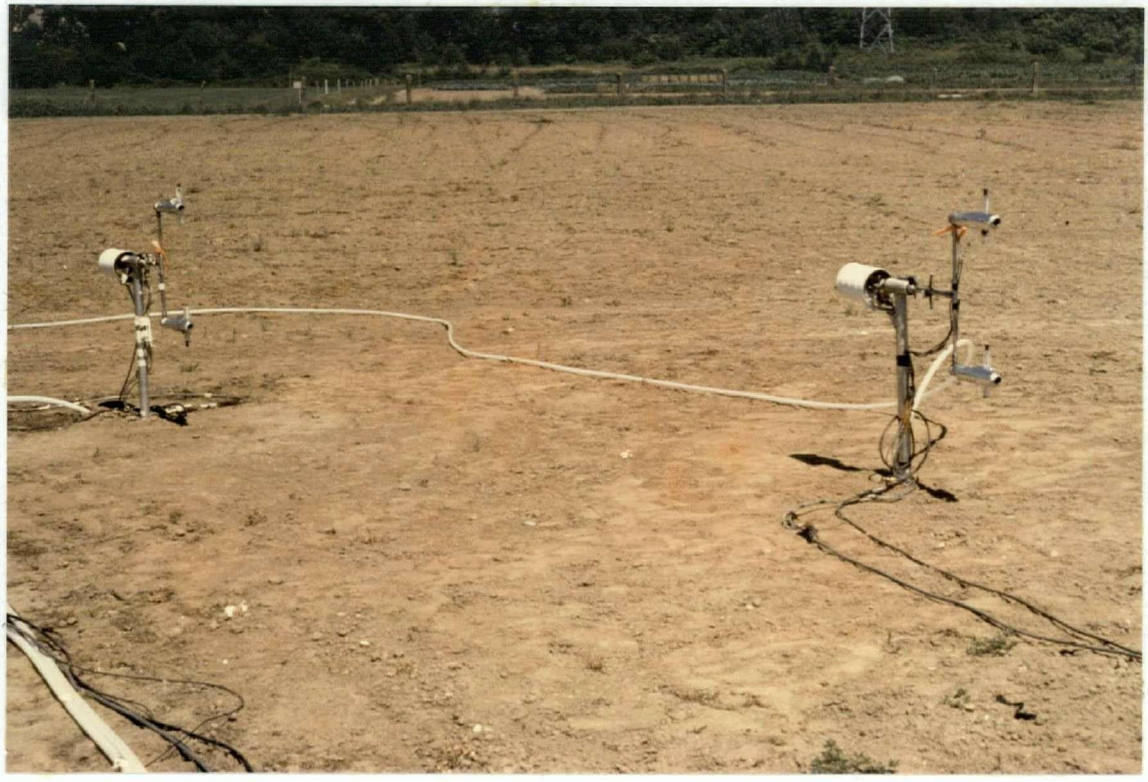

FIGURE 2

FIGURE 3

APPENDIX II

SAMPLE LISTING OF THE COMPUTER PROGRAM THAT CALCULATES SOIL TEMPERATURE FROM THE THEORY DISCUSSED IN CHAPTER 2

SAMPLE LISTING OF THE COMPUTER PROGRAM THAT CALCULATES SOIL TEMPERATURE FROM THE THEORY DISCUSSED IN CHAPTER 2

The first 210 lines listed are the computer program. The next 93 lines are the program input data for both sites; each line respectively contains G_o^{24} (W m^{-2}), albedo, and G_o^d (W m^{-2}). The last 153 lines are the output of the listed program (the example shown is for site 2). The output data for each date are as follows:

LINE 1: Day number, date, d(cm), albedo, C_1 (MJ m^{-3} $°C^{-1}$), k_1 (W m^{-1} $°C^{-1}$), C_2 (MJ m^{-3} $°C^{-1}$), k_2 (W m^{-1} $°C^{-1}$), respectively.

LINE 2: G_o^{24}, G_o^d, and calculated $||G_o||$, all in W m^{-2}, respectively.

LINE 3: Calculated daily average temperatures at 0.0, 1.0, 2.5, 5.0, 10.0, 20.0, 50.0, 100.0 cm depths from left to right, respectively (°C).

LINE 4: Error estimates for the boundary-value calculation at all 8 output depths, respectively (°C).

LINE 5: Error estimates for the initial-value calculation at all 8 output depths, respectively (°C).

LINE 6: Calculated daily maximum temperatures at all 8 output depths, respectively (°C).

LINE 7: Calculated daily minimum temperatures at all 8 output depths, respectively (°C).

LINE 8: Temperatures calculated using the initial-value part of the complete solution at all 8 output depths, respectively (°C). The difference between LINE 3 and LINE 8 is the temperature calculated by the boundary-value part of the solution at each respective depth.

```
C PROGRAM TO CALCULATE SOIL TEMPERATURES USING THE EXACT SOLUTION
C FOR THE CASE OF A COMPOSITE MEDIUM CONSISTING OF A LAYER
C OF DEPTH L AND A SEMI-INFINITE REGION.
C DIMENSION AND EXTERNALIZE THE VARIABLES.
      DIMENSION ALB(75),T(8,75),ERR1(8,75),ERR2(8,75),TD(75)
      DIMENSION NUMD(75),MO(75),TMAX(8,75),TMIN(8,75),TIN(8,75)
      DIMENSION GDAY(75),DDD1(75),C1(75),TK1(75),GABS(75)
      EXTERNAL F1,F21,F22,FN
      COMMON /A1/G(75),THMU1(75),J,TAU,AS,TAA,TO,DDA2,TK,ZK,AL
      COMMON /A2/Z(8),RA(75),D1(75),RB(75),ZL,D2,PI,I
      REAL*8 X,Y,E1,FN
      LOGICAL LZ
C SPECIFY THE REQUIRED INPUT PARAMETERS.
C (A) TIME VARIABLES.
      TAU=1.0
      ND=17
      DO 1 I=1,ND
    1 TD(I)=I-1+0.5
C (B) READ IN THE SURFACE HEAT FLOW AND ALBEDO DATA.
      READ(1,30) (G(I),ALB(I),GDAY(I),I=1,ND)
   30 FORMAT(F5.1,F8.3,F7.1)
      N=1
      IF(N.EQ.1) GO TO 51
      DO 50 I=1,ND
      G(I)=G(I)-4.0
   50 GDAY(I)=GDAY(I)-4.0
   51 CONTINUE
C (C) SPECIFY LAYER DEPTH, THERMAL PROPERTIES (FUNCTIONS OF
C     ALBEDO), AND THEIR DEPENDENT PARAMETERS.
      ZL=7.5
      PI=3.1415927
      CW1=1.55*11.5741
      CD1=0.95*11.5741
      TKW1=0.66
      TKD1=0.35
      C2=2.6*11.5741
      TK2=0.9
      D2=TK2/C2*10000.
      DO 31 I=1,ND
      IF(ALB(I).EQ.0.0) ALB(I)=0.086
      BETA=(0.170-ALB(I))/0.095
      TK1(I)=BETA*TKW1+(1.-BETA)*TKD1
      C1(I)=BETA*CW1+(1.-BETA)*CD1
      D1(I)=TK1(I)/C1(I)*10000.
      THMU1(I)=TK1(I)*C1(I)
      S1=SQRT(THMU1(I))
      S2=SQRT(TK2*C2)
      RA(I)=(S1-S2)/(S1+S2)
      RB(I)=S1/(S1+S2)
   31 CONTINUE
C (D) SPECIFY PARAMETERS FOR THE FUNCTION WHICH DESCRIBES
C     THE INITIAL TEMPERATURE PROFILE.
      TAA=11.5
      TO=19.6
      TK=15.2
      ZK=100.0
      DDA2=SQRT(D2*365./PI)
      X=0.0D0
      Y=2.*PI
      E1=1.0D-5
```

```
      CALL ZERO1(X,Y,FN,E1,LZ)
      AL=X
C (E) SPECIFY PARAMETERS FOR DIURNAL MAX/MIN CALCULATION.
      W=2.0*PI
      DO 5 I=1,ND
    5 DDD1(I)=SQRT(2.0*D1(I)/W)
      DDD2=SQRT(2.0*D2/W)
C CALCULATE THE DAILY AVERAGE SOIL TEMPERATURES USING THE EXACT
C SOLUTIONS.
C FIRST THE CONTRIBUTION FROM THE SURFACE HEAT FLOW.
      DO 2 I=1,8
      DO 2 J=1,ND
      T(I,J)=QINF(F1,0.0,1.E-8,30.0,1.E-2,ERR,5)
      ERR1(I,J)=ERR
    2 CONTINUE
C NOW THE CONTRIBUTION FROM THE INITIAL CONDITION (ASSUMING HOMOGENEITY).
      DO 10 I=1,8
      DO 10 J=1,ND
      AS=SQRT(4.0*D2*TD(J))
      UL=Z(I)/AS
      AI1=CADRE(F21,0.0,UL,1.E-2,0.0,ER1)
      AI2=QINF(F22,0.0,1.E-8,30.0,1.E-2,ER2,5)
      TIN(I,J)=AI1+AI2
      T(I,J)=T(I,J)+TIN(I,J)
      ERR2(I,J)=ER1+ER2
   10 CONTINUE
C CALCULATE THE DAILY MAX/MIN TEMPERATURES USING VAN WIJK'S
C SINUSOIDAL RESULTS.
      DO 6 I=1,8
      DO 6 J=1,ND
      DEN=COS(W*20.5/24.0-1.178)-COS(W*4.5/24.0-1.178)
      GABS(J)=(G(J)-GDAY(J))*16.0/24.0*W/DEN
      IF(Z(I).GE.ZL) GO TO 7
      ZD=Z(I)
      TABS=R(ZD,DDD1,RA,J,ZL)
      TABS=TABS*GABS(J)/SQRT(THMU1(J)*W)
      GO TO 8
    7 TABS=R(ZL,DDD1,RA,J,ZL)
      TABS=TABS*GABS(J)/SQRT(THMU1(J)*W)
      TABS=TABS*EXP(-(Z(I)-ZL)/DDD2)
    8 TMAX(I,J)=T(I,J)+TABS
      TMIN(I,J)=T(I,J)-TABS
    6 CONTINUE
C WRITE OUT THE RESULTS. FIRST CALCULATE DATE INFORMATION.
      NYR=78
      NUMD(1)=5
      MO(1)=7
      DO 3 J=2,ND
      NUMD(J)=NUMD(J-1)+1
      MO(J)=MO(J-1)
      IF(NUMD(J).GT.31.AND.MO(J).EQ.5) GO TO 4
      IF(NUMD(J).GT.30.AND.MO(J).EQ.6) GO TO 4
      GO TO 3
    4 NUMD(J)=1
      MO(J)=MO(J)+1
    3 CONTINUE
      C2=C2/11.5741
      DO 40 J=1,ND
      C1(J)=C1(J)/11.5741
      J1=J+56
```

```
      WRITE(2,41) J1,NUMD(J),MO(J),NYR,ZL,ALB(J),C1(J),TK1(J)
     1,C2,TK2,G(J),GDAY(J)
     2,GABS(J),(T(I,J),I=1,8),(ERR1(I,J),I=1,8),(ERR2(I,J),I=1,8)
     3,(TMAX(I,J),I=1,8),(TMIN(I,J),I=1,8),(TIN(I,J),I=1,8)
   41 FORMAT(I4,I10,'/',I1,'/',I2,F7.1,F8.3,2(F9.2,F5.2)
     1/9X,3G12.4/6(6X,8G12.4/))
   40 CONTINUE
      STOP
      END
C FUNCTION FOR THE IMPROPER INTEGRAL IN THE CONTRIBUTION
C FROM THE SURFACE HEAT FLOW.
      FUNCTION F1(U)
      COMMON /A1/G(75),THMU1(75),J,TAU,AS,TAA,TO,DDA2,TK,ZK,AL
      COMMON /A2/Z(8),RA(75),D1(75),RB(75),ZL,D2,PI,I
      U2=U**2
      EM=EXP(-U2*TAU/2.0)
      A=0.0
      IF(J.EQ.1) GO TO 4
      DO 1 K=2,J
      K2=2*K-3
    1 A=A+G(J-K+1)*EM**K2
      A=A*(1.0-EM**2)/U2
    4 A=A+G(J)*(1.0-EM)/U2
      SD1=SQRT(D1(J))
      B=1.+RA(J)**2-2.*RA(J)*COS(2.*ZL*U/SD1)
      IF(Z(I).GT.ZL) GO TO 2
      C=COS(Z(I)*U/SD1)
      C=C*2.*(1.-RA(J)**2)/PI/SQRT(THMU1(J))
      GO TO 3
    2 SD2=SQRT(D2)
      SD3=SQRT(D2/D1(J))
      C=COS((Z(I)-ZL*(1.-SD3))*U/SD2)
      C=C-RA(J)*COS((Z(I)-ZL*(1.+SD3))*U/SD2)
      C=C*4.*RB(J)/PI/SQRT(THMU1(J))
    3 F1=A*C/B
      RETURN
      END
C PROGRAM TO INITIALIZE THE DEPTH DATA IN COMMON.
      BLOCK DATA
      COMMON /A2/Z(8),RA(75),D1(75),RB(75),ZL,D2,PI,I
      DATA Z/0.0,1.,2.5,5.,10.,20.,50.,100./
      END
C FUNCTION FOR THE PROPER INTEGRAL IN THE CONTRIBUTION
C FROM THE INITIAL CONDITION.
      FUNCTION F21(EPS)
      COMMON /A1/G(75),THMU1(75),J,TAU,AS,TAA,TO,DDA2,TK,ZK,AL
      COMMON /A2/Z(8),RA(75),D1(75),RB(75),ZL,D2,PI,I
      A=EXP(-EPS**2)/SQRT(PI)
      ARG1=Z(I)-AS*EPS
      ARG2=-Z(I)+AS*EPS
      TAB=(TO-TAA)/SIN(AL)
      B1=TAA+TAB*EXP(-ARG1/DDA2)*SIN(AL-ARG1/DDA2)
      B2=TAA+TAB*EXP(-ARG2/DDA2)*SIN(AL-ARG2/DDA2)
      F21=A*(B1-B2)
      RETURN
      END
C FUNCTION FOR THE IMPROPER INTEGRAL IN THE CONTRIBUTION
C FROM THE INITIAL CONDITION.
      FUNCTION F22(EPS)
      COMMON /A1/G(75),THMU1(75),J,TAU,AS,TAA,TO,DDA2,TK,ZK,AL
```

```
      COMMON /A2/Z(8),RA(75),D1(75),RB(75),ZL,D2,PI,I
      A=EXP(-EPS**2)/SQRT(PI)
      ARG1=-Z(I)+AS*EPS
      ARG2=Z(I)+AS*EPS
      TAB=(TO-TAA)/SIN(AL)
      B1=TAA+TAB*EXP(-ARG1/DDA2)*SIN(AL-ARG1/DDA2)
      B2=TAA+TAB*EXP(-ARG2/DDA2)*SIN(AL-ARG2/DDA2)
      F22=A*(B1+B2)
      RETURN
      END
C FUNCTION TO CALCULATE THE AMPLITUDE RATIO IN THE MAX/MIN CALCULATIONS.
      FUNCTION R(Z,DD,RA,J,ZL)
      DIMENSION DD(75),RA(75)
      E1=2.0*Z/DD(J)
      E2=2.0*ZL/DD(J)
      A=EXP(-E1)
      B=2.0*RA(J)*EXP(-E2)*COS(E2-E1)
      C=RA(J)**2*EXP(-2.0*E2+E1)
      D=-2.0*RA(J)*EXP(-E2)*COS(E2)
      E=RA(J)**2*EXP(-2.0*E2)
      F=(A+B+C)/(1.0+D+E)
      R=SQRT(F)
      RETURN
      END
      FUNCTION FN(X)
      REAL*8 FN
      COMMON /A1/G(75),THMU1(75),J,TAU,AS,TAA,TO,DDA2,TK,ZK,AL
      FN=(TK-TAA)*SIN(X)+(TAA-TO)*EXP(-ZK/DDA2)*SIN(X-ZK/DDA2)
      RETURN
      END
```

SITE1 DAILY DATA, 11/5/78 TO 21/7/78

	G24	ALBDO	GDAY
2	19.7	0.0	40.1
3	27.2	0.0	55.3
4	5.1	0.0	18.8
5	7.6	0.0	26.6
6	7.0	0.0	25.7
7	5.9	0.0	21.9
8	15.1	0.077	50.4
9	34.1	0.090	91.0
10	23.6	0.122	71.4
11	27.8	0.143	75.9
12	-24.6	0.119	-2.3
13	-9.3	0.076	14.6
14	20.3	0.124	64.9
15	3.3	0.123	45.1
16	6.0	0.098	33.6
17	10.2	0.096	34.2
18	-2.3	0.068	15.3
19	6.4	0.074	34.3
20	-0.9	0.082	24.2
21	26.7	0.079	69.3
22	21.3	0.137	65.0
23	29.6	0.159	80.5
24	35.1	0.166	89.7
25	33.0	0.164	84.9
26	31.1	0.156	78.5
27	22.0	0.160	73.5
28	14.0	0.151	61.1
29	-6.8	0.147	21.4
30			

31	14.0	0.152	51.1
32	-16.1	0.078	3.1
33	5.6	0.069	35.7
34	13.1	0.084	47.6
35	-9.0	0.092	11.8
36	0.5	0.079	23.8
37	7.9	0.076	40.3
38	-11.1	0.085	-1.4
39	10.1	0.065	30.4
40	20.2	0.113	63.5
41	4.1	0.123	40.3
42	21.0	0.137	66.3
43	21.2	0.146	66.1
44	14.4	0.148	48.3
45	3.3	0.138	31.2
46	9.5	0.141	38.8
47	-4.9	0.114	19.6
48	-5.1	0.072	9.4
49	26.6	0.109	59.7
50	31.8	0.143	77.3
51	30.3	0.151	75.7
52	-15.5	0.107	-1.1
53	0.9	0.093	22.7
54	26.0	0.131	61.4
55	-4.8	0.120	12.8
56	9.9	0.133	34.2
57	-8.6	0.131	6.3
58	16.4	0.133	39.6
59	24.2	0.152	60.1
60	21.1	0.161	68.9
61	-14.8	0.138	0.1
62	-15.0	0.088	-7.6
63	-3.8	0.077	11.4
64	-1.2	0.080	16.7
65	30.4	0.105	75.6
66	26.3	0.134	71.2
67	24.2	0.140	72.0
68	16.5	0.140	53.8
69	-27.0	0.090	-22.3
70	11.3	0.132	33.9
71	23.8	0.154	60.9
72	24.9	0.147	74.1
73	19.5	0.160	69.5
74	22.0	0.156	74.5
75	SITE2 DAILY DATA, 5/7/78 TO 21/7/78.		
76	G24	ALBDO	GDAY
77	16.4	0.140	32.0
78	21.9	0.165	48.0
79	17.4	0.173	50.0
80	-7.7	0.145	3.3
81	-13.6	0.097	-9.2
82	-5.9	0.066	6.3
83	-1.0	0.076	13.3
84	27.4	0.114	64.2
85	29.1	0.145	66.8
86	27.0	0.150	66.2
87	23.1	0.150	56.4
88	-21.5	0.122	-17.7
89	10.2	0.154	31.4
90	21.5	0.164	51.7

```
91      25.3   0.170   65.7
92      21.6   0.162   61.1
93      22.3   0.156   65.9
 1       57        5/7/78    7.5   0.140      1.14 0.45      2.60 0.90
 2                 16.40        32.00        43.57
 3                23.21        22.83        22.34        21.52        20.22        19.06        17.25        15.21
 4              0.6485E-04   0.3816E-01   0.6455E-02   0.2397E-02   0.8547E-02   0.4607E-02   0.8120E-02   0.6600E-02
 5              0.5417E-02   0.5418E-02   0.5417E-02   0.5429E-02   0.5463E-02   0.5561E-02   0.7247E-02   0.6908E-02
 6                30.21        29.06        27.48        25.04        21.91        19.66        17.28        15.21
 7                16.21        16.61        17.20        18.00        18.53        18.45        17.23        15.21
 8                18.92        18.92        18.91        18.89        18.81        18.52        17.24        15.23
 9
10       58        6/7/78    7.5   0.165      0.98 0.37      2.60 0.90
11                21.90        48.00        72.89
12                27.06        26.51        25.57        24.25        22.23        20.42        17.51        15.27
13              0.7599E-02   0.7611E-01   0.3993E-01   0.4130E-01   0.2005E-01   0.1254E-01   0.5102E-02   0.3072E-03
14              0.4791E-02   0.4807E-02   0.4807E-02   0.4807E-02   0.4843E-02   0.4940E-02   0.5645E-02   0.7794E-02
15                41.07        38.90        35.68        30.91        25.16        21.47        17.55        15.27
16                13.06        14.12        15.46        17.60        19.31        19.37        17.46        15.27
17                18.45        18.45        18.44        18.43        18.39        18.21        17.23        15.28
18
19       59        7/7/78    7.5   0.173      0.93 0.34      2.60 0.90
20                17.40        50.00        91.04
21                27.69        27.21        26.41        25.23        23.45        21.70        18.04        15.34
22              0.3857E-01   0.5836E-01   0.4590E-01   0.5295E-01   0.9556E-03   0.2578E-01   0.2769E-02   0.1728E-02
23              0.4395E-02   0.4395E-02   0.4396E-02   0.4395E-02   0.4411E-02   0.4473E-02   0.4919E-02   0.7260E-02
24                46.37        43.70        39.82        33.93        27.14        23.03        18.10        15.34
25                9.004        10.71        13.01        16.52        19.76        20.38        17.98        15.34
26                18.13        18.13        18.13        18.12        18.09        17.95        17.15        15.32
27
28       60        8/7/78    7.5   0.145      1.11 0.43      2.60 0.90
29               -7.700        3.300        30.72
30                20.75        20.93        21.16        21.48        21.87        21.56        18.58        15.47
31              0.1607E-02   0.2636E-01   0.1891E-01   0.3834E-03   0.8386E-02   0.3157E-01   0.9551E-02   0.3218E-02
32              0.4074E-02   0.4074E-02   0.4075E-02   0.4074E-02   0.4084E-02   0.4241E-02   0.4463E-02   0.6400E-02
33                25.85        25.47        24.89        24.02        23.07        21.99        18.60        15.47
34                15.65        16.40        17.42        18.94        20.67        21.13        18.56        15.47
35                17.89        17.89        17.88        17.88        17.85        17.74        17.05        15.35
36
37       61        9/7/78    7.5   0.097      1.41 0.59      2.60 0.90
38              -13.60        -9.200        12.29
39                17.49        17.69        18.01        18.51        19.24        19.77        18.65        15.62
40              0.1751E-02   0.8174E-02   0.2620E-02   0.4177E-02   0.9290E-02   0.1319E-01   0.3666E-02  -0.1369E-01
41              0.3815E-02   0.3815E-02   0.3831E-02   0.3830E-02   0.3821E-02   0.3932E-02   0.4712E-02   0.5747E-02
42                19.04        19.08        19.18        19.35        19.69        19.93        18.65        15.62
43                15.94        16.30        16.85        17.67        18.79        19.61        18.64        15.61
44                17.68        17.68        17.68        17.67        17.65        17.55        16.95        15.37
45
46       62       10/7/78    7.5   0.066      1.61 0.69      2.60 0.90
47               -5.900        6.300        34.07
48                17.24        17.32        17.44        17.64        17.98        18.41        18.28        15.76
49              0.4545E-02   0.6817E-02   0.1321E-02   0.5418E-03   0.1178E-03   0.7606E-02   0.3785E-02   0.5788E-02
50              0.3601E-02   0.3601E-02   0.3602E-02   0.3601E-02   0.3606E-02   0.3690E-02   0.4294E-02   0.5224E-02
51                20.97        20.69        20.30        19.77        19.17        18.84        18.30        15.76
52                13.51        13.96        14.58        15.52        16.79        17.99        18.26        15.76
53                17.50        17.50        17.50        17.49        17.47        17.39        16.85        15.38
54
55       63       11/7/78    7.5   0.076      1.54 0.66      2.60 0.90
56               -1.000        13.30        39.94
57                17.63        17.65        17.67        17.71        17.79        17.93        17.85        15.86
```

```
          0.1331E-02  0.1830E-02  0.1882E-02  0.6611E-03  0.5255E-02  0.1692E-02  0.6125E-02  0.5461E-02
          0.3418E-02  0.3418E-02  0.3418E-02  0.3418E-02  0.3422E-02  0.3489E-02  0.3975E-02  0.4802E-02
           22.20       21.76       21.15       20.28       19.20       18.43       17.88       15.86
           13.07       13.54       14.19       15.14       16.38       17.42       17.83       15.86
           17.34       17.34       17.34       17.33       17.31       17.24       16.75       15.38

64        12/7/78     7.5   0.114      1.30 0.53      2.60 0.90
            27.40       64.20       102.8
           24.12       23.66       22.99       21.86       20.17       18.68       17.58       15.90
          0.4041E-01  0.2448E-01  0.4534E-01  0.1917E-01  0.2915E-01  0.7692E-02  0.1111E-03 -0.2794E-01
          0.3265E-02  0.3265E-02  0.3266E-02  0.3265E-02  0.3268E-02  0.3325E-02  0.3713E-02  0.4460E-02
           38.27       36.30       33.56       29.34       24.01       20.06       17.65       15.90
           9.979       11.01       12.43       14.38       16.33       17.30       17.52       15.90
           17.19       17.19       17.19       17.19       17.17       17.10       16.65       15.37

65        13/7/78     7.5   0.145      1.11 0.43      2.60 0.90
            29.10       66.80       105.3
           28.96       28.26       27.32       25.79       23.37       21.14       17.84       15.88
          0.7416E-02  0.9927E-01  0.6926E-01  0.1564E-02  0.3258E-01  0.2711E-01  0.1220E-01 -0.1356E-01
          0.3113E-02  0.3128E-02  0.3128E-02  0.3128E-02  0.3130E-02  0.3164E-02  0.3491E-02  0.4155E-02
           46.44       43.79       40.12       34.49       27.48       22.61       17.91       15.88
           11.48       12.72       14.52       17.09       19.26       19.66       17.77       15.88
           17.06       17.06       17.06       17.06       17.04       16.98       16.56       15.35

66        14/7/78     7.5   0.150      1.08 0.42      2.60 0.90
            27.00       66.20       109.5
           30.92       30.24       29.31       27.83       25.42       23.05       18.59       15.89
          0.1231E-01  0.1250      0.5443E-01  0.7133E-02  0.4004E-01  0.2597E-01  0.1055E-01  0.9041E-02
          0.3006E-02  0.3006E-02  0.3006E-02  0.3006E-02  0.3008E-02  0.3050E-02  0.3332E-02  0.3907E-02
           49.73       46.93       43.03       37.08       29.73       24.60       18.66       15.89
           12.11       13.54       15.58       18.57       21.12       21.51       18.52       15.89
           16.94       16.94       16.94       16.94       16.92       16.86       16.48       15.33

67        15/7/78     7.5   0.150      1.08 0.42      2.60 0.90
            23.10       56.40       93.00
           31.15       30.79       30.03       28.70       26.60       24.37       19.45       15.98
          0.1343      0.1066      0.1275      0.6393E-02  0.3402E-01  0.2254E-01  0.2706E-01  0.9977E-02
          0.2914E-02  0.2899E-02  0.2915E-02  0.2899E-02  0.2916E-02  0.2939E-02  0.3170E-02  0.3694E-02
           47.13       44.97       41.69       36.57       30.25       25.68       19.51       15.98
           15.18       16.61       18.37       20.84       22.94       23.05       19.39       15.98
           16.83       16.83       16.83       16.82       16.81       16.76       16.40       15.31

68        16/7/78     7.5   0.122      1.25 0.51      2.60 0.90
           -21.50      -17.70       10.61
           20.62       21.06       21.59       22.44       23.62       23.77       20.15       16.17
          0.1444E-01  0.7733E-02  0.4727E-01  0.1120E-01  0.4738E-01  0.1889E-01  0.3538E-01 -0.2003E-01
          0.2823E-02  0.2808E-02  0.2823E-02  0.2823E-02  0.2824E-02  0.2843E-02  0.3046E-02  0.3512E-02
           22.15       22.42       22.72       23.23       24.02       23.91       20.16       16.17
           19.09       19.69       20.45       21.64       23.22       23.63       20.14       16.17
           16.72       16.72       16.72       16.72       16.71       16.66       16.32       15.29

69        17/7/78     7.5   0.154      1.05 0.40      2.60 0.90
            10.20       31.40       59.20
           24.04       23.88       23.55       23.01       22.21       21.72       20.21       16.70
          0.7282E-01  0.5995E-01  0.6439E-01  0.5727E-01  0.2052E-01  0.1025E-01  0.1151E-01  0.8688E-03
          0.2747E-02  0.2747E-02  0.2747E-02  0.2747E-02  0.2732E-02  0.2764E-02  0.2944E-02  0.3358E-02
           34.51       33.17       31.17       28.11       24.55       22.56       20.25       16.70
           13.58       14.60       15.93       17.90       19.87       20.88       20.17       16.70
           16.63       16.63       16.62       16.62       16.61       16.56       16.24       15.26
```

```
118        70        18/7/78     7.5    0.164       0.99 0.37       2.60 0.90
119                    21.50         51.70         84.34
120                  28.86         28.32         27.41         26.15         24.16         22.64         20.04         16.65
121                0.6340E-02    0.7565E-01    0.3857E-01    0.3477E-01    0.7163E-01    0.2719E-01    0.2700E-01    0.2708E-03
122                0.2686E-02    0.2686E-02    0.2670E-02    0.2686E-02    0.2686E-02    0.2701E-02    0.2847E-02    0.3214E-02
123                  44.94         42.55         39.03         33.81         27.54         23.85         20.09         16.65
124                  12.78         14.10         15.80         18.49         20.78         21.42         19.98         16.65
125                  16.53         16.53         16.53         16.53         16.52         16.47         16.17         15.24
126
127        71        19/7/78     7.5    0.170       0.95 0.35       2.60 0.90
128                    25.30         65.70         112.8
129                  32.15         31.48         30.37         28.74         26.24         24.17         20.32         16.80
130                0.3681E-01    0.8952E-01    0.6204E-01    0.7112E-01    0.9312E-01    0.3691E-01    0.3548E-01    0.1316E-03
131                0.2625E-02    0.2625E-02    0.2625E-02    0.2625E-02    0.2625E-02    0.2653E-02    0.2768E-02    0.3077E-02
132                  54.73         51.43         46.60         39.34         30.79         25.80         20.39         16.80
133                  9.579         11.53         14.13         18.14         21.69         22.53         20.24         16.80
134                  16.44         16.44         16.44         16.44         16.43         16.39         16.10         15.21
135
136        72        20/7/78     7.5    0.162       1.00 0.38       2.60 0.90
137                    21.60         61.10         110.3
138                  32.37         31.85         30.92         29.62         27.49         25.45         20.88         16.94
139                0.5341E-02    0.7675E-01    0.4015E-01    0.2081E-01    0.6767E-01    0.2524E-01    0.2589E-01    0.1621E-04
140                0.2579E-02    0.2579E-02    0.2579E-02    0.2579E-02    0.2579E-02    0.2605E-02    0.2723E-02    0.2977E-02
141                  53.07         50.18         45.90         39.53         31.90         27.03         20.95         16.94
142                  11.67         13.52         15.94         19.70         23.08         23.87         20.80         16.94
143                  16.36         16.36         16.36         16.36         16.35         16.31         16.04         15.18
144
145        73        21/7/78     7.5    0.156       1.04 0.40       2.60 0.90
146                    22.30         65.90         121.8
147                  33.18         32.59         31.81         30.48         28.39         26.30         21.49         17.11
148                0.8362E-02    0.1414        0.1441        0.4112E-02    0.5020E-01    0.2173E-01    0.2538E-01    0.1642E-01
149                0.2548E-02    0.2548E-02    0.2548E-02    0.2548E-02    0.2570E-02    0.2558E-02    0.2665E-02    0.2898E-02
150                  55.02         51.96         47.68         41.09         33.21         28.03         21.57         17.12
151                  11.34         13.23         15.94         19.88         23.56         24.57         21.41         17.11
152                  16.28         16.28         16.28         16.28         16.27         16.23         15.97         15.15
153
End of File
```

APPENDIX III

THE MEASUREMENT OF G_o FOR DRY SOIL CONDITIONS

THE MEASUREMENT OF G_o FOR DRY SOIL CONDITIONS

In the null-alignment procedure it was assumed that internal heat sources or sinks were absent and internal convective heat exchange could be neglected in the soil. The integrated form of the heat transfer equation used was

$$G(z,t) = G(z_k,t) - \int_{z_k}^{z} C\frac{\partial T}{\partial t}\, dz \qquad (1)$$

Philip (1957) and Gardner and Hanks (1966) showed that when the soil surface is very dry, evaporation takes place below the surface (generally within the upper 3 cm). In this case (1) should be modified as follows:

$$G(z,t) = G(z_k,t) - \int_{z_k}^{z} C\frac{\partial T}{\partial t}\, dz - \int_{z_k}^{z} h_{LE}\, dz \qquad (2)$$

where $h_{LE}(z,t)$ is the volumetric rate at which energy is being used for evaporation in the soil. Since $h_{LE} > 0$, (2) with $0 < z < 3$ cm and $z_k > 3$ cm shows that near-surface values of G, calculated using (1), as well as corresponding values of k, calculated from Fourier's Law, would be underestimated during the daytime for dry soil moisture conditions. An underestimate occurs because the energy that flows into the soil from the surface, but is used to evaporate water and not warm the soil has been neglected in (1). Below the evaporation zone, both (1) and (2) yield the same values of G since h_{LE} is then 0. Calculation of h_{LE} is difficult since it is determined in the mass transfer equation for water vapour, presented in integrated form as follows:

$$\int_{z_k}^{z} L_w P\frac{\partial \rho_v}{\partial t}\, dz = L_w[q_v(z,t) - q_v(z_k,t)] + \int_{z_k}^{z} h_{LE}\, dz \qquad (3)$$

where P is the porosity of the soil, ρ_v is the density of water vapour in the soil pore space, q_v is the vapour flux density (positive upward), and L_w is the latent heat of vapourization of water (assumed constant).

An upper limit to the correct value of G_o (from (2)) is given by the addition of LE to G_o calculated from (1). For daytime averages at both sites at Agassiz on the final days of the study, this yields values of G_o about $1\frac{1}{2}$ - 2 times greater than those calculated from (1). Consequently the surface values of k reported in Table 1.3 (0.1 - 0.2 W m^{-1} $°C^{-1}$) may be this much in error. Applying this correction improves the agreement between the measured values of k and values reported in the literature (~ 0.2 - 0.3 W m^{-1} $°C^{-1}$ for loam/silt-loam soils with $\theta_v < 0.05$).

To ascertain the effect on the energy balance calculations, consider $z = 0$ and $z_k = d$, where d is a depth below the evaporation zone. The h_{LE} term can be eliminated by combining (2) and (3) as follows:

$$G_o = G(d,t) + \int_o^d C\frac{\partial T}{\partial z}\,dz + \int_o^d L_w P\frac{\partial \rho_v}{\partial t}\,dz + LE \qquad (4)$$

where $LE = L_w q_v(o,t)$ and $q_v(d,t) = 0$. The energy balance equation of the "infinitesimally shallow" $z = 0$ layer is:

$$R_N = H + G_o \qquad (5)$$

Combining (4) and (5) yields

$$R_N = H + LE + G(d,t) + \int_o^d C\frac{\partial T}{\partial t}\,dz + \int_o^d L_w P\frac{\partial \rho_v}{\partial t}\,dz \qquad (6)$$

It is recognized that the sum of the third and fourth terms of (6) is simply the value of G_o calculated from (1). The energy balance components in this thesis were calculated using (6) with the last term neglected. This term represents the rate at which latent heat is stored

in the evaporation zone. An upper limit to the magnitude of $\frac{\partial \rho_v}{\partial t}$ can be calculated by assuming that the soil in the upper 0 - 3 cm goes from saturation to air dry within a half-hour. The increase in ρ_v can be calculated from the ideal gas law

$$\rho_v = \frac{e}{R_v T} \tag{7}$$

with $e = e^*(T)$ and $R_v = 460$ J kg^{-1} °C^{-1}. Assuming that T = 318°K (45°C), so that e = 9.5 kPa, yields $\rho_v = 0.065$ kg m^{-3}. Assuming P = 0.65, d = 0.03 m, and with $L_w = 2.5$ MJ kg^{-1} yields an upper limit of 0.9 W m^{-2} for this term. This is completely negligible compared to the daytime half-hourly values of R_N, G_o, H, and LE. Consequently the energy balance calculations are not significantly in error when evaporation occurs below the surface and G_o is calculated from (1). Furthermore the effect on the similarity assumption ($\kappa_H = \kappa_{LE}$) due to the slightly different source heights for LE and H should be small since 3 cm is only 4% of 70 cm, the height midway between the psychrometers.

Literature Cited

Gardner, H.R., and R.J. Hanks, Evaluation of the evaporation zone in soil by measurement of heat flux, Soil Sci. Soc. Amer. Proc., 30, 425-428, 1966.

Philip, J.R., Evaporation, and moisture and heat fields in the soil, J. Meteorol., 14, 354-366, 1957.